

GENERATION OF INDUCTION HEATED, SEEDED HYDROGEN PLASMAS
AT ONE ATMOSPHERE PRESSURE

A THESIS

Presented to

The Faculty of the Division of Graduate
Studies and Research

By

Robert Allan Benns

In Partial Fulfillment
of the Requirements for the Degree
Doctor of Philosophy
in the School of Nuclear Engineering

Georgia Institute of Technology

August, 1972

GENERATION OF INDUCTION HEATED, SEEDED HYDROGEN PLASMAS
AT ONE ATMOSPHERE PRESSURE

Approved:


J. R. Williams, Chairman

Robert G. Ragsdale

Joseph D. Clement

Date approved by Chairman: 8/11/72

In presenting the dissertation as a partial fulfillment of the requirements for an advanced degree from the Georgia Institute of Technology, I agree that the Library of the Institute shall make it available for inspection and circulation in accordance with its regulations governing materials of this type. I agree that permission to copy from, or to publish from, this dissertation may be granted by the professor under whose direction it was written, or, in his absence, by the Dean of the Graduate Division when such copying or publication is solely for scholarly purposes and does not involve potential financial gain. It is understood that any copying from, or publication of, this dissertation which involves potential financial gain will not be allowed without written permission.

7/25/68

ACKNOWLEDGMENTS

This research project was supported by NASA Grant NCR-11-002-146 and monitored by the Advanced Nuclear Propulsion Concepts Branch of the Lewis Research Center. Mr. R. G. Ragsdale and Mr. C. C. Masser of Lewis Research Center deserve thanks for their personal interest and helpful suggestions toward this research work.

My thesis advisor, Dr. J. R. Williams, has earned my appreciation for his assistance and encouragement during the course of this work. Dr. J. D. Clement, Dr. J. R. Stevenson, and Mr. R. G. Ragsdale, my thesis committee members, have provided invaluable professional support.

I wish to thank Mr. W. E. Bennis and Mr. G. C. Blascoe for their advice and recommendations concerning the practical aspects of designing high power radio frequency equipment. Mr. W. D. Statham of the electronics shop has been helpful in the prompt and efficient assistance he has given concerning electronic design and trouble shooting. Mr. M. Burke, of the machine shop, was always cooperative in helping with the various problems associated with machining the ceramic for the plasma torches. My appreciation is extended to Lydia Geeslin for her typing and editing assistance on this manuscript and other papers.

During this research I have acquired many good friends from among my fellow nuclear engineering graduate students. I am thankful to Steve Thompson for encouraging and aiding me in this research. Danny Corbett,

Harry Majors, and Rich Games have all made helpful contributions to this research effort.

I express my most sincere appreciation to my wife, Chris, for her love and understanding during the times that this research took priority.

TABLE OF CONTENTS

	Page
ACKNOWLEDGMENTS	ii
LIST OF TABLES	vi
LIST OF ILLUSTRATIONS	vii
SUMMARY	x
Chapter	
I. INTRODUCTION	1
II. PREVIOUS EXPERIMENTAL AND THEORETICAL RESEARCH	3
Previous Induction Plasma Research	5
Previous Research on Hydrogen and Tungsten Plasma Absorption Coefficients	10
Tungsten-Hydrogen Aerosol Research	12
III. PRINCIPLES OF INDUCTION HEATING	14
Induction Heating Theory	14
High Power Amplifiers for Induction Plasma Generation	32
IV. EQUIPMENT AND INSTRUMENTATION	52
Radio Frequency Plasma Generator	53
Plasma Torch	73
Aerosol Generators	78
Gas Flow and Aerosol Density Sampling Systems	83
Data Collection Instrumentation	87
V. EXPERIMENTAL PROCEDURE	90
VI. DATA ANALYSIS	97
VII. EXPERIMENTAL RESULTS	107
VIII. CONCLUSIONS AND RECOMMENDATIONS	116
Conclusions	116
Recommendations	117

TABLE OF CONTENTS (Continued)

	Page
APPENDIX	
ABSORPTION OF RADIANT ENERGY IN HYDROGEN AND TUNGSTEN VAPOR.	119
BIBLIOGRAPHY	138
VITA	143

LIST OF TABLES

Table		Page
1.	Properties of Gases Used in RF Plasmas and Resistivity of Materials Used in "Dummy" Loads.	27
2.	Necessary Tube Protection	46
3.	Pi-Matching Network Component Values for Various Plasma Loads.	66
4.	Plasma Generator Operating Parameters	68

LIST OF ILLUSTRATIONS

Figure	Page
1. Object to be Heated in the Magnetic Field of an Inductor.	15
2. Equivalent Circuit of Work Coil and Object.	17
3. The Variation of Current Density and of the Concentration of Absorbed Power with Depth Below the Surface of a Conductor	17
4. Work Coil is Part of Tank Circuit	22
5. Work Coil is Coupled Inductively to the Tank Coil.	22
6. Pi-Matching Network	22
7. Work Circuit Tuning by Use of Movable Taps on the Tank Coil.	24
8. Work Circuit Tuning by Use of a Variable Capacitor	24
9. Effect of Gas on Arc Diameter	29
10. Induction Plasma Torch.	29
11. Single Ended Grid Neutralization.	50
12. The Basic Circuit of Single Ended Grid Neutralization Showing Interelectrode Capacitances.	50
13. Plasma Generator Components	55
14. Plate Power Supply.	56
15. Three-Phase Full-Wave Rectifier	57
16. Final Amplifier	61
17. Servo Tuning System	67
18. Constant Current Characteristics of Eimac 4CX-35000C.	69

LIST OF ILLUSTRATIONS (Continued)

Figure	Page
19. Plasma Generator Protection System.	72
20. Plasma Torch.	79
21. Test Tube Aerosol Generator	80
22. Blender Aerosol Generator	80
23. Gas Flow Control System	84
24. Data Collection System.	88
25. Plasma Generator Operation.	95
26. Laser Beam Passing Through Plasma	98
27. Oscillograph Recordings for Attenuated and Non-attenuated Laser Scans.	99
28. Ratio of Attenuated to Non-attenuated Laser Intensity as a Function of Axial Intensity.	100
29. Errors Encountered in Analyzing Outer Zones of Plasma Torch	103
30. Opacity Profile of Room Temperature Tungsten Seeded Hydrogen.	108
31. Opacity Profile of Tungsten-Hydrogen Plasma with Inlet Aerosol Density of 41.5×10^{-6} gm/cm ³	110
32. Opacity Profile of Tungsten-Hydrogen Plasma with Inlet Aerosol Density of 30.5×10^{-6} gm/cm ³	111
33. Opacity Profile of Tungsten-Hydrogen Plasma with Inlet Aerosol Density of 16.9×10^{-6} gm/cm ³	112
34. Composition of Hydrogen as a Function of Temperature at a Pressure of One Atmosphere.	122
35. Energy Level Diagram of the Model Fuel Atom	127
36. Assumed Oscillator Strength Distribution Used in the Heavy Atom Model as a Function of Photon Energy.	130

LIST OF ILLUSTRATIONS (Continued)

Figure		Page
37.	Spectral Absorption Coefficient of .01 Atmosphere Tungsten Vapor at 6000 K and 10000 K	136
38.	Experimental Emission Spectrum of Uranium Plasma at 8000 K	137

SUMMARY

The gaseous core nuclear reactor is being developed to produce very hot working fluid gases for advanced power and propulsion systems. In the gaseous core nuclear reactor a very hot fissioning core radiates thermal energy to the working fluid. For propulsion systems hydrogen would be the working fluid. Hydrogen gas below about 10000°K is transparent to the radiation emitted by the fissioning core, and must be seeded with submicron-sized metallic particles to enhance absorption of thermal energy in the working fluid. Measurements of the extinction parameter of tungsten-hydrogen aerosols have previously been made as a function of wavelength from 2500 \AA to 5800 \AA at temperatures to 2500°K .

At high temperatures ($4000\text{-}5000^{\circ}\text{K}$) the seed particles vaporize, resulting in an opacity decrease. At temperatures above about 10000°K the hydrogen itself becomes opaque. The temperature range in which the seed has vaporized, but the hydrogen has not become opaque is known as the seed-hydrogen opacity window. Previously only estimates of the seed vapor opacity, based on theoretical considerations, were available in the region of the seed-hydrogen opacity window.

A 125 kilowatt radio frequency induction heater has been designed and constructed to produce tungsten seeded hydrogen plasmas which simulate the working fluid of the gaseous core nuclear reactor. An air cooled plasma torch with flat windows to allow for spectral observation of the plasma has been developed. Initial opacity measurements of the tungsten

seeded hydrogen plasmas have been taken by scanning the plasma with a helium-neon laser, and recording attenuated and non-attenuated laser intensity. These data, which are a function of axial distance from the center of the plasma, are transformed to opacity as a function of radius by an Abel inversion technique. Opacity data have been taken for several tungsten seeded hydrogen plasmas of various tungsten densities. An extinction parameter of $2 \times 10^4 \text{ cm}^2/\text{gm}$ was measured, which indicates that the seed-hydrogen opacity window is not very transparent and that there should be little difficulty associated with heating the working fluid with thermal radiation in the temperature range of the seed-hydrogen opacity window.

CHAPTER I

INTRODUCTION

The gaseous core reactor is being developed to produce very hot working fluid gases for advanced power and propulsion systems.¹⁻⁴ In the gaseous core nuclear reactor the fissioning plasma core is opaque to thermal radiation,⁵ and as a result only the surface of the fissioning plasma emits thermal radiation. The surface temperature is expected to be of the order of 15,000 °K.⁶ Krascella⁷ and Patch⁸ have calculated the absorption parameters of hydrogen as a function of pressure, temperature, and wavelength. The first transition in the Lyman series occurs at 1216 Å, and hydrogen at low temperatures is transparent to radiation of longer wavelengths. The emission spectra of uranium plasma at 8000 °K occurs primarily from 2000 Å to 8000 Å,^{9,10} so low temperature hydrogen is transparent to the emitted radiation. The hydrogen propellant is made opaque to the radiant energy by seeding it with submicron sized tungsten particles. Other types of particles have been ruled out; carbon due to the excessive reaction rate with high temperature hydrogen,¹¹ and alumina and silica, despite being good attenuators, due to their low absorption coefficient. At high temperatures (4000-5000 °K), the seed particles will vaporize, resulting in an opacity decrease. At temperatures above 10,000 °K the hydrogen itself becomes opaque.^{7,8} The temperature range in which the seed has vaporized but the hydrogen is not opaque is known as the seed-hydrogen opacity window. The opacity of tungsten seeded hydrogen has been

measured to 2500°K, but presently only estimates of the seed vapor opacity, based on theoretical considerations, were available in the temperature range of the seed-hydrogen opacity window.

The purpose of this research is to produce radio frequency induction heated hydrogen plasmas seeded with tungsten to simulate the working fluid of the gaseous core nuclear reactor, and to demonstrate the feasibility of utilizing such a plasma for opacity measurements in the temperature range of the seed-hydrogen opacity window. A 125 kilowatt radio frequency induction heater has been designed and constructed to produce one atmosphere tungsten seeded hydrogen plasmas, and an air cooled plasma torch utilizing flat windows has been developed to allow for spectral observation of the plasma. Initial opacity measurements in the temperature range of the seed-hydrogen opacity window have been made by measuring the attenuation of a laser beam traversing the seeded plasma. An Abel inversion technique taking into account absorption is used to arrive at opacity as a function of radius. Other macroscopic properties of the plasma, such as tungsten seed density, plasma size, and plasma radiant heat output, have also been measured.

CHAPTER II

PREVIOUS EXPERIMENTAL AND THEORETICAL RESEARCH

It was in the early part of the nineteenth century that first mention was made in the literature of the use of induced currents for heating metal. Practical application of these devices was first made about the middle of the nineteenth century; the objective of most of these applications was the melting of metal, utilizing a graphite or metallic crucible heated by induction to a temperature above the melting point of the charge, which in turn was melted by thermal conduction from the crucible. Ferranti and Colby both presented data in the later 1800's on an induction melting furnace which induced currents directly into the charge, thereby permitting the use of non-conducting crucibles. These melting furnaces were all operated on relatively low frequencies, ranging from 5 to 60 cycles, largely because no means was available at that time for producing appreciable amounts of electrical energy at higher frequencies. In the early 1900's Dr. E. F. Northrup invented the high-frequency melting furnace. Since the ability to transfer heat energy into the work piece is a function of the frequency of the current, this device was made practical by use of the mercury-hydrogen spark to produce high-frequency energy. Development of induction heating equipment closely followed advances made in the radio field and today induction heaters are available with powers from less than a kilowatt to more than 1,000 kilowatts, utilizing frequencies from 960 cycles to 30 megacycles.¹²

Although high-power, high-frequency induction heaters have been available for many years, it was not until 1960 that T. B. Reed of the Massachusetts Institute of Technology utilized inductive coupling at a frequency of several MHz to generate a stable plasma at atmospheric pressure. Reed's induction plasma torch was a quartz tube, open at one end, with gas supplied at the other end. An rf coil of a few turns surrounded the tube at the center and served to couple energy into the plasma, which had been ignited by forming a small "pilot" plasma upstream (relative to the rf coil) using a conventional 30 amp ac arc operated in argon. The plasma torch was always started in pure argon, and argon mixtures containing 20 percent air, helium, or hydrogen, or 50 percent oxygen were heated in the induction to plasma torch. The power was supplied to the plasma by a commercial (Lepel) rf heating unit with a maximum power output of 10 kW and operated at a frequency of 4 MHz.¹³

Recently only two companies have done research concerned with radio-frequency induction plasmas. They are the TAFA Division of Humphreys Corporation, whose primary objective was to study the heat addition, mixing, and stabilization mechanisms of the gas core reactor utilizing an induction plasma sheath system scaled up to 1000 kW plate power,¹⁴ and United Aircraft Research Laboratories, whose primary objective has been to develop an intense radiant energy source which would be capable of producing radiant energy fluxes equal to those expected in a full-scale nuclear light bulb engine.¹⁵

Previous Induction Plasma Research

Initial work at Humphreys Corporation was done by M. L. Thorpe, who attempted to produce large-diameter, low-velocity, high-enthalpy hydrogen plasmas for transmissivity investigations. An 88 kW oscillator, using a water cooled triode vacuum tube, which coupled electrical energy to a copper work coil was used to heat the plasma. The work coil was part of the tuned-tank of the plate circuit. Thorpe found it necessary to contain the argon-hydrogen mixtures in a water-cooled metal torch rather than a quartz tube because of the high radiant and convective torch wall heating which resulted when greater than 20 percent hydrogen in argon was used at the required minimum sustaining power, which was above 50 kW. Considerable effort was devoted to maximizing hydrogen percentage at a given power level using the 88 kW rf power supply. Within the power range available, it was found that the maximum hydrogen concentration which could be run reliably was 70 percent. Thorpe extrapolated his data and estimated that plate power levels in the range of 160 kW would be required to achieve 100 percent hydrogen operation.¹⁶

P. H. Dundas and C. E. Vogel utilized induction plasma heating in hot binary flow and permeable wall studies to demonstrate that a hot plasma ball could be maintained in the center of a flowing stream of gas with little mixing of the propellant with the plasma. These studies also demonstrated that the plasma forming material could be introduced by vaporizing a solid near the inlet end of the plasma device.^{17,18}

High frequency (450 kHz to 6 MHz) plasma generators utilized by the Humphreys Corporation are generally good for heating small plasmas with

energy requirements up to 300 kW. The depth of heating is inversely proportional to the frequency of the plasma generator. For high powered plasma operation, greater than 300 kW, a motor generator set producing 9,600, 2,800, or 960 Hz, which heats more uniformly through the plasma, is used. Although there is significant overlap in the power levels at which various frequencies are used, the general trend of reduced frequency with increased power is valid. Initial low frequency plasma experiments by Humphreys were operated at 9,600 Hz. Feasibility experiments were run simply to demonstrate that a plasma could be sustained at 9,600 Hz.¹⁹ Three different devices were tested at 9,600 Hz for the feasibility studies. The first was a device with a 15.3 cm ID by 75 cm long plasma chamber constructed with an uncooled opaque fused quartz wall. A second device utilized a 13.9 cm ID by 45.8 cm long water cooled clear quartz tube, and the third was a 30.6 cm ID by 153 cm long uncooled fused quartz cylinder. Two 9,600 Hz power supplies (motor-generator) connected in parallel with a continuous duty rating of 350 kW supplied power. Ignition of the plasma was accomplished with either a high frequency pulse generated flow discharge (argon) inside of the torch at about one mm mercury pressure or by direct self-ignition with 9,600 Hz power at 40-50 microns. Minimum sustaining power for each configuration was determined. The successful operation of a torch at 9,600 Hz led to the design of a feasibility experiment at 960 Hz. A motor-generator set with a continuous duty rating of 1.25 mW was used with a 30.6 cm ID by 153 cm long opaque fused quartz tube in which the plasma was generated. This device was successfully operated at pressures up to 300 mm mercury; however, it was impossible to

operate above 300 mm due to the inability of the power supply to produce its rated capacity.¹⁹

J. W. Poole and C. E. Vogel conducted an experimental program to produce high pressure, high enthalpy arc plasmas which could be used to study various nozzle cooling techniques. This work was directed toward providing experimental input into the design of the nozzle of the gas core nuclear rocket which will have to withstand extremely high thermal loads. Air plasma operation was utilized and yielded enthalpies of 13,000 Btu/lb. The rf power supply used for most of this work consisted of a 190 kW dc plate power TAFE induction plasma system (12,700 volts, 15 amperes dc). When a transpiration cooled nozzle was used there was a significant reduction (25 percent) in the thermal loading to the nozzle wall. The addition of fine particle seeding to the nozzle coolant flow further reduced (10 percent) the thermal loading on the nozzle walls.²⁰

Initial experiments were conducted at United Aircraft Research Laboratories (UARL) by J. S. Kendall and W. C. Roman to develop an intense radiant energy source which would eventually be capable of producing radiant energy fluxes equal to those expected in a full-scale nuclear light bulb engine.²¹

The test program was conducted using the UARL 1.2 mW rf induction heater, which was constructed during 1966 and 1967. This induction heater was designed to deposit approximately 500 kW of rf power into a gas discharge. The rf output was provided by two power amplifier tubes connected in a push-pull configuration to drive a resonant tank circuit. The grids of the power amplifier tubes were driven by the amplified output of a

variable-frequency oscillator at the resonant frequency of the tank circuit (5.5 MHz).^{21,22} The maximum total dc input power to the power amplifiers employed in plasma discharge tests during this program was about 650 kW.²³ The heater has been operated with a salt-water mock-up load at input dc power levels exceeding 750 kW. The resonator section, plate tank circuit, consisted of two arrays of ten vacuum capacitors, each of which was connected in parallel with a single turn, silver-plated, 3.06 inch diameter work coil. Each work coil consisted of five internally cooled copper tubes which were soldered together to form a single structure prior to being silver plated.²¹

Kendall's and Roman's initial program at UARL was to determine the effect of various parameters on the power radiated from the vortex, the power deposited in the peripheral wall of the vortex tube, and the power carried away by convection from the vortex. Both argon discharges with no seed and argon discharges seeded with submicron carbon and tungsten particles were employed. Tests were conducted at discharge pressures up to 6.0 atmosphere absolute and with up to 85 kW of power deposited in the discharge; of this, 35 kW was radiated through a water-cooled transparent wall surrounding the discharge. The 35 kW of radiant energy represented a radiant energy flux of about 12.0 kW/in^2 , corresponding to an equivalent black body radiating temperature of 7600°R . For comparison, the design radiant flux level at the edge of the fuel containment region of a representative nuclear light bulb engine is 178 kW/in^2 ($15,000^\circ \text{R}$).²¹ Roman continued work along these lines, and by 1970 improvements in the plasma system were such that a maximum heat deposition rate per unit volume of

0.57 MW/in³ was achieved and tests had been conducted at pressures to 19.2 atmospheres. The maximum radiant energy flux achieved at the edge of the plasma was 49 kW/in², corresponding to an equivalent black body radiating temperature of 10,860° R.^{22,23}

A. E. Mensing and J. F. Jaminet conducted investigations at UARL in which the amount of heavy gas contained in light gas vortexes was measured for both heated and unheated vortex flows. The 80 kW rf induction heater, which was used in the heated vortex tests, was a driven system in which a 600 W tunable rf transmitter was the drive for the grid of the 80 kW power amplifier. The output of the power amplifier was connected to a $2\frac{1}{2}$ turn, 2.7 inch diameter coil through a pi coupling network. Comparisons were made of the heavy gas partial pressures in the heated and unheated flows. For similar geometries and the same light gas weight flows, the heated vortexes had larger values of the heavy gas partial pressure in the central regions of the vortex, but less heavy gas partial pressure at the greater radii.^{24,25}

P. J. Marteney, A. E. Mensing, and N. L. Krascella conducted theoretical and experimental investigations to determine spectral emission characteristics of argon-tungsten and argon-uranium plasmas. The tungsten and uranium were introduced into the discharge in the form of tungsten hexafluoride or uranium hexafluoride at heavy atom to argon mass ratios of approximately 1.0×10^{-4} and a total pressure of one atmosphere. Experimental integrated line intensities over 100 Å wavelength intervals for argon, tungsten, and uranium were subsequently compared to similar analytical results calculated for the visible region of the spectrum

(2000 to 10,000 Å), with generally poor correlation between experimental and analytical results for tungsten and fairly good correlation for uranium. For the experimental studies, the previously described 80 kW induction heater was used to produce tungsten-argon and uranium-argon plasmas.²⁷

Theoretical analyses were made by A. E. Mensing and L. R. Boedeker at UARL to investigate the power deposition and energy removal in high power, high pressure, radiating rf plasmas used to simulate the thermal environment of the nuclear light bulb reactor. The power deposition and energy dissipation characteristics of infinite cylinder rf heated argon plasmas at pressures of 1.0 and 10.0 atmospheres were studied, assuming that the thermal and electrical conductivities varied with temperature, that the gas radiation per unit volume varied with both temperature and pressure, and that the plasma was optically thin. The coupling between the plasma discharge and the rf generator was studied using an infinite cylinder, constant conductivity model.²⁸

Previous Research on Hydrogen and Tungsten Plasma

Absorption Coefficients

N. L. Krascella at United Aircraft Research Laboratories made theoretical calculations to determine the following characteristics of hydrogen gas: composition (partial pressures of H_2 , H , H^+ , H^- , electrons, and quantum states 1 through 5 of H); opacity (total spectral absorption coefficient and Rosseland mean opacity); thermodynamic properties (enthalpy, free energy, and entropy); and ionization potential lowering. Data were tabulated for fourteen pressures between 1 and 1000 atmospheres and for

21 temperatures between 3000 and 200,000° R. Spectral absorption coefficients were tabulated for 33 wave numbers between 1000 and 400,000 cm⁻¹ at each pressure and temperature.⁷ The Appendix includes a summary of Krascella's research.

A theoretical study was conducted by R. W. Patch at Lewis Research Center to determine the spectral absorption coefficient for hydrogen for photons with wave numbers from 500 to 400,000 cm⁻¹ (infrared, visible, and ultraviolet), neglecting scattering. The plasma was assumed to be in local thermodynamic equilibrium at temperatures from 3000 to 90,000° R and pressures from 100 to 1000 atmospheres. Fifteen absorption processes were included. The Planck and Rosseland mean opacities were derived for a nonscattering plasma with real index of refraction varying with photon wave number and were calculated for hydrogen.⁸

Krascella calculated the composition and spectral opacity of tungsten plasmas at temperatures of 6000° K and 10,000° K. This was done by assuming a semi-empirical atomic model to represent the tungsten species. Neutral tungsten, singly ionized tungsten, and doubly ionized tungsten were considered in the composition analysis. Bound-bound and bound-free transitions were considered.²⁹ A summary of this research is included in the Appendix.

Miller, Wilkerson, and Koopman at the University of Maryland measured absolute opacities of uranium plasma (2800 to 8800 Å) by using a gas driven shock tube. Temperatures obtained were from 7,500° to 12,000° K, and pressures were from 1/50 to 1/5 atmosphere. The gas was composed of .2 to 2.0 percent UF₆ in neon.³⁰

Campbell and Schneider at the University of Florida used a dc arc generator with a tungsten pin cathode and a uranium pellet anode to produce uranium plasmas. A cover gas of helium was used and substantial vaporization of uranium took place. The atomic characteristics of helium and uranium are such that the emitted line radiation originated primarily from singly ionized uranium. Measurements of temperatures, particle densities, emission and absorption coefficients were reported.²⁶

Tungsten-Hydrogen Aerosol Research

Substantial research has been conducted concerning the absorption and scattering parameters of gases seeded with refractory particles. The absorption of thermal radiation by suspended refractory particles was measured by Lanzo and Ragsdale. Seeded air was introduced into an annular heat exchanger and an arc was initiated. The seeded air in the annulus reached higher temperatures than unseeded air under the same conditions, thus showing that particle seeding enhances radiant heat transfer to gases.³¹ Theoretical and experimental studies of radiant heat transfer from a heated tungsten cylindrical enclosure to a particle cloud within it were reported by Keng and Orr. The addition of tungsten or carbon particles to a transparent gas, helium, which was passed through the tube rendered the gas opaque and caused a significant increase in heat absorption.³²

In an experiment performed by Burkig, a cloud of particles in a gas was injected into a transparent quartz tube and exposed to a flash of a xenon flash tube. The temperature rise of the gas was inferred from the pressure rise. The bulk of the work was done with micron-sized particles

of carbon, iron, and tantalum carbide, seeded in helium and hydrogen. During the flash the temperature of the aerosol rose to about 3000°K for about one millisecond.³³

Williams, Shenoy, Partain, and Clement at Georgia Tech have measured the extinction parameters of submicron refractory particles dispersed in hydrogen at temperatures to 2500°K at pressures to 115 atmospheres. A beam of radiant energy was passed through hot hydrogen, first unseeded and then seeded, at a given temperature. Measurements of the transmitted energy for the two cases as a function of wavelength and simultaneous measurements of the aerosol density yielded the extinction parameter of the particle-seeded gas.³³ The scattering amplitude function of submicron carbon, silicon, tungsten, tungsten carbide, and silicon carbide particles suspended in nitrogen and hydrogen at a wavelength of 6328 \AA for scattering angles from 1 to 179 degrees was measured by Jacobs.³⁴

CHAPTER III

PRINCIPLES OF INDUCTION HEATING

Induction Heating Theory

Radio-frequency heating consists essentially of transferring power electromagnetically to an object to be heated. Metals (or any conductor for that matter) and non-conductors act differently in that good electrical conductors cannot be penetrated by or absorb heat energy from electric fields, while non-conductors can be penetrated by electric fields. Conductors are, however, penetrated by magnetic fields, and any fluctuation of these magnetic fields sets in motion the free electrons responsible for the conductivity of the material. The fluctuating magnetic field induces eddy currents in the conductor, and the heat appears as a result of the flow of eddy currents against the resistance of the material (I^2R losses). The greater the rate of change of the flux the greater the induced currents. Non-conductors are heated by being placed in a strong alternating electric field, such as between capacitor plates. Plasmas, having free electrons, are heated by the inductive process.^{35,36,37}

For most applications, the object to be heated is placed inside a work coil in which the rf currents exist, as shown in Figure 1. The purpose of the work coil is to create an alternating magnetic field in the object. Since heating is proportional to rate of change of flux linked with the work, which in turn depends upon the frequency and magnitude of

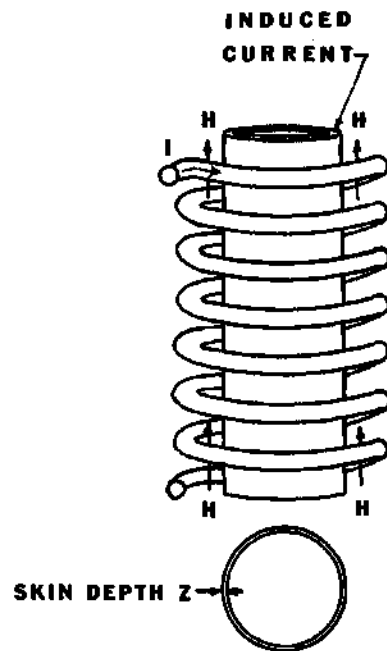


Figure 1. Object to be Heated in the Magnetic Field of an Inductor

current in the work coil, it follows that, at higher frequencies, the current required for a given rate of change of flux will be less.^{35,36,37}

The work coil and object are equivalent to a transformer having a shorted secondary and may be represented by the circuit shown in Figure 2. R_1 and L_1 are the resistive and inductive components of the work coil, and R_2 and L_2 that of the object, while M is the mutual inductive coupling between them. We may write from ordinary coupled theory,

$$i_1(R_1 + j\omega L_1) + j\omega M i_2 = e \quad (1)$$

and

$$j\omega M i_1 + i_2(R_2 + j\omega L_2) = 0 \quad (2)$$

The effective impedance of the work coil is,

$$Z' = R_1 + j\omega L_1 + \left(\frac{M^2 \omega^2}{R_2^2 + \omega^2 L_2^2} \right) (R_2 - j\omega L_2) \quad (3)$$

Separating resistive and reactive components,

$$R_1' = R_1 + \frac{(\omega^2 M^2) R_2}{(R_2^2 + \omega^2 L_2^2)} \quad (4)$$

$$X_1' = X_1 - \frac{(\omega^2 M^2) \omega L_2}{(R_2^2 + \omega^2 L_2^2)} \quad (5)$$

The resistance of the work coil is increased, while the inductance appears to be reduced. Noting that,

$$Q_{\text{work}} = \frac{\omega L_2}{R_2} \quad (6)$$

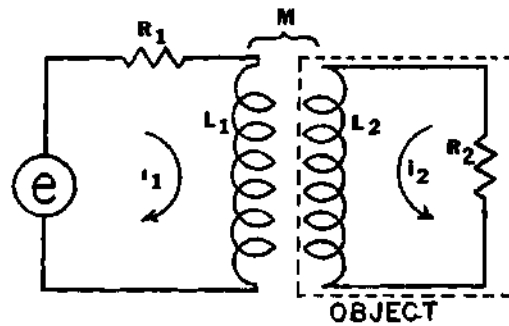


Figure 2. Equivalent Circuit of Work Coil and Object

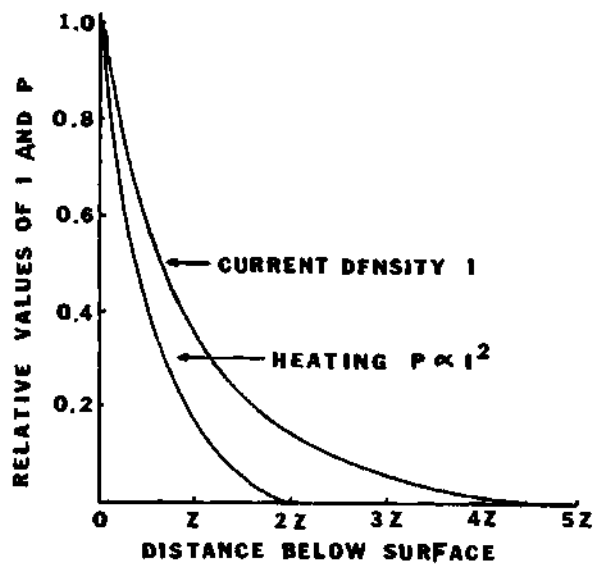


Figure 3. The Variation of Current Density and of the Concentration of Absorbed Power with Depth Below the Surface of a Conductor (Reference 36)

the reflected resistance into the primary becomes,

$$\Delta R_1 = \frac{M^2}{L_2^2} R_2 \left(\frac{Q_W^2}{Q_W^2 + 1} \right) \quad (7)$$

The factor $\frac{Q_W^2}{Q_W^2 + 1}$ closely approaches unity when Q_W is larger than 3, and since this is true except for very small diameter work,³⁶

$$\Delta R_1 \cong \frac{M^2}{L_2^2} R_2 \quad (8)$$

The transfer efficiency or ratio of the useful power in the work to that wastefully dissipated in the work coil is,³⁶

$$\eta = \frac{\Delta R_1}{R_1 + \Delta R_1} \quad (9)$$

which may be written as

$$\eta = \frac{\frac{M^2}{L_2^2} R_2}{\frac{M^2}{L_1^2} R_1 + 1} \quad (10)$$

At high frequencies the whole of the induced current is concentrated in the surface region of the object, and it is of magnitude given by,

$$H = 4\pi I_\ell \quad (11)$$

where I_ℓ is the number of turns per unit length and H denotes the original magnetic field of the inducing coil. We have outside the work piece the

original field H ; inside the rod beyond the surface skin, zero field; and in the surface skin a field which varies from zero to H as we pass outwards through the skin; as shown in Figure 3. Skin depth z may be given by

$$z = (2\pi\mu\omega\sigma)^{-\frac{1}{2}} \quad (12)$$

for small z , where σ is the conductivity of the material and μ is the absolute permeability.³⁵

Since skin depth is proportional to $(f)^{-\frac{1}{2}}$ and resistance is proportional to z^{-1} , rf resistance of the object is proportional to $(f)^{\frac{1}{2}}$, but this also applies to the work coil. It is seen from the equation for transfer efficiency, η , that, if $R_1 = R_2$, the efficiency is independent of frequency, but when R_2 is larger than R_1 , which is usually the case, there is a slight increase in efficiency with frequency.³⁶

For high efficiency of energy transfer, it is necessary that:

1) Work coil resistance R_1 be low. The material of the work coil must be of low specific resistance, e.g., copper, and its cross sectional area must be as large as possible.

2) The resistance R_2 of the object be relatively high (of the order of magnitude of the resistance of graphite). This is largely governed by the nature and temperature of the object.

3) Q of the work ($Q_w = \omega L_2 / R_2$) should exceed three. This is governed by the nature of the work piece because Q will be proportional to the effective permeability of the material and to the square root of the size of the object. It is also proportional to the square root of the

frequency, so for small sized objects a high frequency is preferable.

4) M^2/L_2^2 should be large, where M mutual inductance is given by,

$$M = k(L_1 L_2)^{\frac{1}{2}} \quad (13)$$

So, L_1 should be greater than L_2 , and k should be as close to one as possible. To make L_1 large, the work coil should be of large radius and many turns. The radius is determined by the size of the object, and if many turns are used the resistance becomes large. So the problem is to obtain the greatest inductance for a given length of conductor, and this is facilitated by flattening the circular tubing so that a greater number of turns can be wound in a given coil length; but spacing between adjacent turns is limited by peak voltage across the coil. Strips of mica may be inserted between the coils to help prevent flash-over. The coupling factor k is dependent on the number of flux linkages between the coil and the object, so spacing between coil and object should be kept as small as possible consistent with voltage breakdown requirements.³⁶

With a given rf generator, the power that is available for useful dissipation depends upon the unloaded Q value of the tank coil, Q_0 , and the optimum loaded value, Q_{LO} , which should be small (about ten). The useful power is

$$\text{Useful Power} = \frac{(E_b - v_{a \text{ min}}) I_{ac}}{2} \left(\frac{Q_0 - Q_{LO}}{Q_0} \right) \quad (14)$$

where $(E_b - v_{a \text{ min}})$ is the anode voltage swing, and I_{ac} is the peak value of the ac component of the anode current. There are two main methods of

energizing the work coil. In one the work coil is part of the tank coil, Figure 4, while in the other it is coupled inductively to the tank coil, Figure 5. The first circuit is preferable when energy transfer is efficient, and the coupled circuit should be used when the transfer efficiency is poor.³⁵

The overall arrangement of the coupled system can be regarded as two transformers in series, and the main object of its use is to obtain an impedance match between the object and the loaded tank circuit. When the object is not present, there is already a load imposed on the tank circuit by the closed circuit inductively coupled to it. The heat which is dissipated in R_1 and R_2 should be minimized. The Q value of the tank coil should be as high as space limitations permit. To obtain a high coupling coefficient k_1 , the distance between the tank and coupling coils should be a minimum, with the coupling coil mounted inside the tank coil. The ratio of the number of turns of the tank coil to those of the coupling coil may be about ten to one, and it follows that L_2 will be much smaller than L_1 . Since the coupling factor is usually of the order of .7, the mutual inductance M_1 will be much larger than L_2 , or even $L_2 + L_3$. Coupling circuit current is,

$$i_2 = \frac{-j\omega M_1 i_1}{R_2 + j\omega(L_2 + L_3)} \quad (15)$$

Since M_1 is larger than $L_2 + L_3$, the work coil current will be greater than the tank coil current. This advantage was gained at the expense of a reduced value of tank circuit Q before the work is included.

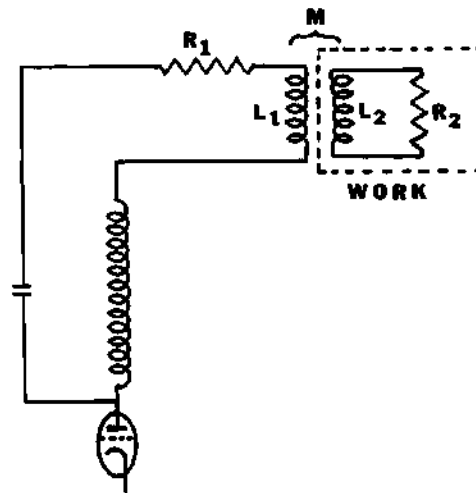


Figure 4. Work Coil is Part of Tank Circuit

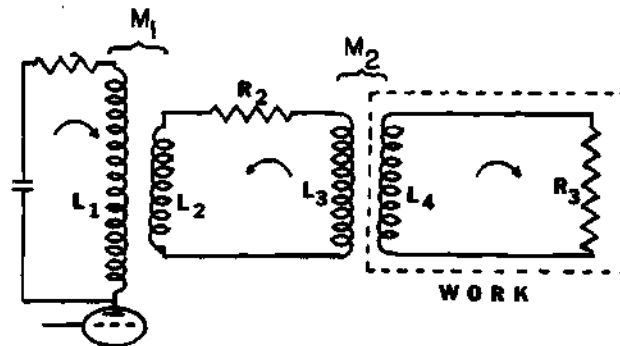


Figure 5. Work Coil is Coupled Inductively to the Tank Coil

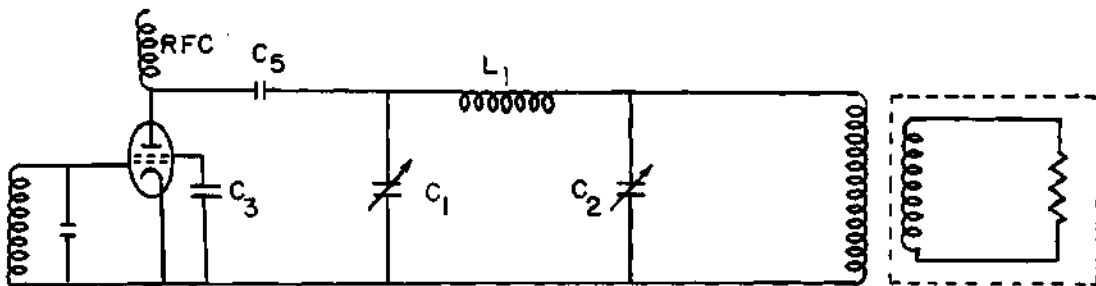


Figure 6. Pi-Matching Network

Q tank circuit alone = $\omega L_1 / R_1$.

$$\text{Q tank circuit + coupling circuit} = \frac{\omega L_1}{R_1 + \left(\frac{M_1}{L_2}\right)^2 R_2} \quad (16)$$

Because of the large value of R_2 , the effective tank coil resistance will be larger than with a direct work coil circuit and less useful power is available from a given generator. The advantage is that difficult to load objects can be made to load to the generator more effectively. These objects will have a Q value lower than three and coupling may be as low as .1. The resistance reflected by the object into the coupling coil circuit is given by,

$$\Delta R_2 = \frac{M_2^2}{L_4^2} \cdot R_3 \cdot \frac{Q_w^2}{Q_w^2 + 1} \quad (17)$$

For very poor work, ΔR_2 may be less than R_3 , but the effect of ΔR_2 on the tank circuit becomes

$$\Delta R_1 = \frac{M_1^2}{(L_2 + L_3)^3} \cdot \Delta R_2 \quad (18)$$

Now $\frac{M_1^2}{(L_2 + L_3)^3}$ is much greater than unity, so we have an enhanced reflected resistance, and thus loading, as compared with that prevailing in a direct work circuit.³⁶

When the object is such that variable loads appear on the generator, it is possible to tune the work circuit by use of a variable capacitor (Figure 8), by use of movable taps on the tank coil (Figure 7), or by use of a pi matching network (Figure 6).³⁶

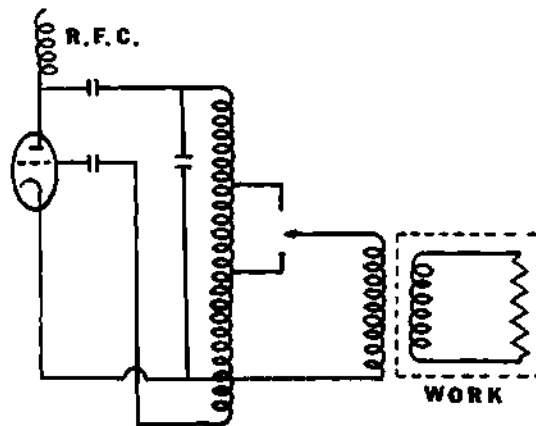


Figure 7. Work Circuit Tuning by Use of Movable Taps on the Tank Coil

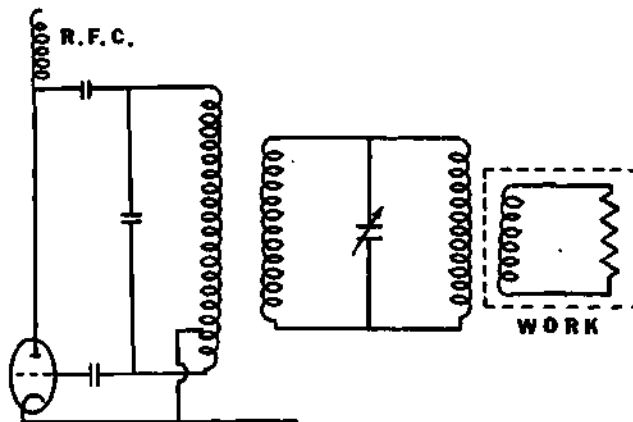


Figure 8. Work Circuit Tuning by Use of a Variable Capacitor

A few simple statements can be made as guidelines concerning the ability of various coils to produce heat in an object. First, the rate of heat generation is proportional to the coil ampere-turns squared. Second, the electrical resistivity of the object governs the rate of I^2R heating in it. Because of the skin effect in high frequency heating (heating is confined to a region close to the surface), and because of the large magnitude of currents employed, forced cooling is customarily used to avoid overheating of the current carrying components. Water cooling is generally used for coils, capacitors, and connecting lines, with forced air cooling used on other circuit components.³⁶

The induction coupled plasma torch is simply a basic induction heating unit with the object being an ionized gas. Added apparatus is necessary to allow for initiation of the plasma.

Practically no power can be coupled from the induction system to a gas if there are no ions present. In order to generate a radio-frequency induction plasma, a small degree of ionization of the gas is required. One procedure to do this is to form a small "pilot" plasma using a conventional dc arc generator. A low power arc discharge is drawn between two electrodes along the centerline of the work coil. The arc is maintained until sufficient coupling of rf power to the arc plasma occurs to produce a sustained rf discharge in the test chamber.³² An alternate procedure is to heat a graphite rod or a refractory wire loop inductively within the rf field and then withdraw it. The heating by conduction of gases in the vicinity of the hot rod lowers the breakdown potential of the gases sufficiently for the plasma to be established in the high rf field present before starting.¹³

Argon is the easiest gas to use for starting and maintaining an rf plasma primarily due to its poor thermal conductivity, low heat capacity at ionization temperatures, and low electron-atom collision cross sections. For these reasons, plasma torches are almost always started with argon and then switched over to mixtures of argon and other gases (such as oxygen, nitrogen, air, hydrogen), or, if enough power is available, entirely to other gases.¹³

Appropriate gas velocity profiles are necessary to stabilize the arc and maintain it within the coil region. If symmetrical flow patterns are not produced the rf arc will move off center and be extinguished or cause wall failure. If the power level or energy density is increased, or diatomic or polyatomic gases used, the preciseness of this flow pattern becomes more important.¹⁶ Once the plasma has formed, it must propagate against the gas flow, otherwise the gas flow will sweep the plasma arc away from the coil and the arc will be extinguished. At low gas velocities, conduction can maintain the plasma, but at higher gas velocities some form of plasma recirculation must occur. The most satisfactory method of arc stabilization and recirculation is vortex stabilization, which is accomplished by feeding the gas into the tube tangentially to cause flow to spiral down the walls creating a low pressure region in the center of the tube. This causes some of the plasma to flow up the tube counter-current to the main flow. The greater the gas flow, the greater the amount of recirculation. The flow along the walls tends to center the arc and to cool the tube walls, thereby permitting operation at higher powers.^{13,16}

Some important parameters affecting the plasma arc are found in Table 1. Also in Table 1 is the resistivity for graphite, steel, and copper. This information is useful when designing "dummy loads" to simulate the plasma when the equipment is tested.

Table 1. Properties of Gases Used in RF Plasmas, and Resistivity of Materials Used in "Dummy" Loads

Material	Resistivity 10% Ionization ohm/cm	Enthalpy 10% Ionization		Thermal Conductivity	Plasma Temperature for 10% Ionization
		kcal/mole	Btu/lb	kw/cm ² K	
Hydrogen	10^{-1}	255	229,000	7×10^{-5}	10,000
Nitrogen	2.5×10^{-2}	400	25,000	2×10^{-5}	11,000
Argon	10^{-2}	90	4,000	$.6 \times 10^{-5}$	12,000
Graphite	10^{-3}	---	---	---	---
Steel	2×10^{-5}	---	---	---	---
Copper	2×10^{-6}	---	---	---	---

It can be shown¹⁶ that the resistance of an induction plasma is given by,

$$r = 2\pi^2 \frac{d}{l} (\mu\rho f)^{\frac{1}{2}} \quad (19)$$

where d = diameter of the plasma, l = length of the plasma, f = frequency, ρ = resistivity of the gas (Table 1), μ = magnetic permeability (one for non-magnetic materials), and r = plasma resistance.

The effect of various gases on arc diameter at constant power is

shown schematically in Figure 9. The argon plasma is relatively large due to the low thermal conductivity and the small amount of energy necessary to ionize the gas (see Table 1) (about 4,000 Btu/lb for 10 percent ionization). A nitrogen plasma is smaller due to its increased thermal conductivity, illustrating the effect known as thermal pinch, and increased ionization energy (about 25,000 Btu/lb for 10 percent ionization). A hydrogen plasma is very difficult to obtain due mainly to the drastic increase in resistivity of the gas.¹⁶

The work coil efficiency can be studied theoretically by considering the case where the work coil has a height, H , large in proportion to its diameter, D , so that a uniform magnetic field is formed in its interior. Assume also that the substance which requires heating is in the form of a long solid cylinder of height, h , large in proportion to its diameter, d (Figure 10). If the frequency, f , of the induced current, i_0 , is high enough, the current flows close to the surface of the cylinder. The magnitude of the current decreases with depth according to the exponential law

$$i = i_0 e^{-x/\epsilon} \quad (20)$$

where x is the distance from the surface and ϵ is the skin of thickness³⁷ where

$$\epsilon = \frac{1}{2\pi} \left(\frac{\rho}{f} \right)^{\frac{1}{2}} \quad (21)$$

If I is the current which circulates in the coil, which has n_1 turns per centimeter, the induced current per centimeter length of load should be $n_1 I$. The load exhibits the properties of a conductor of thickness, ϵ , height, h ,

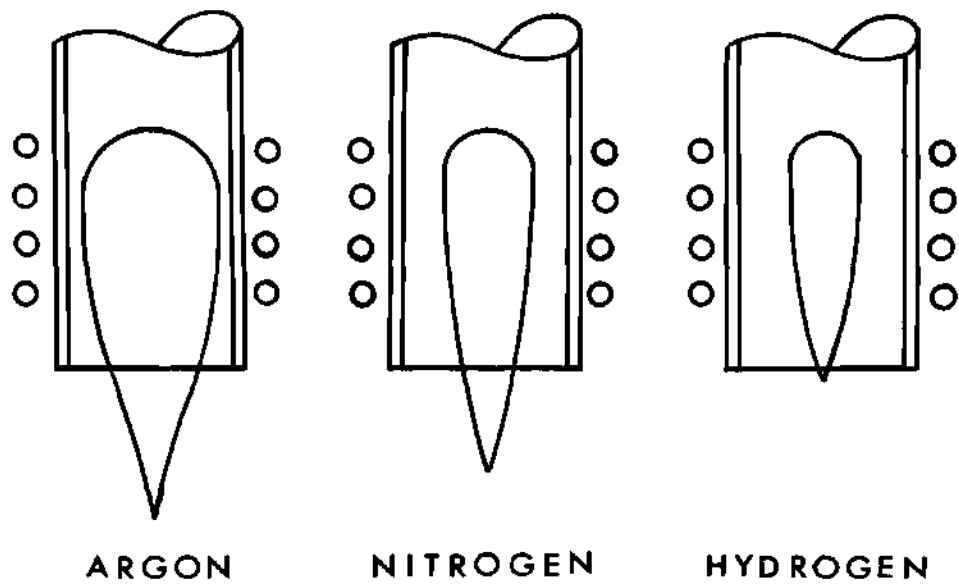


Figure 9. Effect of Gas on Arc Diameter

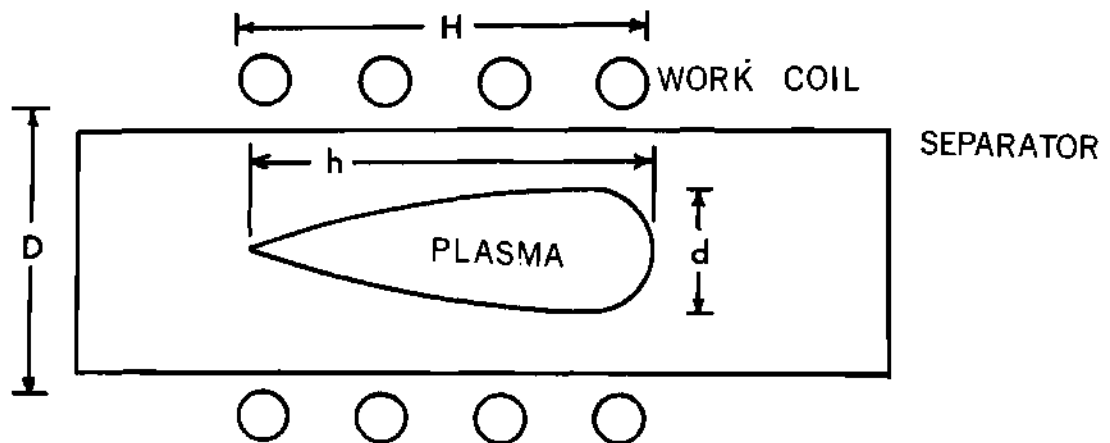


Figure 10. Induction Plasma Torch

and circumference, πd . Its resistance is, therefore,

$$r = \pi \left(\frac{d\rho}{h\epsilon} \right) \quad (22)$$

The total current induced is $n_1 h I$ and the power W_c transformed as heat in the work piece is written

$$W_c = r i^2 = \frac{\pi d \rho h}{\epsilon} n_1^2 I^2 \quad (23)$$

Eliminating skin thickness, the above equation is written

$$W_c = n_1^2 I^2 2\pi^2 dh (\rho f)^{\frac{1}{2}} \quad (24)$$

The energy dissipated as heat in the work coil is found in a similar fashion to be

$$W_e = n_1^2 I^2 \frac{\pi D \rho' H}{\epsilon'} \quad (25)$$

or

$$W_e = n_1^2 I^2 2\pi^2 DH (\rho' f)^{\frac{1}{2}} \quad (26)$$

where ρ' is the resistivity of the work coil and ϵ' is the skin thickness of the work coil. The work coil efficiency can thus be written,³⁷

$$\eta_{wc} = \frac{W_c}{W_c + W_e} = \left[1 + \frac{DH}{dh} \left(\frac{\rho'}{\rho} \right) \right]^{-\frac{1}{2}} \quad (27)$$

In order to sustain a discharge in a gas, a minimum electric field

strength within the plasma must be maintained. The plasma is equivalent to a one turn secondary coil of a transformer. If a current i flows in the plasma, then the minimum voltage around the turn is V_{\min} , where

$$V_{\min} = E_s \pi d \quad (28)$$

and E_s is the required field strength for sustaining the plasma. According to von Engle,³⁸ this field strength is a function of current, i , and over a certain range the following approximate empirical relationship holds

$$i = J_o / E_s^4 \quad (29)$$

where J_o is a constant.

The resistance, r , of the gas load can be written

$$r = \frac{V_{\min}}{i} = \frac{E_s^5 \pi d}{J_o} \quad (30)$$

but the resistance of the gas load can also be expressed in terms of the skin thickness, ϵ ,

$$r = \frac{\pi d \rho}{\ell} = 2\pi^2 \frac{d}{\ell} \rho^{\frac{1}{2}} f^{\frac{1}{2}} \quad (31)$$

The resistivity of the gas load, ρ , is a function of the sustaining voltage and the induced current,³⁸ according to the following relationship.

$$\rho \approx \frac{10E_s}{i} = \frac{10E_s^5}{J_o} \quad (32)$$

Eliminating r from the above equations

$$r = 2\pi^2 \frac{d}{\ell} 10 \frac{E_s^{\frac{5}{2}} f^{\frac{1}{2}}}{J_o^{\frac{1}{2}}} = \frac{E_s^5 \pi d}{J_o} \quad (33)$$

The power required to sustain the discharge can now be written¹⁴

$$W_{\text{req}} = V_{\text{min}} i = \frac{E_s \pi d J_o}{E_s^4} \quad (34)$$

Therefore

$$W_{\text{req}} = \frac{\pi}{(2\pi)^{\frac{6}{5}}} \cdot \frac{J_o^{\frac{6}{5}}}{10^{\frac{3}{5}}} \cdot \frac{d \ell^{\frac{6}{5}}}{f^{\frac{6}{5}}} \quad (35)$$

Employing absolute cgs units, for argon $J_o = 6.25 \times 10^{35}$, and for hydrogen $J_o = 2.56 \times 10^{39}$.³⁸ From the above relationship, the power required to sustain an argon plasma of dimensions $d = 2.5$ cm, and $\ell = 5^{\cdot 8}$ at a frequency of 4×10^6 hertz is 2.43 kW. The power required to sustain a similar hydrogen plasma is 69 kW. Therefore, it requires 28 times the power to sustain a hydrogen discharge as it does to sustain an argon discharge.¹⁴

High Power Amplifiers for Induction Plasma Generation

The previous section described the production of plasmas using high frequency induction heating. The two primary sources of high frequency power are the motor-generator set and the vacuum tube amplifier (or oscillator). The vacuum tube amplifier is used in this research to produce tungsten seeded hydrogen plasmas.

In the vacuum tube the electric current flows through a vacuum. This is only possible when free electrons are introduced into the vacuum. In an evacuated space, free electrons are attracted to positively charged objects and repelled by negatively charged objects. Electrons are introduced into the vacuum by heating a thoriated tungsten element to incandescence in the vacuum. Thorium is added to the tungsten in the process of making tungsten wire. About 1.5 percent thorium is added in the form of thorium dioxide (ThO_2). By proper processing during vacuum pumping of the tube envelope, the metallic thorium is brought to the surface of the filament wire, and emission increases about 1000 times. At a typical operating temperature of 1900°K , a thoriated-tungsten filament will produce a specific peak emission of about 70 to 100 milliamperes per watt of filament heating power. The electrons emitted from the cathode tend to form a cloud or space charge about the cathode preventing emission of any more electrons.^{39,40} If a positively charged conductor is also placed in this vacuum, the electrons are attracted and current flows through the device. If this second electrode, commonly known as the plate, is negatively charged, no current flows. This two element tube diode allows current to flow in only one direction, and, if an alternating current is applied to the plate, current will flow only during the positive half cycle, and the ac current is rectified to an intermittent direct current.³⁹

A third tube element, of control grid, can be inserted between the cathode and plate to control the effect of the space charge. If this element is given a positive voltage with respect to the cathode, the space charge will tend to be neutralized, allowing increased plate current. The

grid will also attract electrons and grid current will flow. It is desired that most of the current flow in the tube be to the plate so the grid is made in the form of a wire mesh of spiral which allows electrons to go through the open spaces in the grid to reach the plate. If the grid is made negative with respect to the cathode, the negative charge on the grid will add to the space charge and reduce the number of electrons that can reach the plate at any selected plate voltage. The grid thus can act as a valve to control the flow of plate current, having a much greater effect on plate current than the plate voltage by being located physically close to the cathode.³⁹

Since a small voltage change on the grid has the effect of a large voltage change on the plate, amplification is possible. The amplified output power is not obtained from the tube itself, but from the voltage source connected between the plate and cathode. The tube controls the power from this source by means of the control grid, changing it to the desired form. An impedance must be connected to the plate or output circuit to act as a load.⁴⁰

Some important tube characteristics are: 1) the plate resistance, which is the ac resistance of the path from cathode to plate, for a given grid voltage it is the quotient of a small change in plate voltage divided by the resultant change in plate current; 2) the amplification factor, which is defined as the ratio of the change in plate voltage to the change in grid voltage to effect equal changes in plate current; 3) the transconductance, or mutual conductance, which is the change in plate current divided by the change in grid voltage that caused the change.⁴⁰

The amplifier plate current flows during the entire excitation cycle (360 degrees) for the class A amplifier. Class A amplifiers are operated so that the output wave forms of the plate current are practically the same as those of the exciting grid voltage. Class B amplifiers are a type which is operated with a negative grid bias approximately equal to the plate current cut-off, so that the plate current is almost zero when the grid excitation is removed. When the grid signal goes positive, plate current flows. Class B operation is characterized by larger power output and higher efficiency than class A. A class C amplifier is one in which high power output is the primary consideration. The grid is negatively biased to a point considerably beyond the cut-off point so that no plate current flows when there is no grid excitation. The grid excitation voltage is large and is often sufficient to cause the plate current to reach saturation on the positive swings. Plate current is allowed to flow during less than 180° of the operating cycle. The advantage of class C operation is that plate efficiency is increased to 70-80 percent.⁴⁰

Each pair of elements in a tube forms a small capacitor. In a triode there are three such capacitances; that between the grid and cathode, that between the grid and plate, and that between the plate and cathode. The capacitances are small, of the order of picofarads, but they frequently have a very pronounced effect on the operation of an amplifier circuit. The grid to plate capacitance can be reduced to a negligible value by inserting a second grid between the control grid and the plate. This second grid, called the screen grid, acts as an electrostatic shield to prevent capacitive coupling between the control grid and the plate. The screen

grid, which is in the form of a coarse screen, is operated at a positive potential to help attract electrons to the plate. In traveling toward the screen, the electrons acquire a higher velocity so that most of them pass between the screen wires and then are attracted to the plate. A small fraction strikes, with the result that a current also flows in the screen grid circuit.³⁹ The screen must be connected to the cathode through a circuit that has low impedance at the frequency being amplified. A bypass capacitor from screen to cathode is generally used.⁴¹

In designing equipment using power grid tubes, electron emission from the control and screen grids must be considered. The grid materials will emit electrons as a primary emitter if the work function of the grid surface material is low enough. Primary grid emission is usually quite low in a thoriated tungsten filament type tube, because grid materials can be used which have high work functions. Another type of grid emission is secondary emission from the screen grid. The screen grid is operated at a relatively low potential in order to accelerate the electrons emitted from the cathode. As the electrons pass through the screen grid on the way to the plate some are intercepted by the screen grid. As they strike the screen grid electrons, called secondary electrons, are emitted from the screen. Some of these secondary electrons are attracted back to the screen. Most of those which are emitted into the region between the screen grid and the plate are attracted to the plate. The result is an electron flow from screen to anode. The control grid is not in this region and thus has virtually no control over the number of secondary electrons flowing. It is possible that, during any part of the operating cycle

of the tube, more electrons will leave the screen grid than will arrive, in which case a dc current meter can be used to indicate a reverse electron flow. On the other hand, if on the average more electrons arrive than leave the screen grid, the dc screen meter will indicate a forward current flow. Reverse screen current is quite normal for high power tetrode tubes, so the circuit must be designed to provide a low impedance path for this flow.⁴¹ If the screen power supply impedance is too high in the reverse current direction, the screen voltage will tend to increase to the plate voltage. Most regulated power supplies have low impedance in the forward direction only. As the screen voltage rises the secondary and plate currents increase and the tube is in a runaway condition,⁴⁰ that is, the current increases until tube failure occurs, or overcurrent protection devices react.

The power supply requirements for a triode are straightforward. The necessary degree of regulation and permissible ripple depend upon the requirements of the amplifier system. Linear rf amplifiers require good plate power supply regulation to prevent the plate voltage from dropping during the time the plate is conducting current. This tendency for the voltage to drop will result in distortion of the output signal. The dc high voltage for high power rf amplifiers is usually obtained from rectifier type power supplies.

The negative control grid voltage can be obtained either from a separate dc power supply or by using a resistor connected in series with the cathode. The direction of plate current flow is such that the end of the resistor nearest the cathode is positive. The voltage drop across the

resistor, therefore, results in a negative voltage on the grid. This negative bias is obtained from the dc component of the plate current, whereas a capacitor provides a low impedance path for the rf component. The magnitude of the negative grid bias is the product of the dc component of the plate current and of the bias resistor. Another method for obtaining control grid bias utilizes a resistor in the grid circuit to develop a negative bias whenever grid current flows. This resistor must also be bypassed by a capacitor to provide a low impedance path for the rf component of the grid current. The type of bias which depends on the flow of current in the plate or grid circuits is known as an operating bias. A fixed negative control grid voltage is often used to obtain a form of protective bias which helps to prevent the tube from being severely damaged during fault conditions. Many amplifiers are designed using both protective and operating bias.^{39,40}

Voltage for the screen grid of a low power tetrode can be readily provided by the power supply used for the plate of the tube. In this case a series resistor, or potential dividing resistor, is chosen so that when the intended screen current is flowing the voltage drop across the resistor provides the desired screen voltage. Use of a potential dividing resistor is the preferred technique for those tubes with significant secondary screen emission. The screen voltage can also be provided by a low voltage supply, which can often be an already available source in the system. A combination is sometimes used with a dropping resistor used in conjunction with a low voltage or intermediate voltage supply. Frequently a combination of series resistor voltage sources and power supplies

can be chosen so that the rated screen dissipation will not be exceeded regardless of the variations in screen current. With a fixed screen supply there are advantages in using an appreciable fixed grid bias so as to provide protection against loss of excitation. If the screen voltage is taken through a dropping resistor from the plate supply, there is usually little point in using a fixed grid bias because an unreasonably large bias would be required to protect the tube if the excitation failed. When a screen dropping resistor is used, most of the bias is normally supplied through a grid resistor and other means are used for tube protection. Under operating conditions with normal screen voltage, the cutoff bias is low. When a stage loses excitation and runs statically, the screen current falls close to zero. If the screen voltage is obtained through a simple dropping resistor from the plate supply, the screen voltage will then approach the full plate voltage. The grid bias required is much greater than the bias desired under normal operating conditions because the cutoff bias required is proportional to the screen voltage.^{39,40}

A portion of the high frequency power in the plate circuit of an amplifier can be fed back into the grid circuit to provide feedback. If the power from the plate circuit is returned to the grid circuit 180° out of phase with the signal acting on the grid, the feedback is considered to be negative, or degenerative. If this power is fed back in phase with the signal, the feedback is called positive, or regenerative. With negative feedback, the amplitude of the signal acting between the grid and cathode is reduced and the result is a decrease in amplification. When properly utilized, the greater the negative feedback, the more independent

tube characteristics and circuit conditions become of the amplification. This tends to make the frequency response characteristics of the amplifier flat. This is not a necessary characteristic for amplifiers used in induction heating applications.⁴⁰

Positive feedback, which increases voltage amplification, can be useful in induction heaters. The amplification tends to be greatest at one frequency, and less drive is necessary. If enough energy is fed back, a self sustaining oscillation, in which energy at essentially one frequency is generated by the tube itself, will be set up. In such a case, all the signal voltage on the grid can be supplied from the plate circuit, no external signal is needed because any small irregularity in the plate current will be amplified and thus give the oscillation an opportunity to build up. Positive feedback finds a major application in such oscillators.⁴⁰ Oscillations normally occur at only one frequency, and a desired oscillation frequency can be obtained by using a resonant circuit tuned to that frequency.

Rf power amplifiers are often operated under class C conditions, with the main objective being to deliver as much power as possible into a load without exceeding the tube ratings. The load resistance R may be in the form of a transmission line, the grid circuit of another amplifier, or some type of matching network to a reactive load. A further objective is to minimize harmonic energy which is a product of the rf wave form distortion present in all class C amplifiers. In attaining these objectives, the Q of the tank circuit is of importance. The Q of a parallel resonant circuit loaded by a resistive impedance is the parallel load resistance

divided by the reactance of one leg of the parallel resonant circuit. The effective Q of a circuit loaded by a parallel resistance becomes higher when the reactances are decreased. A circuit loaded with a relatively low resistance must have low reactance elements (large capacitance and small inductance) to have reasonably high Q . With respect to all of these factors, a tank Q of 10 to 20 is usually considered optimum. A significantly lower Q will result in less efficient operation of the amplifier tube, greater harmonic output, and greater difficulty in coupling inductively to a load. A significantly higher Q will result in higher tank currents with increased power losses in the tank coil.³⁹

In designing the output circuit of an amplifier, it is necessary to specify the resonant load impedance of the tube, the loaded Q of the circuit, and the desired output impedance of the network. The resonant plate load impedance of the tube is determined by dividing the plate peak rf voltage swing by the plate peak fundamental rf current.⁴⁰

A pi-section tank circuit may be used in coupling to a resistive or reactive load. Within reasonable limits, a properly set pi matching network can transform any resistive load into any desired resistance, with the reactance of the load, provided it is relatively small, being eliminated by small changes in the second capacitive leg of the network (Figure 6). Charts are available which give values of reactance for C_1 , C_2 , and L_1 for practically all practical applications.^{40,42}

When the load R is located for convenience at some distance from the amplifier, or when maximum harmonic reduction is desired, it is normal to transmit the power to the load through a low impedance coaxial cable.

The shielded construction of the cable prevents radiation and makes it possible to install the line in any convenient manner without danger of unwanted coupling to other circuits. By adjusting the effective load resistance and using a matching network to match the impedance of the cable, losses in the cable can be reduced and the coupling adjustments at the amplifier made independent of cable length. The amplifier can be coupled to the transmission line by using a coupled circuit tuned to the operating frequency. This circuit provides additional selectivity and aids in the suppression of spurious radiations. Properly adjusted, the line characteristics do not change appreciably with frequency, and the input impedance of the line will be essentially resistive and equal to the total impedance of the line. With a coaxial cable, a circuit of reasonable Q can be obtained with practicable values of inductance and capacitance connected in series with the line's input terminals. The Q of the coupling circuit often may be as low as two before difficulty is encountered in getting adequate coupling to a properly designed tank circuit. Power transfer is obtained with less coupling if the line input is tuned to resonance.³⁹

In adjusting a tetrode rf amplifier for proper excitation and loading, the procedure is different depending on whether the screen voltage is taken from a fixed supply or a dropping resistor supply. In the case where both the screen bias and grid bias are provided by fixed sources with good regulation, the plate current is almost entirely controlled by the rf excitation. First the excitation is varied until the desired plate current is reached. The loading is then varied until the maximum power

output is obtained. Following these adjustments, the excitation is then decreased along with the loading until the desired control grid and screen grid currents are obtained. In the case of an rf amplifier where both the screen and grid bias are provided by sources with poor regulation, the stage will tune very much like a triode rf power amplifier. The plate current is adjusted principally by varying the loading, and the excitation is trimmed to give the desired control grid current. In this case, the screen current will be almost entirely set by the choice of the dropping resistor. Excitation and loading will vary the screen voltage considerably and these should be trimmed to give about normal screen voltage.^{43,44}

Typical tetrode operating values for a particular value of screen voltage are given on the published technical data sheet. The screen voltage is not critical for most applications and the value used has been chosen as a convenient value consistent with low driving power and reasonable screen dissipation. If lower values of screen voltage are used, more driving voltage is required. Thus, high power gain can be achieved provided the circuit has adequate stability. Care should be observed that the screen dissipation limit is not exceeded. The value of screen voltage can be chosen to suit available power supplies or amplifier conditions.⁴⁰

If isolation of the output and input circuits is to be maintained, some thought must be given to the location of the component parts of the amplifier. All component parts of the grid or input circuit and any earlier stages must be kept out of the plate circuit compartment. Simi-

larly, plate circuit parts must be kept out of the input compartment. It must be noted, however, that in the case of the tetrode the screen lead of the tube and connections via the tube socket are common to both the output and input resonant circuits. Due to the plate to screen capacitance of a tetrode, the rf plate voltage (developed in the output circuit) causes an rf current to flow out the screen lead to the chassis. Similarly, due to the grid to screen capacitance of the tube, the rf voltage in the input circuit will cause an rf current to flow in this same screen lead to the chassis. The mutual coupling from the screen lead to the input resonant circuit is a possible source of trouble.⁴⁵

Some of the interconnecting lead wires close to the tube should be designed with extremely low inductance to minimize the formation of possible VHF parasitic circuits. The lead lengths of radio-frequency circuits involving the fundamental can be fairly long, the length depending on the fundamental frequency. All of the dc and control circuit wires can be quite long if properly filtered and arranged away from the active rf circuits. Filament and screen by-pass leads, suppressor by-pass leads, and leads from the grid and the plate to the tuning capacitor of the rf circuit and return should preferably have quite low inductance. For a lead to have low inductance, it must have a large surface and be short in length, as in a strap or a ribbon. Low inductance by-pass capacitors should be used in by-passing the filament. It is good practice to place a capacitor directly between the filament socket terminals. If the circuit permits, filament should be strapped directly to the chassis, and if not, a second by-pass capacitor from one terminal to the chassis can be provided. Low inductance leads are generally used for screen grid

terminal connections. For all frequencies, it is normal to route the screen by-pass capacitors directly from the screen to one filament terminal.^{40,41}

Most power grid tubes are designed to stand considerable abuse. For instance, the excess anode dissipation resulting from detuning the plate circuit of the tube will have no ill effects if not applied for periods of time sufficient to overheat the envelope and the seal structure. Similarly, the control and screen grids will stand some excess dissipation. The maximum dissipation for each grid indicated on the data sheet should not be exceeded, except for time intervals of less than one second. The maximum dissipation rating for each grid structure is usually considerably above typical values used for maximum output so that ample operating leeway is provided. The time of duration of overloads on a grid structure is necessarily short because of the small heat storage capacity of the wires. Furthermore, grid temperatures cannot be seen, so no visual warning of accidental overload is apparent.⁴⁰

The type and degree of protection required in an rf amplifier against circuit failure will vary with the type of screen and grid voltage supply. Table 2 is a chart indicating the location of suitable relays which should act to remove the principal supply voltage from the amplifier to prevent damage to the tube.

For screen voltage taken through a dropping resistor from the plate supply, a plate relay provides almost universal protection. For a fixed screen supply, a screen relay provides protection in most cases. For protection against excess loading and consequent high plate dissipation, a

Table 2. Necessary Tube Protection (Ref. 40)

CIRCUIT FAILURE	FIXED SCREEN SUPPLY		SCREEN VOLTAGE THROUGH DROPPING RESISTOR	
	FIXED GRID BIAS	RESISTOR GRID BIAS	FIXED GRID BIAS	RESISTOR GRID BIAS
Loss of Excitation	No Pro- tection Required	Plate Current Relay	Plate Current Relay	Plate Current Relay or Screen Control Circuit
Loss of Loading	Screen Current Relay	Screen Current Relay	Grid Current Relay	Nothing Required
Excess Loading	Screen Under- current Relay	Screen Under- current Relay	Plate Current Relay	Plate Current Relay
Failure of Plate Supply	Screen Current Relay	Screen Current Relay	Grid Current Relay	Nothing Required
Failure of Screen Supply	Grid Current Relay	Nothing Required	----	----
Failure of Grid Bias Supply	Plate Current Relay or Screen Current Relay	----	Plate Current Relay Grid Current Relay	----

screen undercurrent relay may also be used. The plate, screen, and bias voltages may be applied simultaneously to a tetrode. In a grid driven amplifier, the grid bias and excitation can usually be applied alone to the tube, especially if a grid leak resistor is used. Plate voltage can be applied to the tetrode before the screen voltage with or without excitation to the control grid. Screen voltage is never applied before plate voltage. The only exception would be when the tube is cut off so that no space current (screen or plate current) will flow, or when the excitation and screen voltage are low. If screen voltage is applied before the plate voltage, a screen current can flow; the maximum allowable screen dissipation will almost always be exceeded and tube damage will result.^{40,45}

The basic steps for checking self-oscillation of an rf amplifier are:

(a) The amplifier is operated without rf excitation and without fixed grid bias, with light loading and with low voltages applied to the plate and to the screen. The voltage applied should be high enough to develop full plate dissipation, and a grid leak bias should be applied. The rf circuits should be tuned off resonance to see if self-oscillation of the amplifier can be initiated. The indication of any grid current means that self-oscillation is present.

(b) The frequency of the self-oscillation, if present, is determined. A simple neon bulb will indicate whether the frequency of oscillation is high or low. The lower the frequency, the more orange will be the glow. A purple color indicates VHF or UHF oscillation. An oscilloscope can then be used to determine the exact frequency.

(c) After the frequency of oscillation is measured, it is necessary to identify the circuit supporting the oscillation, and the circuit must then be altered without disturbing the performance of the amplifier at the normal frequency of the amplifier.⁴⁵

Self-oscillation in rf power amplifiers usually falls in the following three classes: (a) Oscillation in the VHF range from about 40 MHz to 200 MHz, (b) Self-oscillation at the fundamental frequency of the amplifier, and (c) Oscillation at a low radio frequency below the normal frequency of the amplifier. Low frequency oscillation in an amplifier usually involves the rf chokes, especially when chokes are used in both the output and input circuits. Oscillation near the fundamental frequency involves the normal resonant circuits and indicates improper neutralizing of the rf amplifier, which will be discussed later. When a parasitic self-oscillation is found at a very high frequency, the interconnecting leads of the tube, the tuning capacitor and the by pass capacitors are involved. Placing a small coil and resistor in the plate lead between the plate of the tube and the tank circuit usually eliminates the VHF parasitic oscillation. The resistor-coil combination is usually made up of a non-inductive resistor of about 25 to 100 ohms, shunted by three or four turns of approximately one-half inch diameter, frequently wound right around the resistor. In some cases it is necessary to use such a suppressor in both the plate and grid leads. The resistor-coil combination operates on the principle that the resistor loads the VHF circuit but is shunted by the coil for the lower fundamental frequency.^{40,43,45}

As previously mentioned, oscillation near the fundamental frequency

involves the normal resonant circuits, with feedback occurring due to the interelectrode capacitances of the tube. When the interelectrode capacitance between the input and output circuits is cancelled, the tube is completely neutralized. Cancellation of these impedances between the input and output theoretically prevents oscillation. As the gain of the amplifier increases, the need to cancel feedback voltage becomes much more necessary. For this reason, it is often necessary to neutralize tetrodes, despite the fact that the screen grid reduces interelectrode capacitance. At frequencies below the VHF region, neutralization usually employs a capacitance bridge circuit, as shown in Figure 11, to balance out the feedback due to the residual plate to screen capacitance. This assumed that the screen is well by-passed to ground and so provides the expected screening action. In this method the input resonant circuit is taken slightly off ground by making the input circuit by-pass capacitor, C , somewhat smaller than usual. The voltage to ground across the capacitor, C , is out of phase with the grid voltage and can be fed back to the plate to provide neutralization. In this case the neutralizing capacitor, C_n , is considerably larger than the grid-to-plate capacitor. The basic circuit can be redrawn as a capacitance bridge showing clearly the grid neutralization circuit, Figure 12. Balance is obtained when

$$\frac{C_n}{C} = \frac{C_{gp}}{C_{gf}} \quad (36)$$

where C_{gp} is the feedback capacitance grid-to-plate of the tetrode, and C_{gf} is the total input capacitance, including tube and stray capacitance.^{39,40}

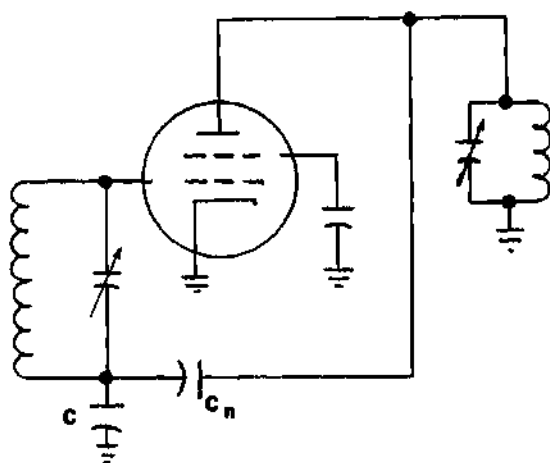


Figure 11. Single Ended Grid Neutralization

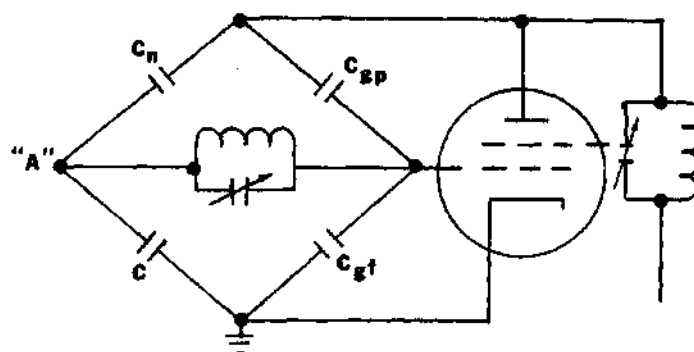


Figure 12. The Basic Circuit of Single Ended Grid Neutralization Showing Interelectrode Capacitances (Reference 39)

The first step in the neutralization procedure is to break the dc connections of the plate voltage and screen voltage leaving the rf circuits intact. If the dc current path is not broken, some current can flow in either one of these circuits even though the voltages are zero. The presence of this current causes the amplifier to work in the normal manner, generating rf power in the plate circuit. It will then be incorrect to adjust for zero power in the plate circuit. Sufficient rf grid drive must be applied to provide some grid current or to cause a sensitive rf meter coupled to the plate to give an indication of feed through power. When the plate circuit is tuned through resonance, the grid current will dip when the circuit is out of neutralization or the rf meter will peak. The neutralization adjustments are made until the indication is minimum. When the amplifier is operating and the plate circuit is tuned through resonance, the minimum plate current, maximum control grid current, and maximum dc screen current should occur simultaneously.^{40,43,45}

CHAPTER IV

EQUIPMENT AND INSTRUMENTATION

The equipment is designed to produce high temperature hydrogen plasmas seeded with metallic particles. The plasma, seeded with sub-micron metallic particles, simulates the propellant of a gaseous core nuclear reactor. The plasma torch, which couples the radio frequency energy to the plasma and contains the plasma, is constructed to allow for the measurement of the transmission of radiant energy through the plasma and to permit spectral observations of the plasma. One major objective of producing seeded hydrogen plasmas contained in such a plasma torch is to measure the opacity of the plasma as a function of radial distance from the center of the plasma. This is accomplished by scanning the seeded hydrogen plasma with a helium-neon laser and measuring the transmitted intensity as a function of axial distance from the center of the plasma. The transmitted intensity is then measured with no plasma or seed present, and the ratio of the two intensities gives the attenuation. This attenuation, which is a function of axial distance, is changed to a radial function by an Abel inversion technique. Such macroscopic properties as seed density, plasma size, and plasma radiant heat output are also measured.

Radio Frequency Plasma Generator

There are four types of high frequency induction heaters which are practical for use in producing seeded hydrogen plasmas. These are the grid driven rf triode amplifier, the grid driven rf tetrode amplifier, the rf triode oscillator, and the rf tetrode oscillator. These are the only practical types for several reasons. As shown in the section on induction heating theory, the minimum power required to sustain a plasma is an inverse function of frequency. For seeded hydrogen plasmas to be sustained with reasonable power levels (i.e., less than 500 kW), high frequencies are necessary. This means an electronic generator (oscillator or amplifier) is required. Since the power requirements are large even in the high frequency range (2-30 MHz), the tube element in the electronic generator must be either a triode or tetrode, as these are the only types of tubes normally available capable of handling input powers of 100 kW necessary to produce hydrogen plasmas.

The radio frequency generator which has been developed to produce seeded hydrogen plasmas is a high power vacuum tube amplifier which operates at input power levels of 125 kW with a single air-cooled Eimac 4CX-35000C tetrode as the tube element. Output power available is about 85 kW. The plasma generator is designed to operate at four MHz, but by appropriate changes in certain components and amplifier retuning, operation from 2-30 MHz could be achieved.

A tetrode amplifier design was chosen rather than one of the three other choices for two basic reasons. First, a tetrode was selected due to the low drive requirements of the tetrode, as discussed in the section

on rf amplifiers for plasma generation. A triode producing 85 kW output would require an rf driver producing in excess of 10 kW, while a similar tetrode would require less than one kW of drive. Had the oscillator been selected, the need for a driver stage would have been eliminated, but it was decided to avoid using an oscillator because of the experimental and unstable nature of the plasma load and because of the basic instabilities associated with oscillators. The amplifier would be more easily controlled by the plasma generator operator than would the oscillator.

The plasma generator consists of five more or less separate components shown in Figure 13; the rf driver stage, the plate dc power supply, the final amplifier stage utilizing the Eimac 4CX-35000C, the plasma torch and the monitor and control system. The plate dc power supply is located on a fenced-in concrete pad adjacent to the building containing the electronics of the amplifier. The driver, amplifier, and plasma torch are located in a copper shielded room to prevent spurious radiations of the amplifier from interfering with radio communication in the Atlanta area. All control and monitoring devices utilized in amplifier start up and operation are located in this shielded room. This enables the operator to be physically close to the amplifier, enabling him to better detect equipment failures not noted by the protection and monitor system.

The essential elements of the dc high voltage supply, as shown in Figure 14, are the two unitized rectifiers manufactured by Magnatran, Inc. and supplied to Georgia Tech by the Sperry Rand Corporation. Each unitized rectifier is a pair of three-phase full-wave mercury vapor rectifiers, Figure 15, which can be connected either in series, to produce

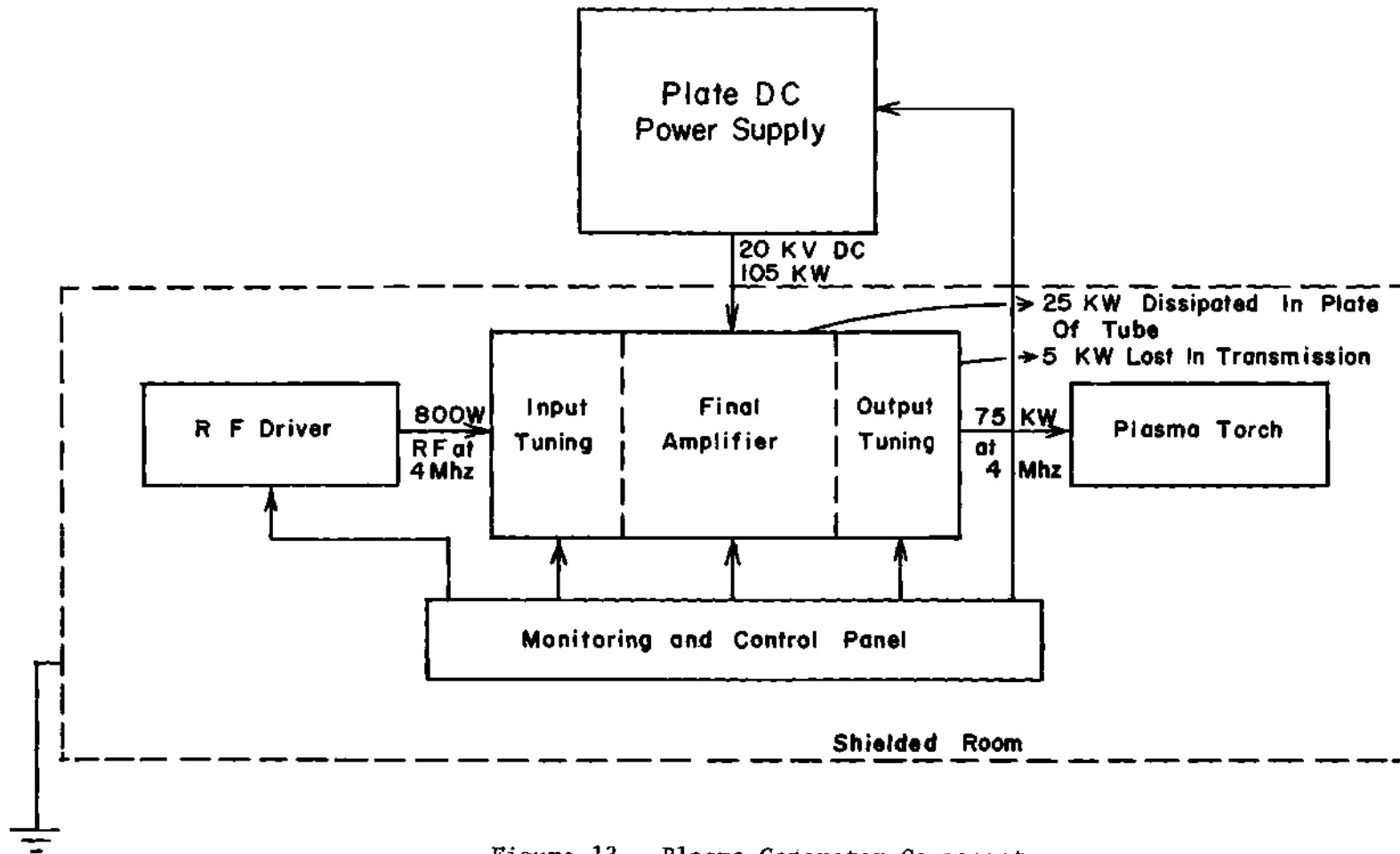


Figure 13. Plasma Generator Components

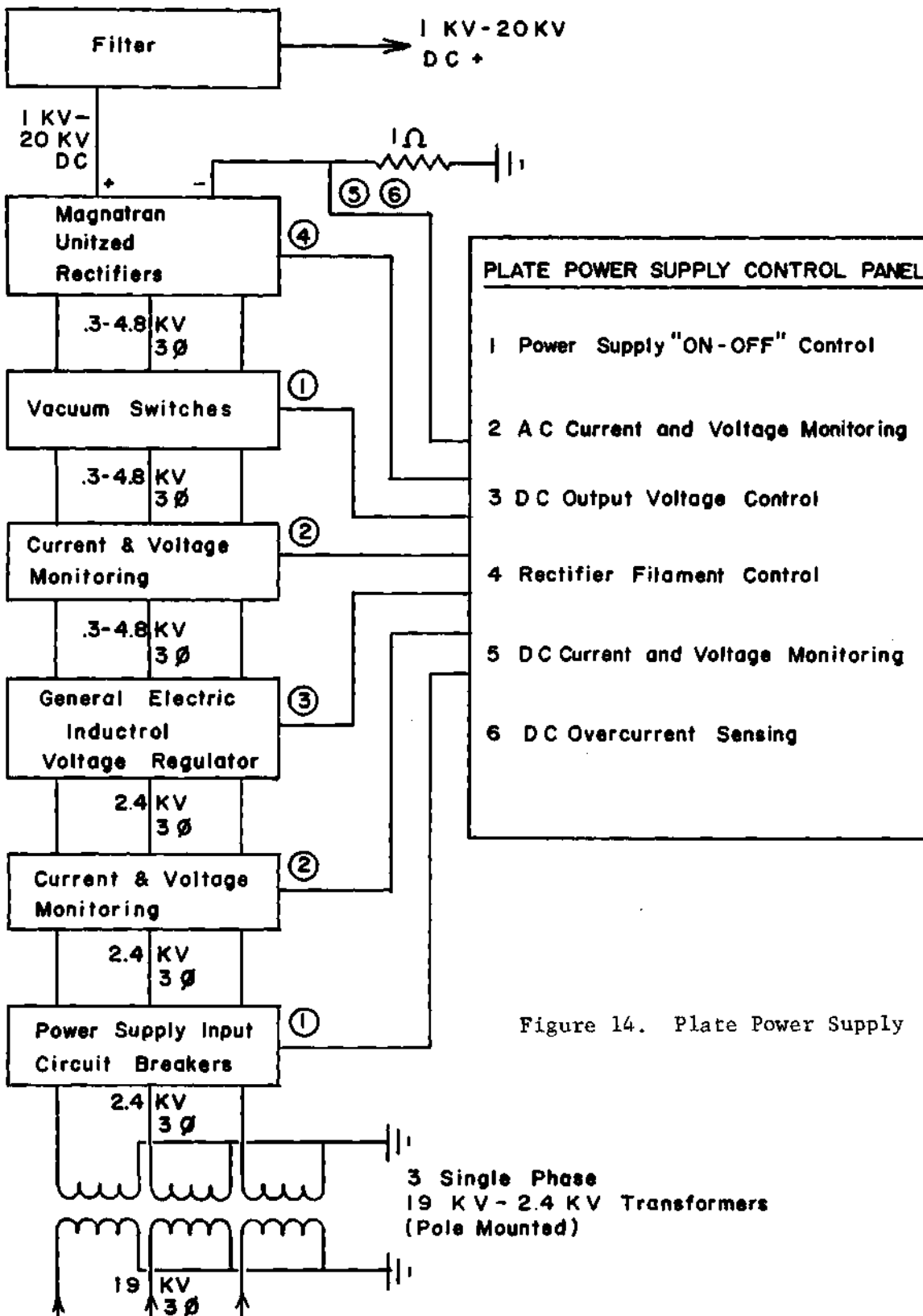


Figure 14. Plate Power Supply

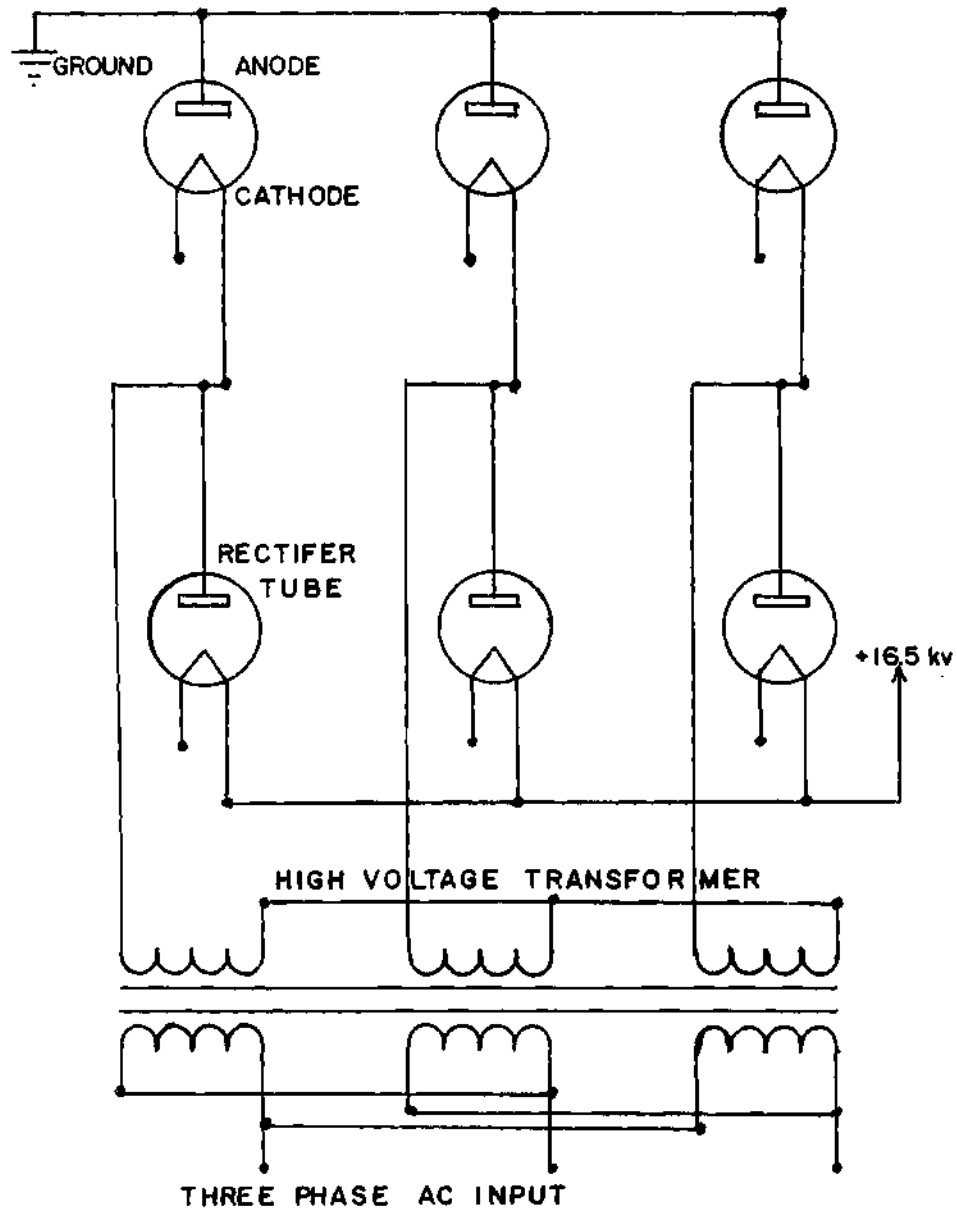


Figure 15. Three-Phase Full-Wave Rectifier

33 kv dc at 6.5 amps, or in parallel, to produce 16.5 kv dc at 13 amps. The high voltage power supply was wired to deliver 16.5 kv maximum, since the final amplifier tube utilized, the Eimac 4CX-35000C, is designed for a maximum plate voltage of 20 kv, and 19 kv is the recommended typical operating value. Operating at a lower voltage would lessen the possibility of damaging the tube during fault conditions.

The three phase ac power for the unitized rectifiers is supplied by a General Electric Inductrol Voltage Regulator, which has a variable output of from 300 to 4800 volts three phase, and requires a 2400 volt three phase input. The inductrol voltage regulator maintains a constant voltage under varying load conditions and allows for remote controlled variations in plate voltage. This varying plate voltage is essential for the expected variations in operating parameters in plasma operation.

The 2400 volt three phase ac input of the inductrol voltage regulator is obtained from the Georgia Tech 19 kv power line, transformed by three 19 kv to 2.4 kv single phase transformers donated by the Georgia Power Company.

The input power to the plate power supply is controlled by a General Electric Circuit Breaker which has current limiting features to protect the Georgia Tech power line from any faults occurring in the plate power supply. The three phase supply is monitored for current and voltage for each phase, both before and after the inductrol voltage regulator. Output switching of the voltage regulator is controlled by three vacuum switches.

The dc output of the rectifiers has about a six percent ripple,

which is excessive, so it is filtered by a choke input filter system consisting of a ten henry inductor and a 24 microfarad capacitor bank. The entire power supply is capable of supplying 428 kW high voltage dc.

All controls and monitor devices for the plate power supply are located on the plate power supply control panel in the shielded amplifier room. From this control panel the operator controls the General Electric power supply input circuit breaker, the vacuum switches which activate ac power to the rectifiers, the General Electric Inductrol Voltage Regulator output, and the rectifier filament voltage. The operator also monitors the three phase input and output voltages and currents of the voltage regulator, and the dc output of the Magnatran unitized rectifiers.

The radio frequency driver for the final amplifier is made up primarily of amateur radio equipment. A Heathkit transmitter, model DX-100 serves as oscillator and driver for a Henry 2-K linear amplifier. The Heathkit DX-100 delivers from 120 to 140 watts continuous wave into a 50 to 600 ohm nonreactive load. The frequency of the Heathkit DX-100 is set by a variable frequency oscillator. This oscillator is variable in certain bands from 2-30 MHz. After the desired frequency is selected (four MHz for the plasma generator), the Heathkit DX-100 is tuned by increasing the grid drive and maximizing the grid current of the amplifier stage of the DX-100. The plate loading is then increased and the plate circuit tuned by minimizing the plate current. Power output of the DX-100 is controlled by varying the amplifier plate voltage. The output of the DX-100 is connected to the input of the Henry 2-K by a short length of coaxial cable.

The Henry 2-K utilizes a pair of Eimac 3-500 triodes operated in parallel and delivers up to 1000 watts CW, requiring a drive of from 60-150 watts. The output of the Henry 2-K is a 50 ohm transmission line which is used to feed the grid input tuning network of the final rf amplifier. Placed in the transmission line is a five ampere rf ammeter used to monitor power output of the driver stage, and a standing wave ratio meter used to assure proper impedance matching of the driver stage to the grid input tuning network. The Henry 2-K is tuned by setting the frequency selector knob at the desired band setting, as determined by the frequency of the oscillator of the DX-100, and minimizing plate current by adjusting the plate loading and plate tuning controls. The output power of the Henry 2-K is determined by the amount of drive selected for the DX-100.

The final amplifier is a grid driven, class C, vacuum tube amplifier, utilizing an Eimac 4CX-35000C forced-air cooled tetrode, with a plate dissipation of 35 kW, and a 110 kW output capability. The Eimac 4CX-35000C vacuum tube and socket are held in place by a plastic support which has an opening for a 10 inch duct which supplies the air for cooling. A 10 horsepower motor drives a New York Blower which delivers 2200 cubic feet per minute at a pressure 20 inches of water. This air is forced through the cooling fins of the tube. The air is exhausted from the shielded room by an exhaust fan and duct. Figure 16 is a schematic of the final amplifier. The final amplifier stage is connected to the driver stage by a 50 ohm transmission line. Power is coupled to the grid of the 4CX-35000C through coupling coils to the tuned grid tank

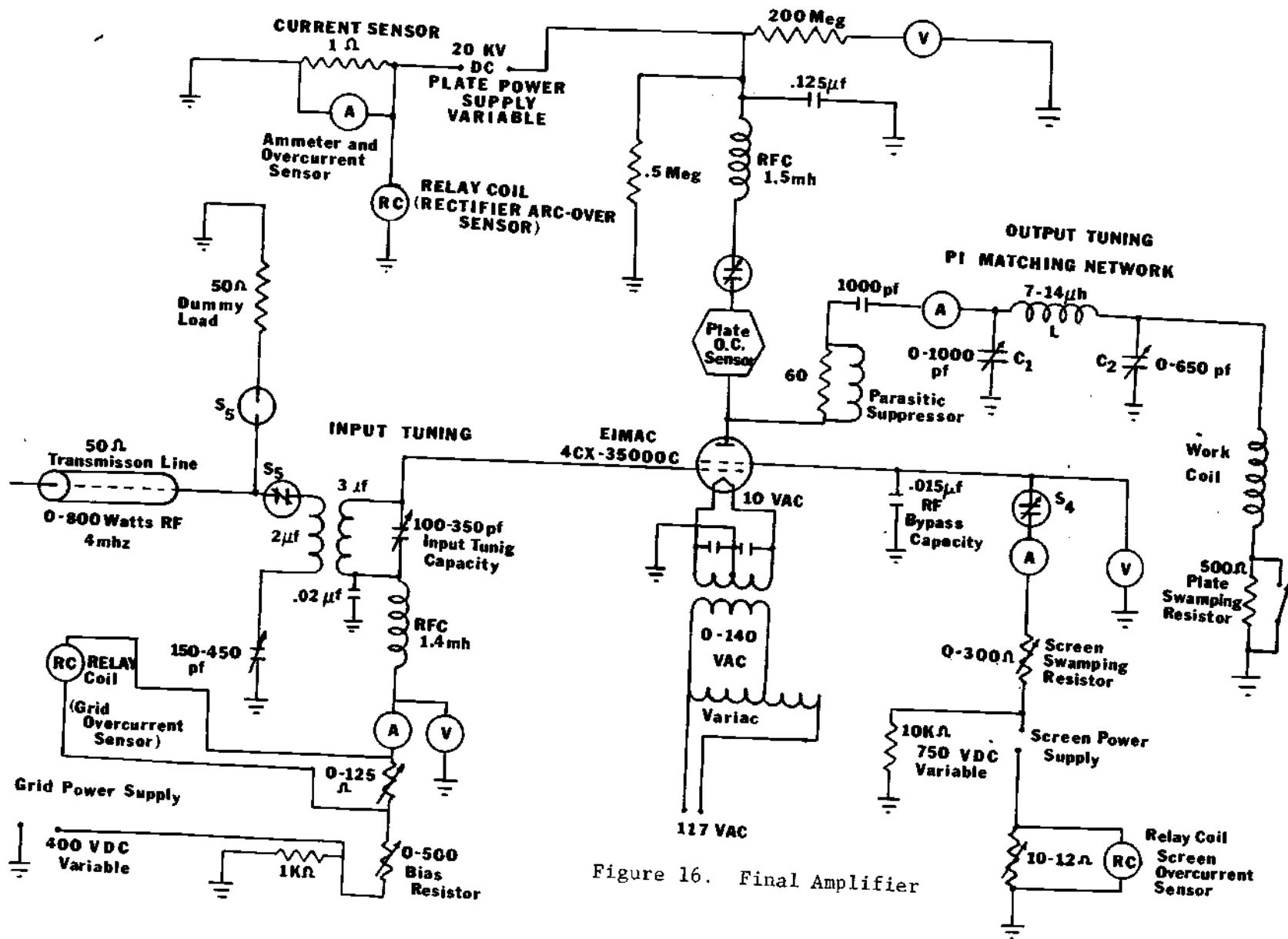


Figure 16. Final Amplifier

circuit. The amount of drive can be varied by changing the excitation fed to the Henry 2-K amplifier, and by changing the value of the link tuning capacitor. The grid tank circuit is tuned to resonance by varying the input tuning capacitor. The approximate component settings are determined by placing a light bulb between the grid of the Eimac 4CX-35000C and ground. The filament voltage of the 4CX-35000C is not applied. Drive is applied to the input tuning network until the bulb is observed to glow. The link tuning capacitor and input tuning capacitor are varied simultaneously until the bulb is at maximum brightness. The bulb is then replaced with a 1000 ohm nonreactive resistor, which is a close approximation to the actual load, and the link tuning capacitor and input tuning capacitor are varied until the standing wave ratio in the 50 ohm transmission line is at a minimum. Usually, a ratio of 1.5 : 1 can be obtained, indicating a good match between the driver stage and the grid of the 4CX-35000C.

Contactors S_5 controls the application of rf drive to the grid of the 4CX-35000C. When the rf drive is switched from the final amplifier tube it is switched to a 50 ohm dummy load. This is done to avoid terminating the 50 ohm transmission line from the Henry 2-K in an open circuit and possibly damaging the driver stage before output of the driver can be reduced. The output of the Heathkit DX-100 can only be varied manually, while the plate high voltage of the Henry 2-K is automatically removed from the final amplifier tube.

Grid bias is a combination of fixed and grid leak bias. This combination was chosen to give adjustment over a wide range of values

because of the experimental nature of the amplifier. The fixed grid voltage supplies protective bias during fault conditions, and the variable grid bias resistor supplies the operating bias. As the dc grid current increases, the operating bias increases, tending to stabilize the amplifier. The 0-125 ohm sensor resistor supplies a voltage to operate the grid overcurrent relay coil during grid overcurrent conditions. The control grid power supply is variable from 0-750 volts, and will supply 750 milliamps. Grid current and voltage are monitored by the operator. The output of control grid power supply is connected to the grid of the 4CX-35000C without regard to other circuit conditions. This is done because the application of a negative dc voltage to the control grid tends to stabilize and cut off an amplifier. The grid power supply is shunted by a 1000 ohm bleeder resistor to stabilize output voltage despite varying amplifier conditions. Rf is prevented from reaching the grid power supply by a 1.4 mh radio frequency choke, which has 35,000 ohms of inductive reactance at four MHz. The rf circuit is connected to ground by a .02 microfarad capacitor connected at the bottom of the input tuning tank circuit. The screen voltage of the 4CX-35000C is also derived from a separate supply because of the unusual nature of the load. The 0-300 ohm screen swamping resistor lowers the screen voltage during periods of high screen current. The 10,000 ohm resistor across the screen power supply provides a reverse current path to ground. Overcurrent conditions are detected by the 10-20 ohm resistor across the screen overcurrent relay coil. A .015 microfarad capacitor is the rf ground for the screen grid. Contactor S_4 connects the screen power supply, a

1200 volt, 750 milliamp unit, to the screen. The screen voltage and current are monitored by the plasma generator operator.

Filament voltage for the Eimac 4CX-35000C is supplied by a 10 volt, 300 amp centertapped transformer. The centertap of the secondary is connected to ground, and .5 microfarad capacitors connect the transformer secondary to the centertap position, providing an rf path to ground. A General Radio, 117 vac., 50 amp Variac supplies power to the filament transformer. A Variac is required since the filament voltage must be increased slowly in a warm-up procedure.

The plate high voltage dc circuit has a one ohm current sensing resistor on the ground side of the power supply. This resistor supplies voltage for the plate ammeter and for the plate voltage control panel overcurrent sensor. The plate power supply is bled by a 500,000 ohm resistor bank. Rf is prevented from reaching the plate power supply by the 1.5 mh rf choke and the .125 microfarad bypass high voltage capacitor. Overcurrents are sensed by a Jennings plate high voltage instantaneous overcurrent relay which operates the vacuum switch, S_3 . This overcurrent sensor is set to operate at seven amps dc. The Jennings overcurrent sensor reacts in about three milliseconds, helping to protect the tube during internal arc conditions. A five ohm, 100 watt, wire-wound resistor is also connected in the plate circuit to help protect the 4CX-35000C in case of internal arc conditions. In the event of an internal arc this resistor acts to limit the instantaneous current available from the plate power supply filter capacitor. As the current increases rapidly during an arc the resistor will also self-destruct due

to the small size of the resistance wire used in the resistor. When the resistor self-destructs, the tube is disconnected from the filter capacitor preventing any further arcing. The current in the 200 megohm resistor bank is a measure of the plate dc voltage. This current is monitored by the operator on the dc plate voltage meter. The .5 megohm bleeder resistor bank allows the plate power supply filter capacitors to discharge when the power supply is turned off. This is partly a safety precaution to prevent the operator from coming into contact with the fully charged filter capacitors. As a further precaution, a knife switch connecting the dc plate high voltage circuit to ground is utilized whenever the operator is working on or near the plate circuit.

The output tuning network enables the operator to match the plasma and torch to the amplifier. The amplifier and tube characteristics determine the optimum amplifier loading, which is close to 1000 ohms for the Eimac 4CX-35000C. This value is determined from the tube operating curves supplied from the manufacturer. The plasma load varies from about 2000 ohms for argon to about 8000 ohms for hydrogen. A pi-matching network was chosen to transform the plasma load to the 1000 ohm load most favorable to the amplifier. This particular network was chosen over the inherently simpler T-network since, for the pi-network, it is possible to permanently set the inductive leg at some value and provide the necessary match by varying the two capacitive legs. Variable vacuum capacitors are well suited for the servo operation which is necessary in making the rapid changes in the reactive values of the pi-network to compensate for changes in the plasma load. The servo motors which drive

the variable vacuum capacitors of the pi-matching network also drive two variable resistors. Figure 17 is a schematic of the servo tuning system. The operator monitors a voltage drop across these resistors which, after a correlation measurement, enables the operator to continuously monitor the reactances of the two capacitive legs. Table 3 shows the range of plasma conditions and the corresponding values for the pi-matching network.

Table 4 lists the theoretical operating parameters of the plasma generator during seeded hydrogen operation. The theoretical parameters were determined from the constant current curves of the 4CX-35000C, Figure 18, as supplied by Eimac. The line AB on Figure 18 is the positive half of the operating line, which is determined by dc plate voltage, dc grid voltage, rf plate voltage, and rf grid voltage.

Table 3. Pi-Matching Network Component Values for Various Plasma Loads

	Plasma Load (ohms)	Amplifier Load (ohms)	Inductor L (μ h)	C ₁ (pf)	C ₂ (pf)	Q
Argon	1000	1000	8	400	400	10
	2000	1000	8	482	342	12
	3400	1000	8	564	305	14
	4900	1000	8	645	289	16
	6800	1000	8	728	276	18
Hydrogen	9000	1000	8	800	267	20

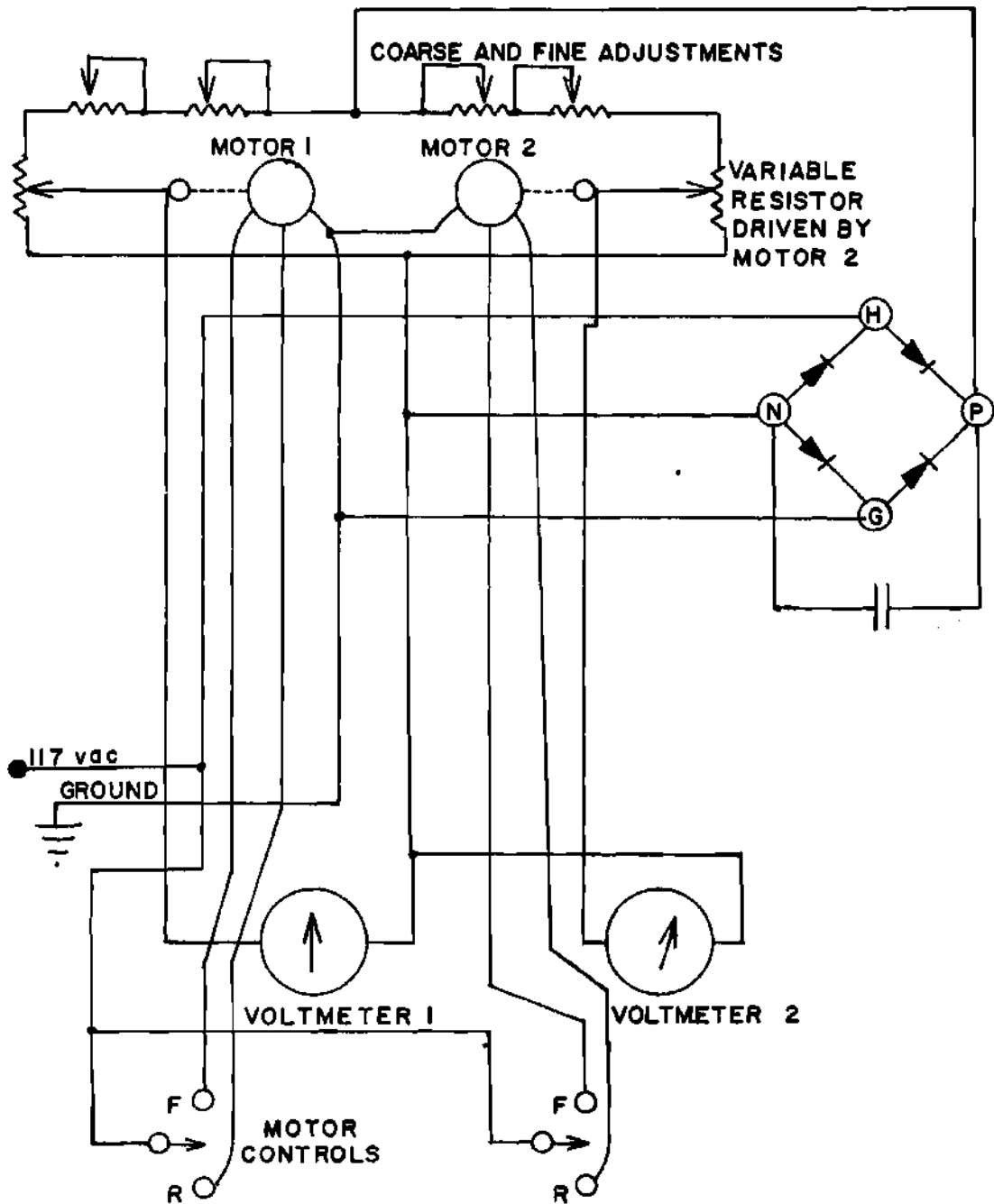


Figure 17. Servo Tuning System

Table 4. Plasma Generator Operating Parameters

	Operating Value	Maximum Rating
dc plate voltage	16,500 volts	20,000 volts
dc grid voltage	- 400 volts	
dc screen voltage	750 volts	2,500 volts
dc plate current	6.2 amperes	15 amperes
dc grid current	.14 amperes	
dc screen current	.50 amperes	
peak rf plate voltage	15,900 volts	
peak rf plate current	9.3 amperes	
peak rf grid voltage	500 volts	
peak rf grid current	.28 amperes	
input impedance	1,785 ohms	
output impedance	1,892 ohms	
total plate input power	102,000 watts	
plate dissipation	28,000 watts	35,000 watts
grid dissipation	14 watts	500 watts
screen dissipation	200 watts	1,750 watts
grid driving power	70 watts	
plate output power	74,000 watts	
plate efficiency	72.5 percent	

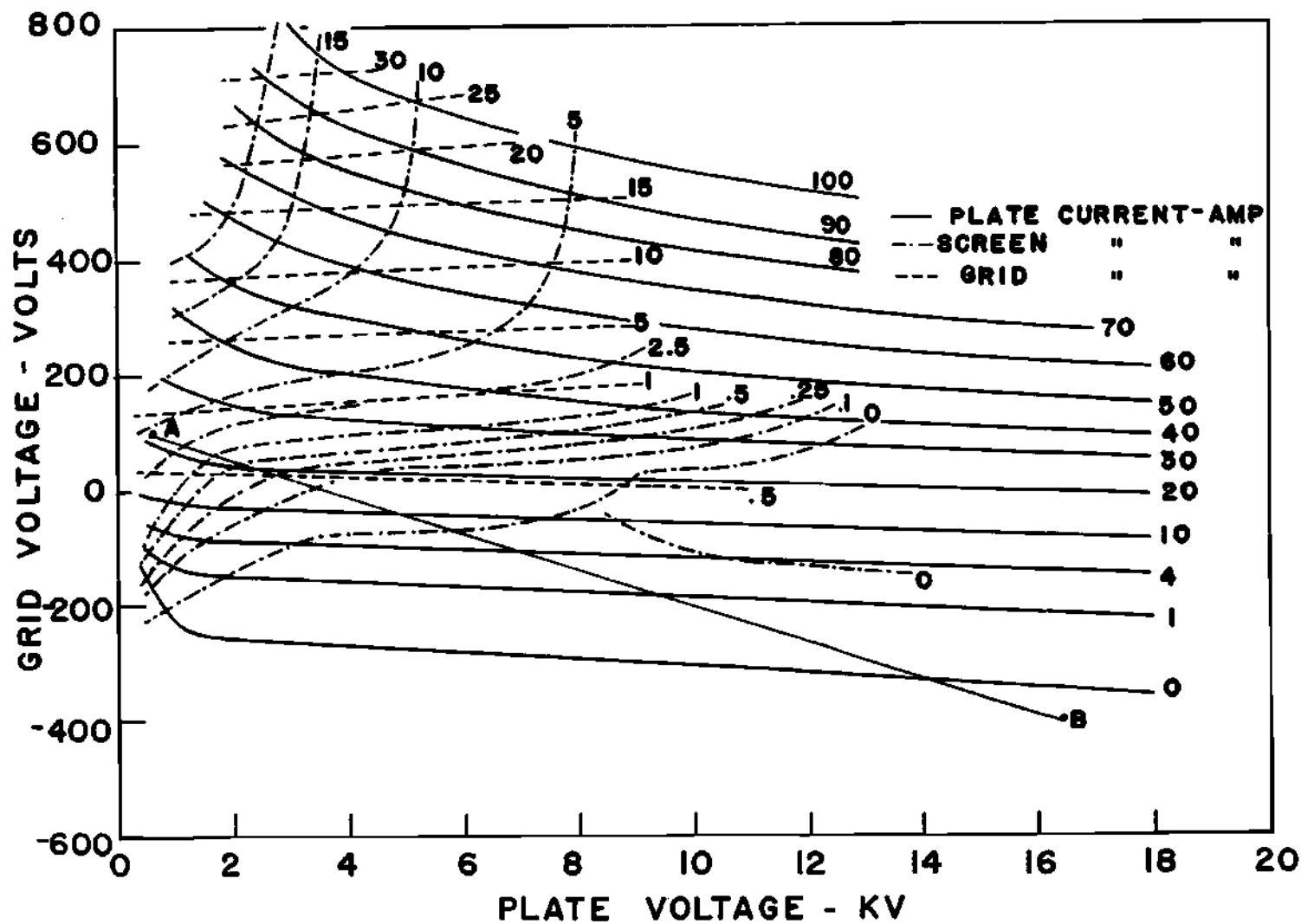


Figure 18. Constant Current Characteristics of Eimac 4CX-35000C
(Reference 41)

All monitor and control functions of the plasma generator are located in the copper shielded room. The three primary functions of the monitoring and control system are (1) to initiate and control the plasma generator, (2) to monitor pertinent voltages and currents, and (3) to protect the rf plasma generator components from fault conditions.

Since certain components would be damaged if not allowed sufficient time to warm up, or if they were not turned on in proper sequence, the correct turn on sequence must be closely followed. In order to insure that this is followed, all important controls have time delays and interlocks to prevent improper operation. An interlock system prevents the amplifier control panel from being activated until the operator has turned on the cooling fans and blowers, adjusted the final amplifier tube filament voltage to ten volts, turned on the grid power supply, turned on the plate power supply, and turned on the screen power supply. When these steps have been taken the interlock system activates the ac power to the amplifier control panel and the "cascade off" system can be set by the operator. The "cascade off" system is part of the amplifier protection system. The control system is also interlocked to prevent application of screen or plate voltage in the incorrect sequence. The grid voltage is applied to the tube when the grid power supply is turned on. Plate voltage is next applied to the tube, and screen voltage applied last. Screen voltage must not be applied prior to plate voltage because excessive screen currents would occur. Figure 25 in Chapter V illustrates the proper rf plasma generator operational sequence.

The different monitors of the rf plasma generator are:

1. Plate power supply ac input voltage and current (three phases),
2. Inductorial ac output voltage and current (three phases),
3. DC plate voltage of final amplifier,
4. DC plate current of final amplifier,
5. Grid and plate current of Heathkit DX-100 (signal generator),
6. Plate voltage of Heathkit DX-100,
7. Grid and plate current of Henry 2-K amplifier,
8. Plate voltage of Henry 2-K amplifier,
9. Rf current output of driver stage,
10. Standing wave ratio of rf output of driver stage,
11. Filament voltage,
12. DC grid current and voltage of the final amplifier,
13. DC screen current and voltage of final amplifier,
14. Pi-matching network capacitor settings,
15. RF output current,
16. Relay control voltage.

The protection network is designed to (1) detect dangerous over-currents, (2) remove voltage causing overcurrent, (3) turn the amplifier off in proper sequence, and (4) indicate the component in which the over-current occurred. Figure 19 shows the complete protection system and the way in which the different protective devices are related to insure plasma generator turn-off. For example, if a rectifier tube arc occurs, the sensor opens the plate power supply input vacuum switches, S_2 , which causes the interlock system to turn off the amplifier control panel

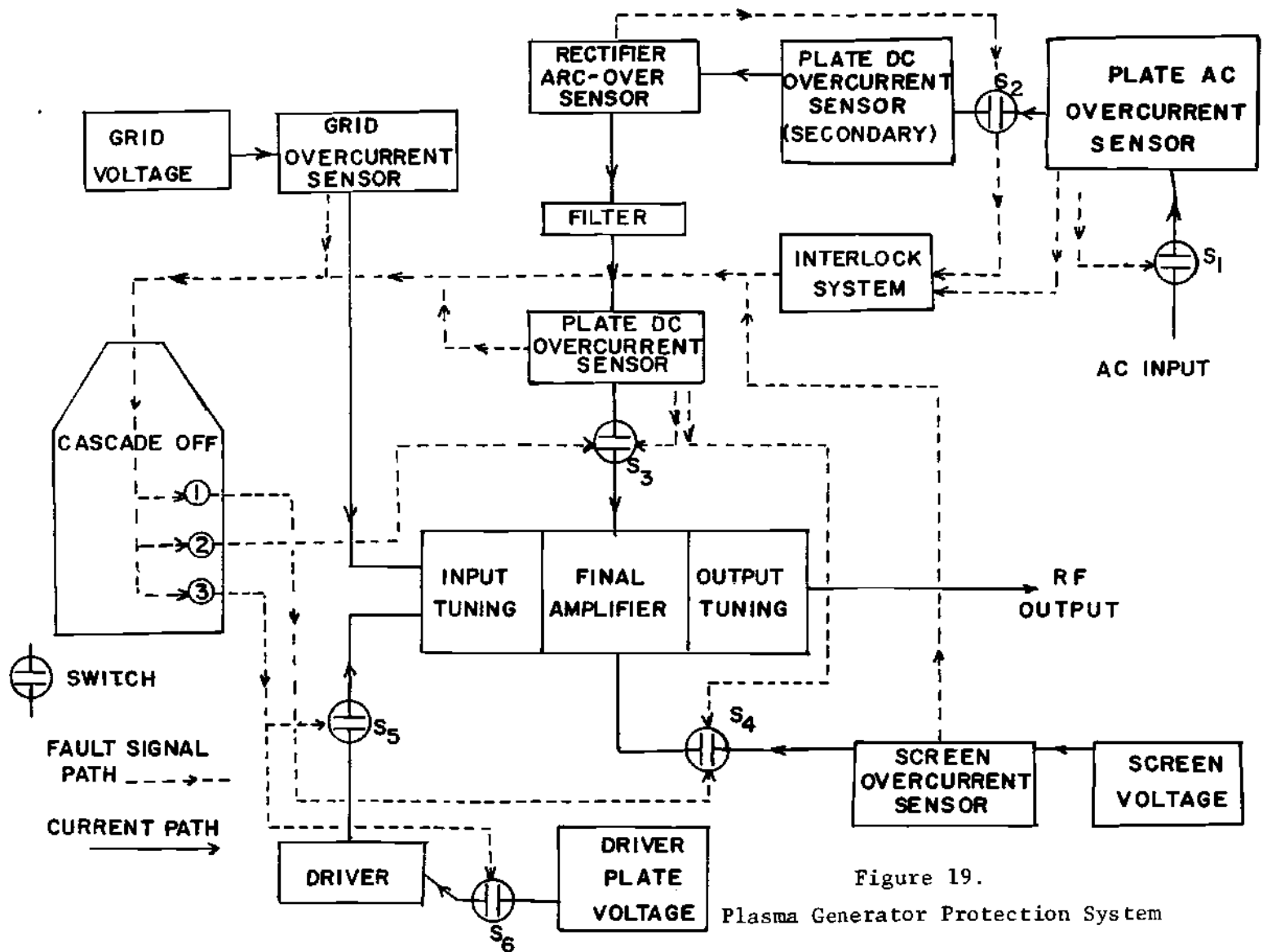


Figure 19.
Plasma Generator Protection System

power, thereby activating the "cascade off" relay network which turns off, in order, the screen voltage, S_4 , dc plate voltage, S_3 , the rf drive voltage, S_5 , and the driver plate voltage, S_6 . In the case of a plate dc overcurrent, the plate dc vacuum switch, S_3 , and the screen voltage switch, S_4 , are both directly activated by the sensor. This is because plate overcurrents can seriously damage the tube elements, and voltages must be removed as quickly as possible. The screen voltage is also directly removed by the plate current sensor since application of screen voltage after the removal of the plate voltage could damage the screen grid. The protection network is such that any overcurrent removes all voltages from the tube, except the grid voltage, which tends to cut-off the tube.

Plasma Torch

Work with particle-seeded hydrogen plasmas has shown that seeded plasmas are easier to sustain than unseeded plasmas. The increase in the electrical conductivity of the plasma resulting from thermionic emission by the particles has been predicted theoretically and confirmed experimentally. Waldie and Fels⁴⁶ measured the conductivity of suspensions of barium oxide particles in argon and showed that the results were of the same order as predicted theoretically by several other researchers. The purpose of their work was to demonstrate the feasibility of using particle seeds in MHD generators. Cory and Bennett⁴⁷ showed that the electrical conductivity of an aerosol of tantalum carbide particles in helium increased to about 20 mhos/cm when the aerosol was flash heated to about 4000°K for about two milliseconds, and that the opacity increased at the

same time the conductivity increased. The increase in conductivity was far greater than that which would have been obtained by heating helium alone. The expected increase in conductivity of hydrogen plasmas due to particle seeding makes seeded plasmas easier to sustain than unseeded plasmas.

The plasma torch consists of a work coil, which couples radio frequency energy to the seeded plasma and transparent quartz tube. The work coil is typically a five to seven turn of one-fourth inch water-cooled copper tubing. This type coil, coupling energy to an argon plasma, reflects a load to the pi-matching network of approximately 2000 ohms, and a hydrogen plasma reflects a load of about 8000 ohms.¹⁶

A 30 foot section of rubber hose carries the cooling water to the copper coupling coil. The long section of rubber hose is needed since the hot side of the coupling coil is typically at a 30 kilovolt rf potential, and the cooling water has not been distilled. The cooling water is not a good insulator and a long path length is required to insulate the coupling coil from ground.

The plasma is confined within an air cooled transparent quartz tube (50.8 mm OD, 1.75 mm w.t.). Air cooling is supplied by one 208 vac, three phase, one-half horsepower blower and two 28 vdc, one-half horsepower blowers. The original design was to scan the transparent circular quartz tube with a laser in order to obtain the transmitted intensity as a function of axial distance. Several problems were experienced in attempting to take opacity data by scanning the circular quartz tube. The first problem encountered was a refraction of the laser beam in scanning near

the outer edge of the circular tube. A series of converging lenses was designed to focus the refracted laser beam onto the photomultiplier tube. This system was not adequate, however, since no information could be obtained from the outermost regions of the plasma torch. The opacity in the outer regions must be known in order to accurately compute the opacity as a function of radius. The other problem associated with scanning the plasma through the circular quartz tube is that the quartz walls are quickly discolored due to impurities in the carrier gas and to the tungsten aerosol. The quartz would usually be discolored before a substantial percentage of hydrogen and tungsten seed could be added to the argon used to start the plasma. These two difficulties made it impossible to take any useful opacity data on tungsten-hydrogen plasmas by scanning through a simple quartz tube.

A new type of torch was designed to solve these problems. A flat window was needed to solve the refraction problems, and this flat window would have to be physically removed from the aerosol and plasma to prevent discoloration. This is done by removing a section about three-sixteenths inch thick from the quartz wall. The slit extends just over halfway across the tube, since all the necessary information can be obtained by scanning half of the plasma. A one-half inch plate of ceramic material is machined to slide down over the slit in the quartz tube. A slit is machined in the ceramic to match the slit in the quartz tube, and flat windows are bonded over the slit in the ceramic to seal the torch. The torch is further sealed by bonding the ceramic and quartz tube with a castable ceramic. Two types of machinable ceramics are used; Aremco

Aremcolox 502-1300 and American Lava AlSi Mag 222. Aremco Ceramabond 503 is used to bond the ceramic to the quartz tube, and Ceramacast 511 is used to seal the openings between the quartz and ceramic. There must be a good seal between the quartz and ceramic because of the high potential differences between the plasma and the work coil. Whenever there is an air path less than about three inches long between the plasma and the work coil, the plasma tends to arc to the work coil causing an amplifier screen overcurrent. During seeded hydrogen operation arcing between plasma and work coil and from turn to turn of the coil is a severe problem. The quartz temperature during hydrogen operation is very close to the softening point of quartz and the plasma often arcs directly through the quartz. If for some reason there are any hot spots on the quartz tube, this type of arcing prevents increasing the power level to the point where seeded hydrogen can be run. Small glass tubes were originally used to separate the work coil from the quartz tube, but they caused hot spots on the quartz tube and subsequent arcing. The work coil is now held in position by the castable ceramic.

The region of the quartz tube surrounded by the ceramic is not cooled as well as the remainder of the quartz tube. It is this region of the plasma torch which limits torch lifetime. Under ideal conditions, the plasma torch operates from 60 to 180 seconds with a seeded-hydrogen plasma before the quartz in the region of the slit has softened to the point where the quartz either deforms to disrupt gas flow, or flows over the window preventing any further laser scanning. The same type torch operates almost indefinitely during seeded-argon operation.

The base of the plasma torch consists of a rubber stopper taped firmly in place. All aerosol and gas lines, and the negative electrode of the dc arc plasma starting system, enter the plasma torch through the rubber stopper. The negative electrode of the dc arc plasma starting system is a one-fourth inch stainless steel tube which enters through the center of the electrode and extends up the torch to within three inches of the bottom of the coupling coil. The plasma is initiated by flowing pure argon through the torch, contacting the hand held positive electrode to the negative electrode, and drawing a dc arc through the work coil region. A standard, 300 ampere dc arc welder is used as the plasma starter system.

The aerosol is injected tangentially at the bottom of the torch by two one-fourth inch sections of copper tubing, pinched closed at the end, and drilled with a one-sixteenth inch hole on the tube wall. The tangentially injected aerosol spirals up the torch to aid in gas recirculation and plasma arc stabilization. Two types of torches have been utilized. One has an inner glass tube which extends up to within three inches of the bottom of the coupling coil. In this torch the aerosol is injected up through the inner glass tube. There is about one-eighth inch clearance between the outside wall of the inner glass tube and the inside wall of the quartz tube. A high velocity flow of argon or hydrogen (no tungsten aerosol) passes up through this region. This design was developed while the circular quartz tube was being used, and discoloration of the torch was a severe problem. This higher velocity outer flow of gas helped to prevent severe discoloration of the quartz. It was also

hoped that this sheath of gas would cool the wall of the torch, extending torch life, but this did not appear to be the case. When the torch was modified for flat windows, discoloration of the quartz tube was no longer a factor, since the laser did not scan through the quartz wall, and this inner glass tube was removed in order to simplify the torch. Since this glass tube was very close to the plasma arc region, it would often soften and disrupt the proper flow of aerosol into the arc region. The aerosol still enters the torch tangentially through the one-fourth inch copper tubes and spirals up the torch. The gas feed line for the outer sheath of gas was retained. Gas is allowed to enter the plasma torch through this line after a data run to remove all traces of aerosol to permit an accurate laser scan with no attenuation.

The hot hydrogen continuously burns off as it exits the top of the torch. A hood covers the exit of the plasma torch and a high volume fan evacuates all plasma products to the outside. The plasma torch is shown in Figure 20.

Aerosol Generators

Three different types of aerosol generators were used in the course of this research. The first two efforts were discarded for not producing sufficiently dense aerosols to feed into the plasma torch. It was desired that the tungsten vapor be of such a density that at least five percent absorption occurred in the plasma region.

The first aerosol generator consisted of a large test tube with gas inlet and outlet tubes, as shown in Figure 21. The gas inlet tube was positioned so that the tungsten placed in the bottom of the tube was

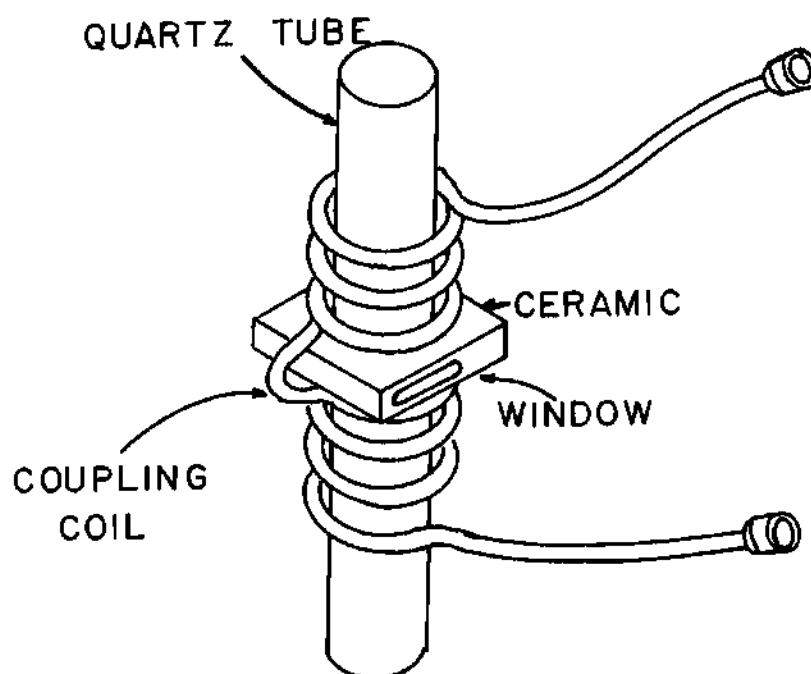


Figure 20. Plasma Torch

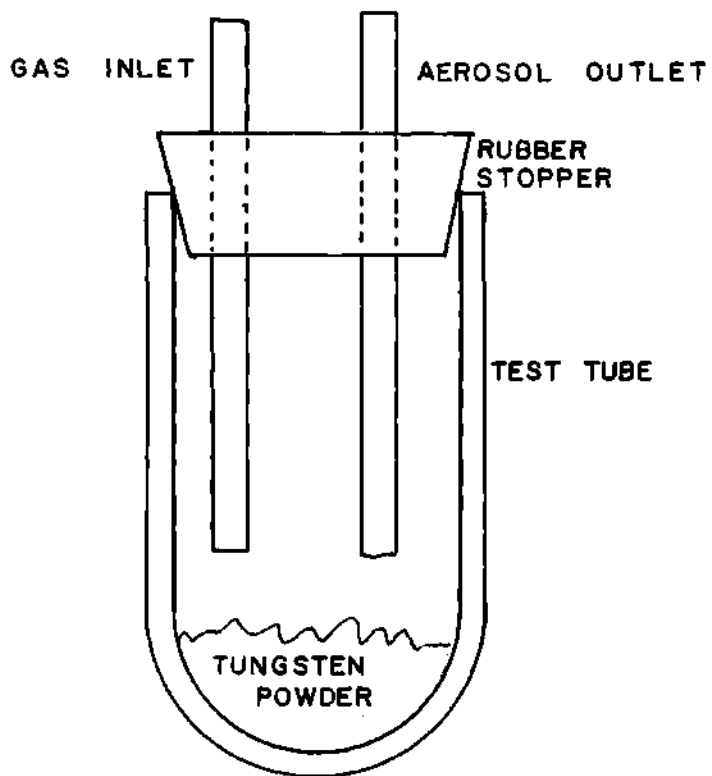


Figure 21. Test Tube Aerosol Generator

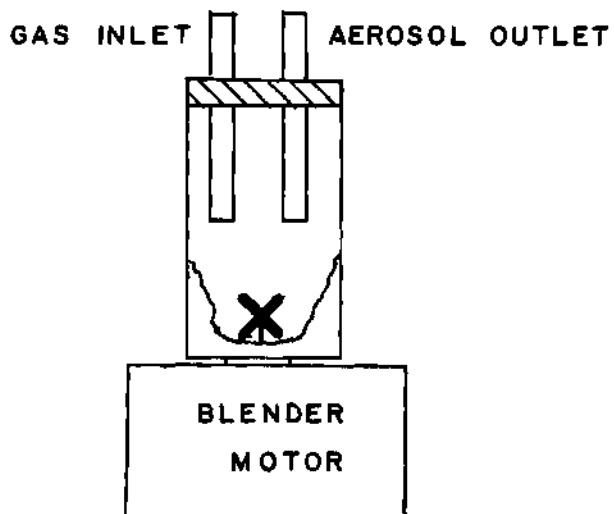


Figure 22. Blender Aerosol Generator

agitated by the incoming gas forming an aerosol. This aerosol generator had two drawbacks, the most important being that the aerosols formed were not dense enough to cause sufficient absorption of the laser beam. The other problem was the large internal volume of the aerosol generator. This caused the time lapse between changes made in the argon-hydrogen gas concentration entering the aerosol generator and the gas mixture entering the plasma torch to be excessively long. It is desired that this time lag be as short as possible due to the relatively short lifetime of the plasma torch during seeded hydrogen operation.

The second type aerosol generator consisted of a commercial food blender, illustrated in Figure 22. The mixing blades of the blender served to agitate the tungsten powder to form the aerosol. However, tungsten tends to settle rapidly and during blender operation the tungsten would form powder structures around the mixing blades and deposit them on the walls of the blender. Thus, even though the blender would produce dense aerosols when first operated, the aerosol density would rapidly decrease. The large internal volume of the blender aerosol generator also presented a problem as in the test tube aerosol generator.

A type of aerosol generator which produces consistently dense aerosols and has a very small internal volume is the Wright Dust Feed Mechanism developed by Wright.⁴⁷ This aerosol generator is the one used in the high temperature, high pressure seeded-hydrogen research of Partain. The tungsten powder is packed into a threaded seed chamber which is slowly advanced onto a scraper head. The carrier gas passes over the scraper head forming the aerosol. Both the seed chamber and the

scraper head are gear driven by a variable speed, reversible drill motor, but the gear ratios are slightly different so that the scraper head advances into the seed chamber. The advantages of the Wright Dust Feed Mechanism are the positive entrainment of the tungsten seed material in the aerosol lines, producing a relatively consistent aerosol and that the aerosol density can be varied by varying the speed of the scraper drive motor.

The tungsten seed material of .04 micron particles is stored in a vacuum oven to drive out any moisture, which would cause the particles to agglomerate. For this research the size of the agglomerates is not critical since it has been shown that micron sized particles are essentially in thermal equilibrium with the carrier gas.⁴⁶ This means that there is no danger of tungsten particles existing within the high temperature plasma region. That is, all the tungsten particles are vaporized within several milliseconds of entering the plasma region.⁴⁶ The actual size of the agglomerates is only of importance in measuring the opacity near the outer edges of the plasma torch where the temperature is below the vaporization point of tungsten. The opacity of this region is due to the seed particles, and it is necessary to know the approximate particle size to compare the measured opacity with previous experimental and theoretical research. Partain³³ utilized an electrostatic precipitator to collect seed samples on electron microscope slides, and analyzed the results to evaluate the particle size distribution. The results of this work showed the particle size to be about .2 micron. The seed material and aerosol generator used in this research are the same as used by

Partain and it is safe to assume that the same agglomerate size applies in this study.

Gas Flow and Aerosol Density Sampling Systems

Figure 23 shows the gas flow control system and the aerosol density sampling system. The gas flow control system is designed to (1) allow the operator to start the plasma with pure argon and thereafter run any desired gas mixture from pure argon to pure hydrogen at the desired flow rates, (2) allow the operator to run any desired portion of the total gas flow through the aerosol generator, and (3) allow the operator to flush the plasma torch with pure argon or hydrogen. The aerosol density sampling system allows for determination of the tungsten seed density of the aerosol entering the plasma torch.

Located within the shielded room containing the rf plasma generator are cylinders of commercial argon and hydrogen gas, each fitted with a pressure reducer, regulator, and valve. The pressure of the argon flow line is set at 40 psi, and the pressure of the hydrogen flow line is set at 45 psi. If the hydrogen line pressure is not run slightly higher than the argon line pressure, it is very difficult to mix in small amounts of hydrogen during the initial period of changing from argon flow to hydrogen flow following plasma start-up. If the operator does not have complete control of the hydrogen flow rate, the plasma is easily extinguished.

The gas flow lines for argon and hydrogen both divide off immediately at the exterior of the gas cylinders. A valve for each line controls the flow of argon and hydrogen into a gas line which by-passes the remainder of the gas control and aerosol generating system. This line

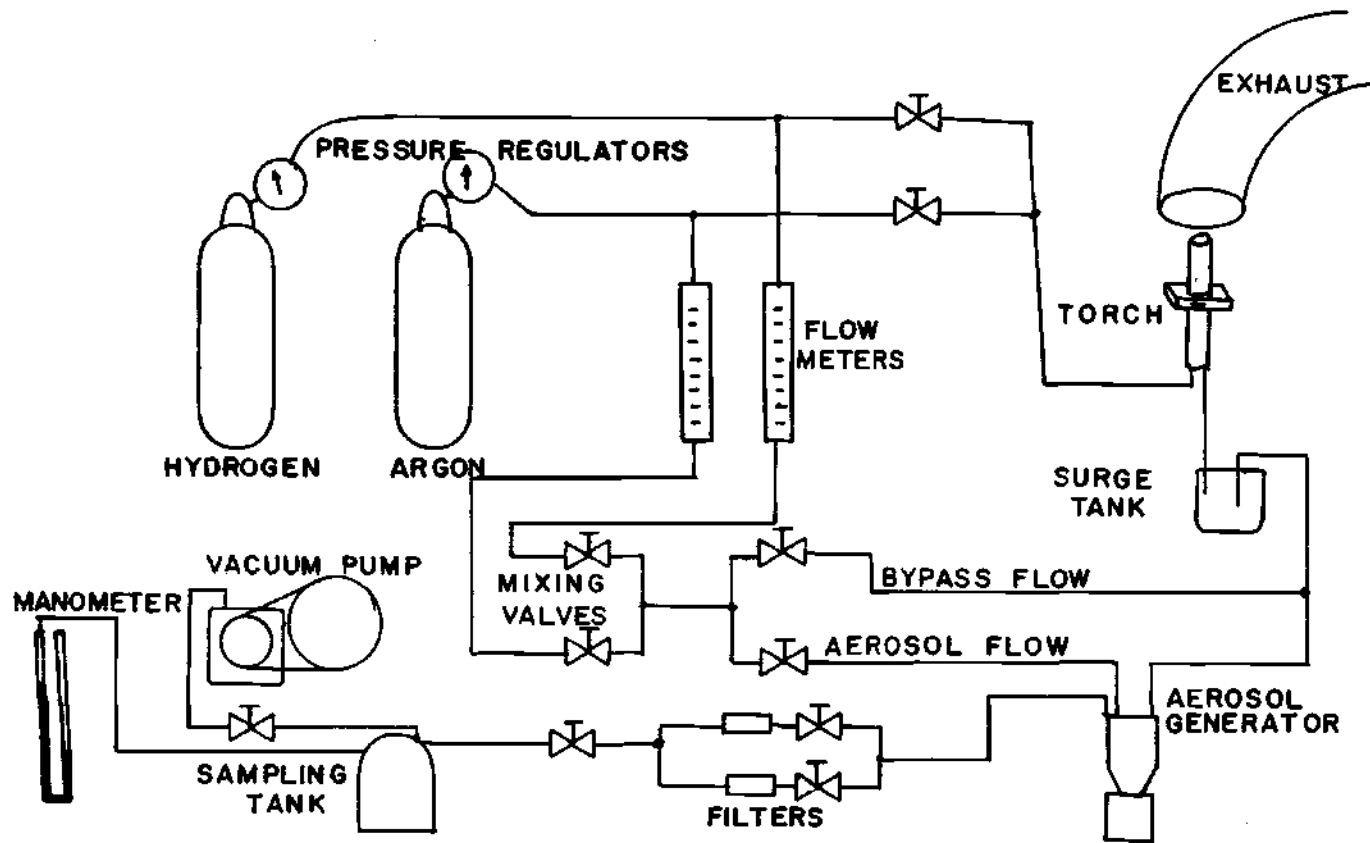


Figure 23. Gas Flow Control System

leads directly to the plasma torch. One torch design utilized a central flow of aerosol, and a surrounding stream of higher velocity argon and hydrogen. It was hoped that this outer region of gas would help to cool the plasma torch walls and keep the discoloration at a minimum. This feature of the plasma torch was discarded since it was felt that the desired goals were not being accomplished. This gas line and torch fittings were retained and are used to clear the torch of all aerosol after the torch has been turned off. The aerosol must be cleared out in order to take a final laser scan of the torch to use as a laser intensity reference.

The argon and hydrogen gas lines then go to the gas flow control panel where the flow of argon and hydrogen are separately controlled by valves. The gas flows from these valves to gas flow meters which monitor the volume flow of the argon and hydrogen and allow the operator to adjust the valves controlling the gas flow to the desired percentage of hydrogen. The argon and hydrogen lines are joined at this point to mix the two gases, and then, after mixing has occurred, this line is split and fed to two valves on the gas flow control panel which allows the operator to feed the desired percentage of gas through the aerosol generator. This aerosol generator by-pass valve gives the operator one control of the aerosol density entering the torch. The other control is the speed of the motor driving the Wright Dust Feed Aerosol generator. The aerosol line from the aerosol generator is joined to the aerosol generator by-pass line and fed into a small, .25 liter surge tank. The surge tank smooths any fluctuations in the aerosol density. The surge tank has two aerosol outlets located close to one another. One outlet goes to the plasma torch and the other to the aerosol density sampling system. The aerosol

line to the plasma torch splits into two torch inlets, which enter through the rubber stopper at the bottom of the torch and inject the aerosol tangentially at the bottom of the torch.

Aerosol density sampling is taken directly from the surge tank since there was no way to sample the aerosol in the torch itself, and it was found that inserting a T connection directly into the aerosol line allowed tungsten deposits to collect in the sampling line adjacent to the aerosol line. When an aerosol sample was taken, part of this buildup of tungsten would be swept along with the aerosol and collected on the filter paper, causing the aerosol density calculation to be inaccurate. The aerosol sampling line feeds the aerosol into one of two filter holders. Each filter holder is a two piece stainless steel holder three inches long and one and one-half inches in diameter. The two halves screw together clamping a fiberglass filter in place. A cutoff valve on each filter holder provides a means of rapidly interchanging filters so that only one fitting has to be disconnected. The sample volume measurement tank is evacuated by a vacuum pump. Gas lines running from the measurement tank to the vacuum pump and to the filter holders are opened and closed by solenoid valves controlled by the operator at the gas flow control panel. After the measurement tank is evacuated and the evacuation solenoid reset to its closed position, the pressure in the tank is read from a manometer. When it is desired to take an aerosol sample, a solenoid valve located between the evacuated tank and the fiberglass filter is activated, drawing an aerosol sample from the surge tank. After the aerosol has been sampled the manometer is read again.

Data Collection Instrumentation

All data collection related instruments are located in the room adjacent to the shielded plasma generator room. A mirror system allows the laser, photomultiplier tube, and related recording instrumentation to be located outside the shielded plasma generator room. If the data recording instrumentation is not located outside the shielded plasma generator room, the rf produced by the plasma generator would interfere with the recording instruments, making the collection of data impossible. The copper shield prevents the electromagnetic radiation produced by the plasma generator from affecting the recording instruments. A small hole, about three inches by six inches has been knocked out of the wall joining the two rooms to allow the laser to scan the plasma. Figure 24 illustrates the data collection system.

A helium-neon laser is the light source for this research. The laser output is one milliwatt at 6328 \AA . The laser beam scans the plasma by means of a movable right angle mirror system. The laser and photomultiplier tube remain fixed while a platform with the mirrors mounted on it is driven at a constant speed by a reversible synchronous motor. A system of microswitches and relays causes the synchronous motor to reverse at the end of each scan.

A photomultiplier tube with a response range of 3000 \AA to 8000 \AA is used to measure the attenuation of the laser beam. The photomultiplier tube is housed in a light-tight box which has a series of spatial and spectral filters to reduce the background light intensity. A high voltage power supply, with an output voltage of from zero to 3000 volts, is

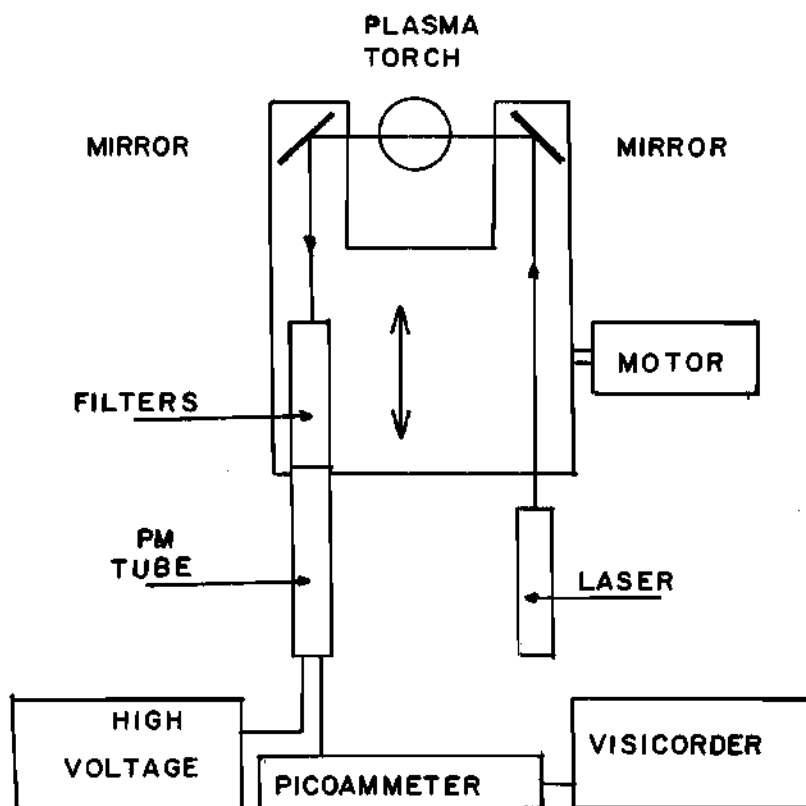


Figure 24. Data Collection System

the voltage supply for the photomultiplier tube. Typical operating values range from 1000 volts to 1500 volts. These voltages are within the linear operating range of the photomultiplier tube. A picoammeter measures the output of the photomultiplier tube, and an oscillograph monitors the picoammeter output. Transmitted laser intensity as a function of axial distance from the center of the plasma is recorded as the right-angle mirror system scans the plasma.

CHAPTER V

EXPERIMENTAL PROCEDURE

Outlined in this chapter is the overall preparation and technique involved in operating the radio frequency plasma generator with a tungsten seeded hydrogen plasma and collecting opacity data.

A plasma torch, which has been constructed as described in the chapter on equipment and instrumentation, is selected and placed in position on the plasma torch air cooling mount. The torch is held in place by two adjustable clamps located at the top and bottom of the torch. The adjustable clamps allow the scanning system to be lined up prior to installing the torch. The right-angle mirrors are adjusted so that the laser beam scans across the torch region in a horizontal plane and enters a pinhole on the face of the photomultiplier tube container. When the laser, photomultiplier tube, and right-angle mirrors are properly lined up, the laser beam is always directed upon the same point on the cathode of the photomultiplier tube when the right-angle mirrors are scanned across the plasma region. The adjustable clamps allow the plasma torch to be lined up so that the laser beam scans across the center of the torch windows. The torch is also adjusted so that the laser beam is as close to perpendicular to the torch window as possible. After the plasma torch is clamped into position, the coupling coil is connected with swagelock connectors to the cooling water supply, pi-matching network,

and rf ground. The rubber stopper torch base is taped into position, and the gas and aerosol lines are connected. An aluminum brace prevents the stopper from coming out during operation and gives the plasma torch further support. At this point the torch and scanning system are checked for proper alignment by turning on the photomultiplier tube high voltage, the picoammeter, and the visicorder. The photomultiplier voltage is adjusted so that the desired output is obtained. The plasma torch is scanned by the laser and the photomultiplier tube output is recorded by the visicorder. The visicorder output is then examined to assure that the laser beam is not being obstructed in any manner. This output trace is kept for comparison with a trace made after the data have been collected to assure that the windows of the torch have not discolored and that the laser beam has not been obstructed in any way.

The tungsten powder is removed from the vacuum drying oven and packed into the aerosol generator and pre-weighed filter papers are placed in the filter holders. The vacuum pump connected to the sample tank is turned on. The tank is evacuated, and the manometer reading is recorded.

At this point all steps necessary prior to plasma generator operation have been completed, and the blower which cools the final tube is turned on. This blower must be operating prior to heating the filaments of the 4CX-35000C. Filament voltage is then slowly raised to ten volts to allow for proper warm-up of the filaments.

Before operating the plate power supply, the knife switch which grounds the power supply for operator protection is opened. The plate power supply circuit breaker is activated, which allows the plate power

supply control panel to be turned on. Filament voltage is applied to the rectifier tubes. A three minute time delay prevents premature application of the ac operating voltage to the rectifiers. When the plate power supply is ready, the power supply dc output voltage is adjusted to five kilovolts.

The screen and grid power supplies are turned on at the same time the plate power supply circuit breaker is activated to allow ample warm-up time. The screen supply is set at +700 volts and the grid supply is set at -400 volts. When the previous steps have been properly completed, the interlock system, which prevents amplifier control panel turn on and premature application of screen and plate voltages to the 4CX-35000C, is activated.

The amplifier control panel is turned on and the "cascade off" system is set. This activates the switching system which allows for application of plate voltage, screen voltage, and rf drive to the 4CX-35000C. The radio frequency driver stage is allowed proper warm-up time. The driver stage is tuned in accordance with the steps outlined in Chapter IV prior to an experimental run. Retuning of the driver stage for each run is not necessary.

Grid voltage, which controls the final tube, was applied when the grid voltage power supply was set at -400 volts. This occurs because the grid power supply is tied directly to the grid of the 4CX-35000C. Plate voltage, which was set at 5000 volts, is applied prior to applying the screen voltage.

Although the loading characteristics of the amplifier when there is no plasma in the torch are different than the loading characteristics

which exist during plasma operation, experience has shown that a limited amount of rf drive can be applied to the final amplifier prior to plasma operation. The pi-matching network is tuned into a seeded argon-hydrogen load prior to the experimental run, and the servo operated tuning capacitors of the pi-matching network are left in the position which resulted in the best plasma operation. When the plasma is to be restarted, the rf drive is increased until the screen current is about the maximum allowable value of 750 milliamperes, and plate current is about 500 milliamperes. Since, with no plasma load, the amplifier is not properly tuned, a small amount of rf drive will result in this high screen current. After the coupling coil cooling water has been turned on, and with about 80 cubic feet per hour of pure argon at STP entering the plasma torch, the argon plasma is ignited. This is done by contacting the dc electrodes of the plasma starting system and drawing an arc through the coupling coil region. An arc of about six inches can be maintained with this system in argon. The dc arc allows the plasma generator, which is operated at this point with reduced rf drive, to couple some energy to the ionized gas produced by the dc arc. A stable argon plasma is generated by increasing the rf drive and withdrawing the starting electrode. Rf drive and plate voltage are adjusted until the plate current is 1.5 amperes and the plate voltage is 7.5 kilovolts. Screen current runs at less than 100 milliamperes, and grid current is less than 50 milliamperes. Before the power level is further increased, or any hydrogen is added to the gas flow, the negative starting electrode is removed from ground. If this is not done, a large percentage of the plasma power leaks to ground through the starting

electrode. Another laser scan is usually taken of the pure argon plasma to determine if starting procedures have caused the plasma torch to move and obstruct the laser beam. Approximately half of the gas flow is allowed to pass through the aerosol generator which is turned on at slow speed to produce a relatively light aerosol, and the power level is increased to about 30 kilowatts by increasing the rf drive and by increasing the plate voltage to 12 kilovolts.

The hydrogen flow control valve is adjusted until about two cubic feet per hour of hydrogen is mixed with the argon gas flow. When the hydrogen is added to the gas flow the plasma contracts to a smaller size. Power level is increased to about 110 kilowatts input by increasing the rf drive and raising the plate voltage to 16.5 kilovolts. The flow rate of hydrogen is increased to eight cubic feet per hour and the flow of argon is stopped. During seeded-hydrogen operation the screen current is about 600 milliamperes, and the grid current is about 150 milliamperes. Figure 25 shows the sequences of steps necessary to operate the plasma generator.

Following the initiation of tungsten seeded hydrogen plasma operation the seed density is increased to the desired value by increasing the speed of the motor driving the aerosol generator and the scanning system and visicorder are turned on. During the laser scan the solenoid valve which controls the aerosol density sampling line is activated for about four seconds. This length of time was determined to yield a measurable seed sample on the filter paper. After several scans across the seeded hydrogen plasma to record the attenuated laser intensity, the plasma

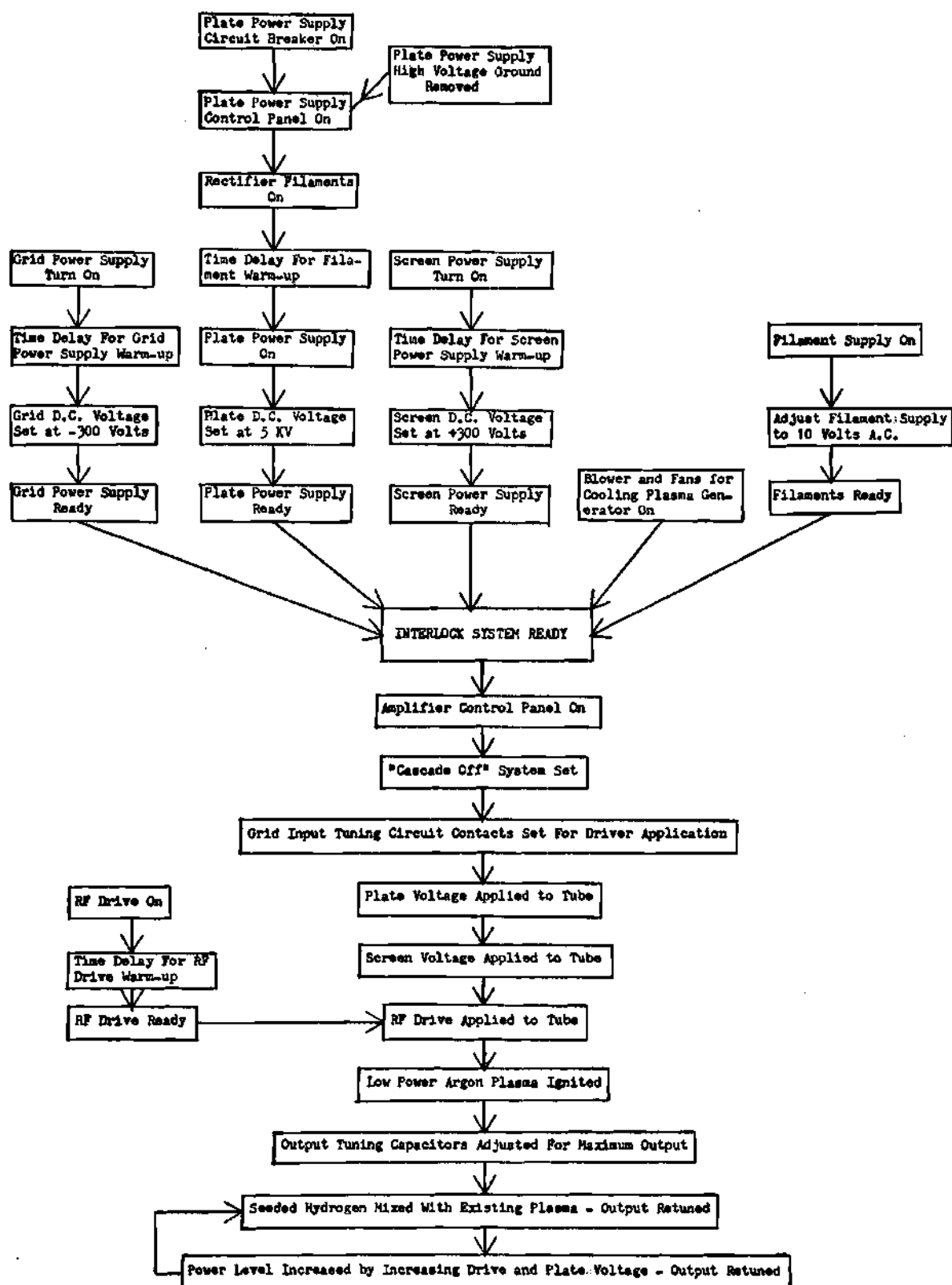


Figure 25. Plasma Generator Operation

generator is shut down by throwing the "cascade off" switch and reducing the rf drive to zero. The aerosol flow is shut off and pure argon is allowed to flush the torch region. After the torch is cleared of all aerosol, a final laser scan is recorded to measure the intensity of the unattenuated laser beam. The unattenuated laser beam intensity is taken following the seeded hydrogen operation to insure that no changes in plasma torch position or torch window discoloration are interpreted as plasma attenuation of the laser beam. The pressure of the aerosol sampling tank and the final weight of the filter are recorded as final steps of opacity data collection.

The equivalent black body radiating temperature of the plasma is determined from the surface area of the plasma and the power radiated from the plasma. The surface area is estimated from visual observations of the plasma during seeded hydrogen operation. The power deposited in the plasma is determined by subtracting power losses in the plasma generator from the plate input power. The plate input power is the product of plate dc voltage and plate dc current, which are recorded during a seeded hydrogen plasma run. The theoretical amplifier plate dissipation is found by analyzing the constant current characteristics of the 4CX-35000C, as shown in Table 4. The theoretical result is compared with an experimental value determined by recording the inlet temperature and outlet temperature of the air cooling the plate of the 4CX-35000C. The power lost in the matching network and coupling coil is estimated from known power losses of similar matching networks used in high powered radio transmitters.

CHAPTER VI

DATA ANALYSIS

The oscillograph recordings of the attenuated and non-attenuated laser scans are a function of y , the distance the beam passes from the axis or the plasma, as shown in Figure 26. In order to determine the transmitted intensity profile, the ratio of the attenuated laser beam intensity to the laser beam intensity without the plasma in place is measured. Figure 27 illustrates some data of the attenuated and non-attenuated laser scans as recorded by the oscillograph. The fluctuations of the recorded laser intensity are due to the physical characteristics of the plasma torch and are reproducible from one data run to another provided that the system is not changed. The spatial and spectral filters attached to the photomultiplier tube reduce the background intensity of the plasma to a level about three orders of magnitude below the laser intensity. Figure 28 is a typical graph of the transmitted intensity profile as a function of axial distance.

The transmitted intensity data as a function of axial distance, y , are transformed to opacity as a function of radius by a modified Abel inversion technique. This is done by considering a given cross section of the plasma to be divided into M zones of radii R/M , $2R/M$, ..., and R , as indicated in Figure 26. The laser beam is passed through the plasma at various distances y from the axis and the attenuation $I(y)/I_0$ is

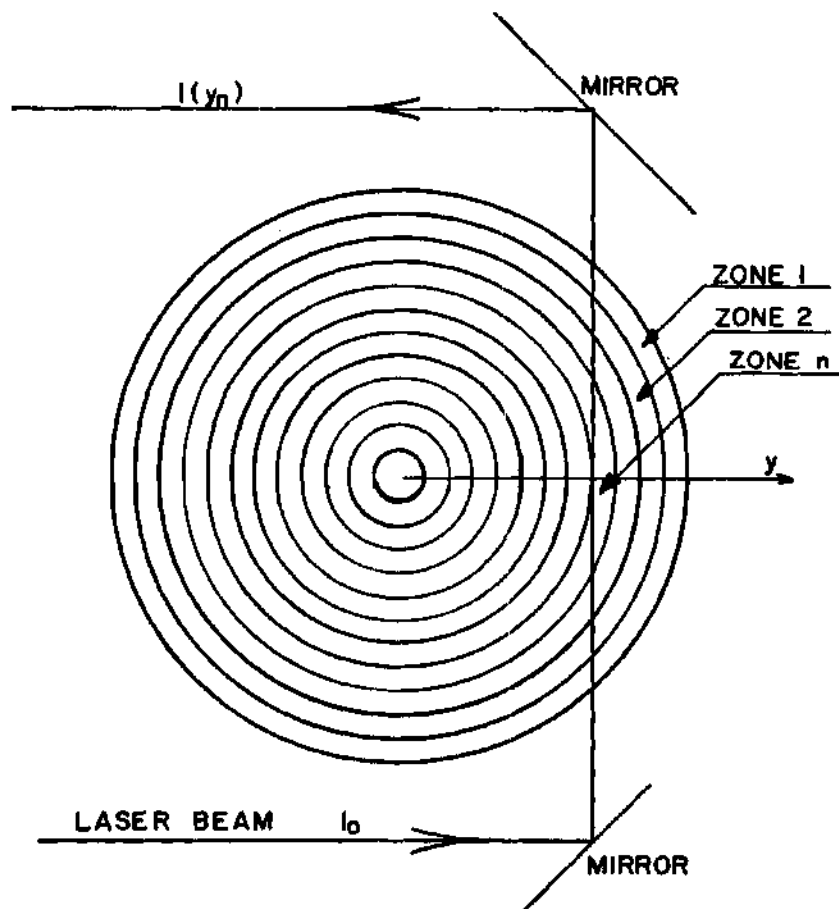


Figure 26. Laser Beam Passing Through Plasma

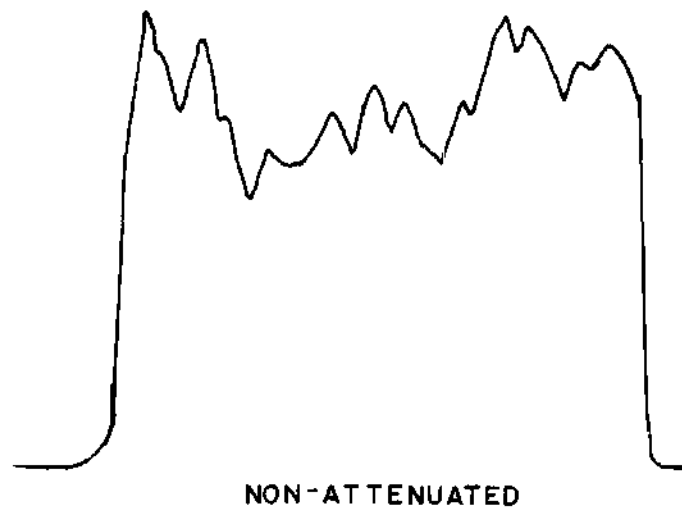
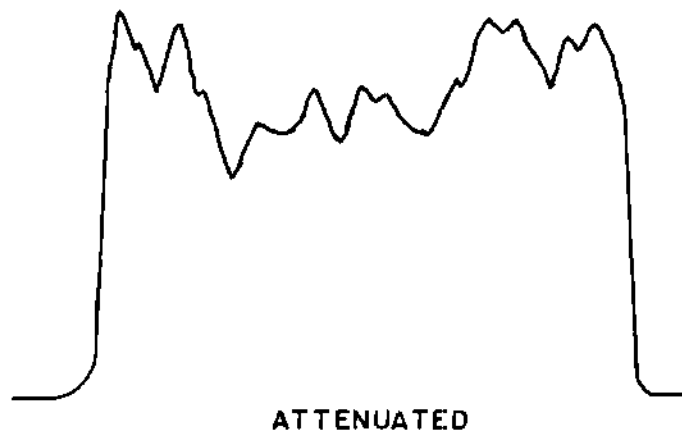


Figure 27. Oscilloscope Recordings for Attenuated and Non-attenuated Laser Scans

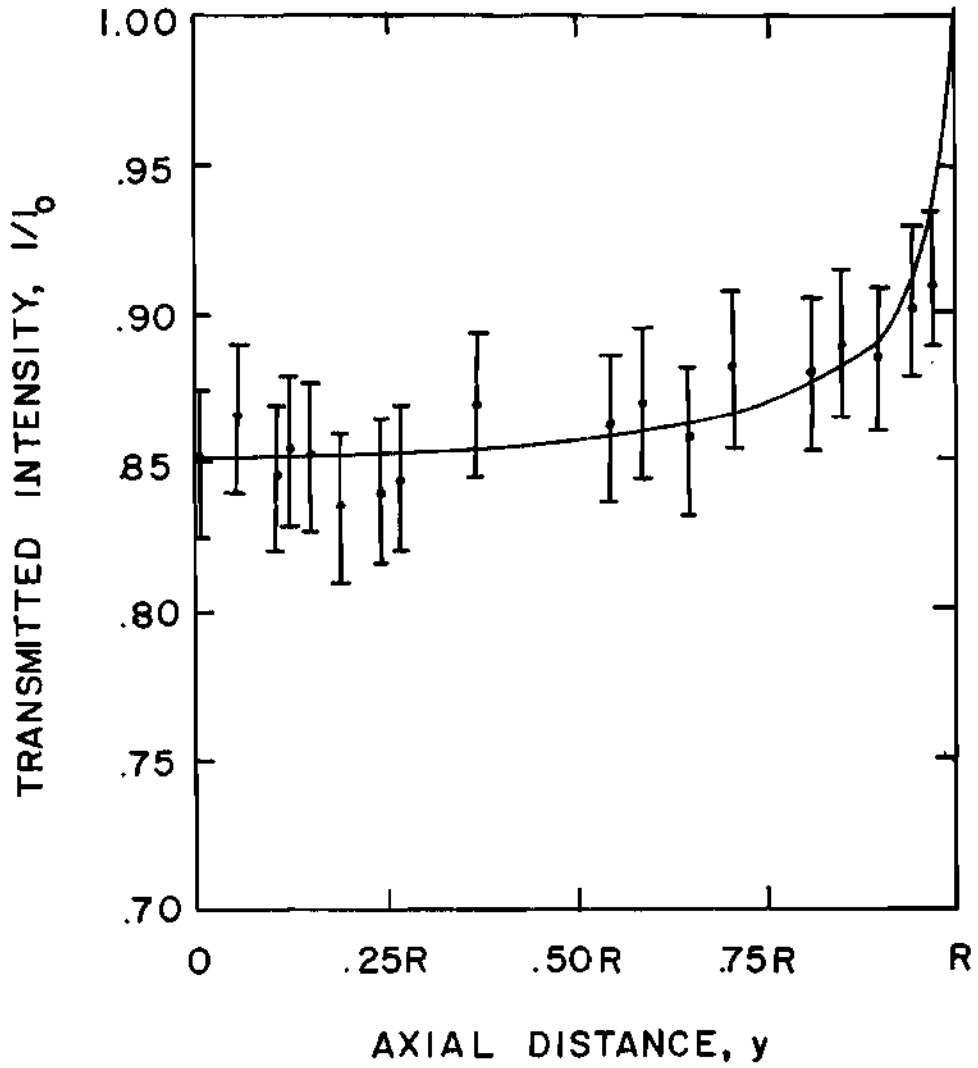


Figure 28. Ratio of Attenuated to Non-attenuated Laser Intensity as a Function of Axial Intensity

measured, as is illustrated by Figure 28. The radius R is taken to be the distance from the axis at which the attenuation is zero ($I(R)/I_0 = 1$). For the purpose of this analysis, the zones will be numbered 1 through M starting with the outermost zone. The thickness Δy of each zone is R/M . Consider now a laser beam passing a distance $y_1 = R - \Delta y$ from the axis of the plasma. This beam will be attenuated by $I(y_1)/I_0$ after passing through a distance $2X_1^1$, where $X_1^1 = [R^2 - (R - \Delta y)^2]^{\frac{1}{2}}$, of zone 1. Thus the opacity k_1 of zone 1 is given by

$$k_1 = -\frac{1}{2X_1^1} \ln \frac{I(y_1)}{I_0} \quad (37)$$

When the laser beam passes a distance $y_2 = R - 2\Delta y$ from the axis, it passes first through a thickness X_2^1 of zone 1, then a thickness $2X_2^2$ of zone 2, then finally a thickness X_2^1 of zone 1, and is attenuated by $I(y_2)/I_0$. X_2^1 and X_2^2 are given by

$$X_2^2 = [R - \Delta y]^2 - (R - 2\Delta y)^2]^{\frac{1}{2}} \quad (38)$$

$$X_2^1 = [R^2 - (R - 2\Delta y)^2]^{\frac{1}{2}} - X_2^2 \quad (39)$$

then

$$\frac{I(y_2)}{I_0} = e^{-k_1 X_2^1} \times e^{-2k_2 X_2^2} \times e^{-k_1 X_2^1} \quad (40)$$

or

$$e^{2k_1 X_2^1} \frac{I(y_2)}{I_0} = e^{-2k_2 X_2^2} \quad (41)$$

and

$$k_2 = -\frac{1}{2X_2^2} \ln \left[\frac{I(y_2)}{I_0} e^{2k_1 X_2^1} \right]. \quad (42)$$

If this analysis is continued, it can be shown that, in general, the opacity of the n^{th} zone is given by

$$k_n = -\frac{1}{2X_n^n} \ln \left[\frac{I(y_n)}{I_0} e^{2 \sum_{i=1}^{n-1} k_i X_n^i} \right] \quad (43)$$

where $y_n = R - n\Delta y = R$ (44)

and $X_n^i = R \left[\left(1 - \frac{i-1}{M}\right)^2 - \left(1 - \frac{n}{M}\right)^2 \right]^{\frac{1}{2}} - \sum_{j=i+1}^n X_n^j$ (45)

where $i = 1, 2, \dots, n$ and $X_n^{n+1} = 0$.

Although the Abel inversion uses 40 zones, the transmitted intensity as a function of axial distance is not calculated specifically for these 40 zones. As seen from Figure 27, the oscillograph recordings of the attenuated and non-attenuated laser scans are not perfectly smooth, but rather have a series of peaks and depressions. The transmitted intensity curve, Figure 28, is calculated only at points easily identified. The transmitted intensity curve which is used in the Abel inversion is not this raw data, but a smooth curve which best fits the 20 to 30 points calculated for the transmitted intensity profile.

The transmitted intensity profile is further modified in order to correct for known errors in the outermost zones. One source of error in the outer zones is due to the fact that the torch and laser beam are not necessarily lined up perfectly, shown in Figure 29. This improper alignment of the laser beam with the plasma torch results from a rotation of the plasma torch, which does not exceed two degrees. If the laser

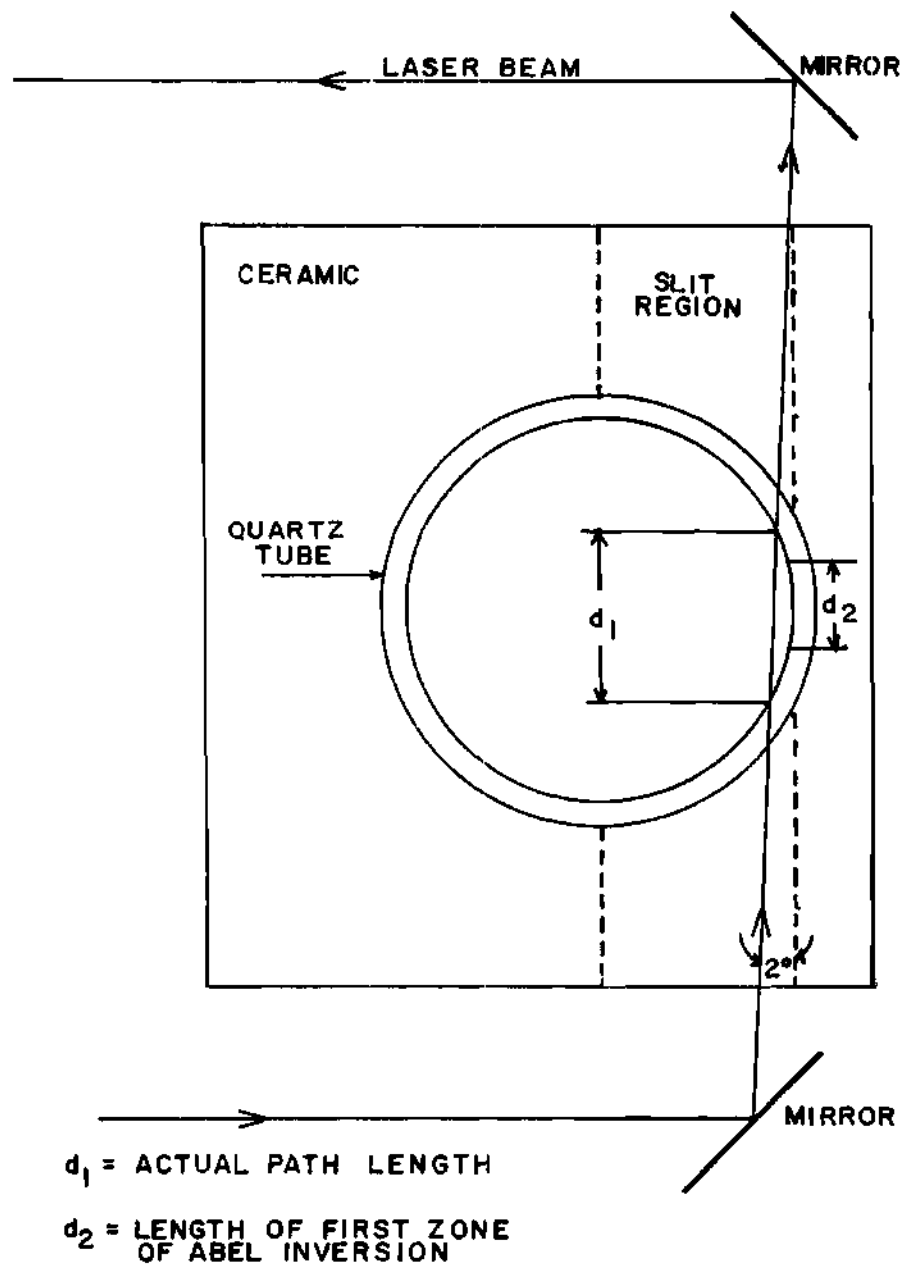


Figure 29. Errors Encountered in Analyzing Outer Zones of Plasma Torch

beam does not pass precisely through the outermost zone, it is seen from Figure 29 that the initial information recorded by the oscillograph does not correspond to the laser beam being attenuated by the first zone of the Abel inversion method. The actual path length over which the laser beam is attenuated for a two degree rotation of the plasma torch is 30 percent greater than the path length corresponding to the first zone of the Abel inversion. The error due to improper alignment of the torch decreases very rapidly after this first zone. Another source of error for the outer zones is due to the aerosol penetrating into the slit region of the plasma torch. Visual observation of aerosol flow indicates that, for the time periods which the aerosol is allowed to flow while data are being taken which are as short as possible, the aerosol penetrates about .05 inch into the slit region. This penetration of the aerosol into the slit region of the torch results in actual attenuated path length of the outermost zone being 50 percent greater than the path length used in the Abel inversion. This error is reduced to 11 percent by the fourth zone, which corresponds to .9 R. These two sources of error tend to make the calculated opacity of the outer zones higher than the actual opacity of these zones, and the Abel inversion carries these errors through in calculating the opacity of the remaining zones.

In order to minimize these errors, the transmitted intensity profile is not used exactly as recorded, but modified in the first three zones. These zones correspond to a region of the plasma torch within .1 inch of the torch wall, well outside the plasma region. The greatest thermal gradients within the plasma torch occur at the edge of the plasma,²¹

and it is reasonable to believe that the thermal gradients near the wall of the torch are relatively flat. It is assumed that the actual opacity of these first four zones does not vary greatly from zone to zone, and the transmitted intensity profile is modified to reflect this assumption. The transmitted intensity for the first three zones is changed so that the calculated opacity of these three zones is about the same as the opacity of the fourth zone (.9 R). The errors due to the rotation of the plasma torch and penetration of aerosol into the slit region should total no more than 12 percent for the fourth zone.

It has been determined by recording the helium-neon laser output with the oscillograph that variations in laser intensity and recording instruments do not deviate more than one percent from the average. An error of less than one percent is encountered in measuring the attenuated and non-attenuated laser intensity from the oscillograph recording. The total error in measuring each point for the transmitted intensity profile is thus three percent, as shown by Figure 28. It is important that many different points be plotted so that a curve fitting these points is clearly established. Although the error in the transmitted intensity curve is only three percent, the error in the opacity profile is greater because the Abel inversion technique which calculates the opacity is sensitive to small changes in the shape of the transmitted intensity curve. It has been found that changing the transmitted intensity curve within the expected limits of error causes changes of about 25 percent in calculated opacity.

The errors associated with determining the aerosol seed density are related to weighing the filter paper and seed sample and reading the

manometer connected to the sampling tank. The filter paper and seed sample are weighed within .0005 gram. The weight of a seed sample taken from a thin aerosol is about .0200 gram, indicating a maximum error of 3.5 percent due to weighing. The mercury manometer can be read within 1 mm. A typical change in pressure of the sampling tank is 50 mm, so the maximum error in recording sampling tank pressure is two percent. The aerosol density is calculated from

$$\rho = \frac{(w_2 - w_1) H_1}{(H_1 - H_2) V} \quad (46)$$

where w_2 and w_1 are final and initial filter weights, H_2 and H_1 are the final and initial manometer readings, and V is the volume of the sampling system. This indicates that the total error in seed density should be less than five percent; however, it is possible that there are other errors which are not so easily estimated. A certain amount of the seed sample collects on the aerosol line leading to the filter holder. This line has been designed to duplicate as closely as possible the aerosol line going to the plasma torch so that the aerosol reaching the sample filter should be nearly the same as the aerosol entering the plasma torch. It is the belief of the author that the total error in measuring aerosol density entering the plasma torch does not exceed 20 percent.

The error in calculating the extinction parameter (opacity/seed density) is the square root of the sum of the squares of the percent errors in opacity and aerosol density. The estimated error in calculating the extinction parameter is 32 percent.

CHAPTER VII

EXPERIMENTAL RESULTS

A 125 kilowatt radio frequency induction heater, as described in Chapter IV, has been designed and constructed to produce one atmosphere pressure hydrogen plasmas seeded with submicron sized metallic particles. These seeded plasmas simulate the working fluid of a gaseous core nuclear reactor. An air cooled plasma torch utilizing flat windows has been developed to allow for spectral observation of the plasma region, and initial opacity measurements of the seed-hydrogen opacity window have been made.

In order to test the accuracy of the laser scanning and attenuation measurement system, data were taken using a standard plasma torch with a flow of tungsten seeded hydrogen. For these data the plasma generator was not operated. As was the case for each data run, the size of the tungsten particles was from .1 to .2 micron. This data run was taken to duplicate the one atmosphere room temperature experimental data taken by A. Shenoy,³³ and to determine if the transmitted intensity profile and Abel inversion technique yielded a relatively flat opacity profile. A flat opacity profile would indicate equal distribution of the aerosol throughout the plasma torch. The calculated opacity profile, Figure 30, for this aerosol varied from a low of $.146 \text{ cm}^{-1}$ to a high of $.168 \text{ cm}^{-1}$; a very low range, indicating the relative accuracy of the data

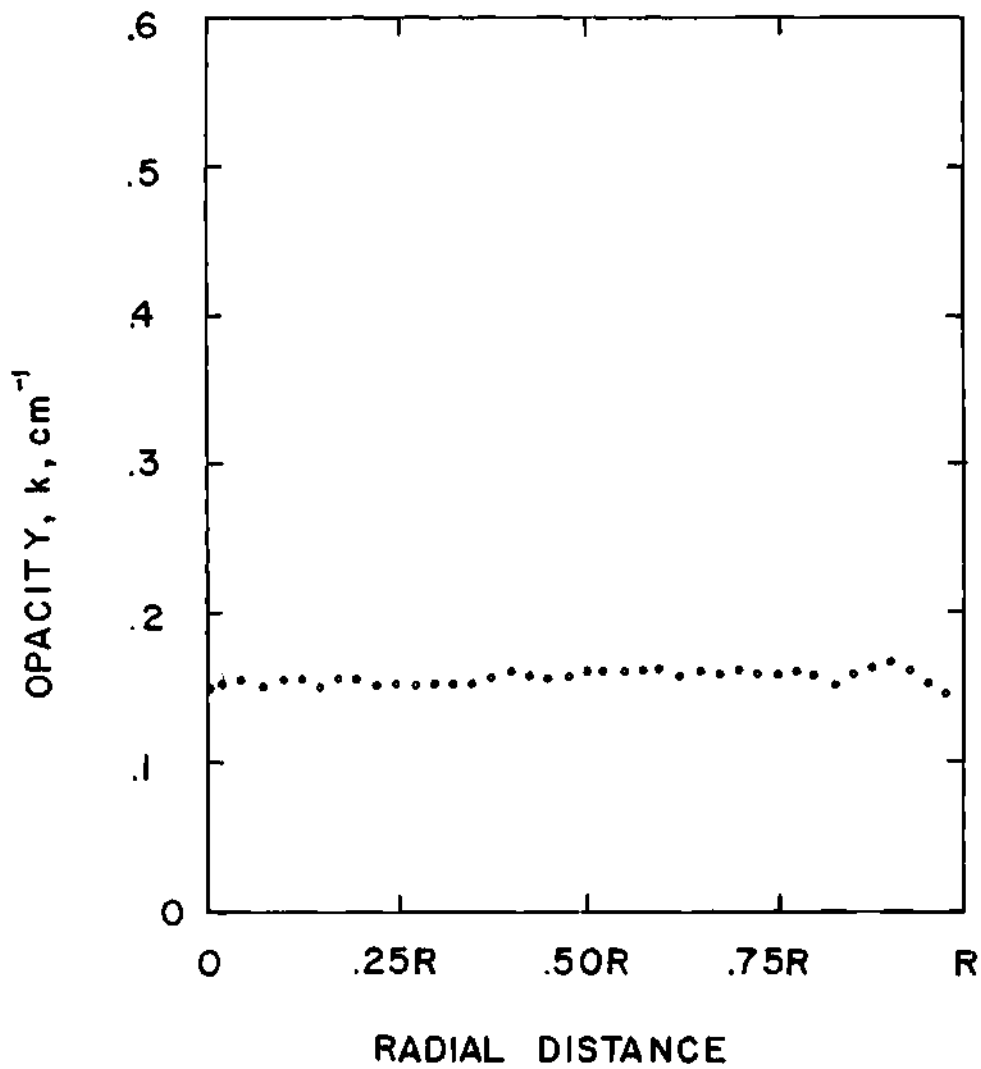


Figure 30. Opacity Profile of Room Temperature Tungsten Seeded Hydrogen

analysis method utilizing the modified Abel inversion technique. The aerosol density for this room temperature (295°K) data run was measured at $12.3 \times 10^{-6} \text{ gm/cm}^3$. This corresponds to an extinction parameter (k/ρ) of $1.27 \times 10^4 \text{ cm}^2/\text{gm}$ when an average value of $.157 \text{ cm}^{-1}$ is measured for k . This compares very well to the value of $1.01 \times 10^4 \text{ cm}^2/\text{gm}$ measured by A. Shenoy³³ for the same sized tungsten particles at the same wavelength of 6328 Å.

Once a degree of confidence was established in the scanning system and the Abel inversion technique, initial data were taken in the seed-hydrogen opacity window with a helium-neon laser. The data presented in Figures 31, 32, and 33 represent the results of the best and most accurate of many data runs. A large proportion of data runs were unsuccessful for various reasons. About 25 percent of the torches constructed arced from the starting electrode to the coupling coil during plasma starting operation. Of the torches which were successfully started, another 15 percent arced before the power could be raised high enough to sustain a seeded hydrogen plasma. Even for the torches which were capable of sustaining a seeded-hydrogen plasma, further difficulties sometimes were encountered. Several attempted data runs were unsuccessful because of failure of the scanning system or recording system to operate properly, or because of failure to take a proper seed sample at the correct time. Occasionally what appeared to be a good seeded hydrogen data run was ruined because the quartz of the torch had softened and obstructed any further scanning by the laser, which meant that the laser scan of the torch after a data run was impossible.

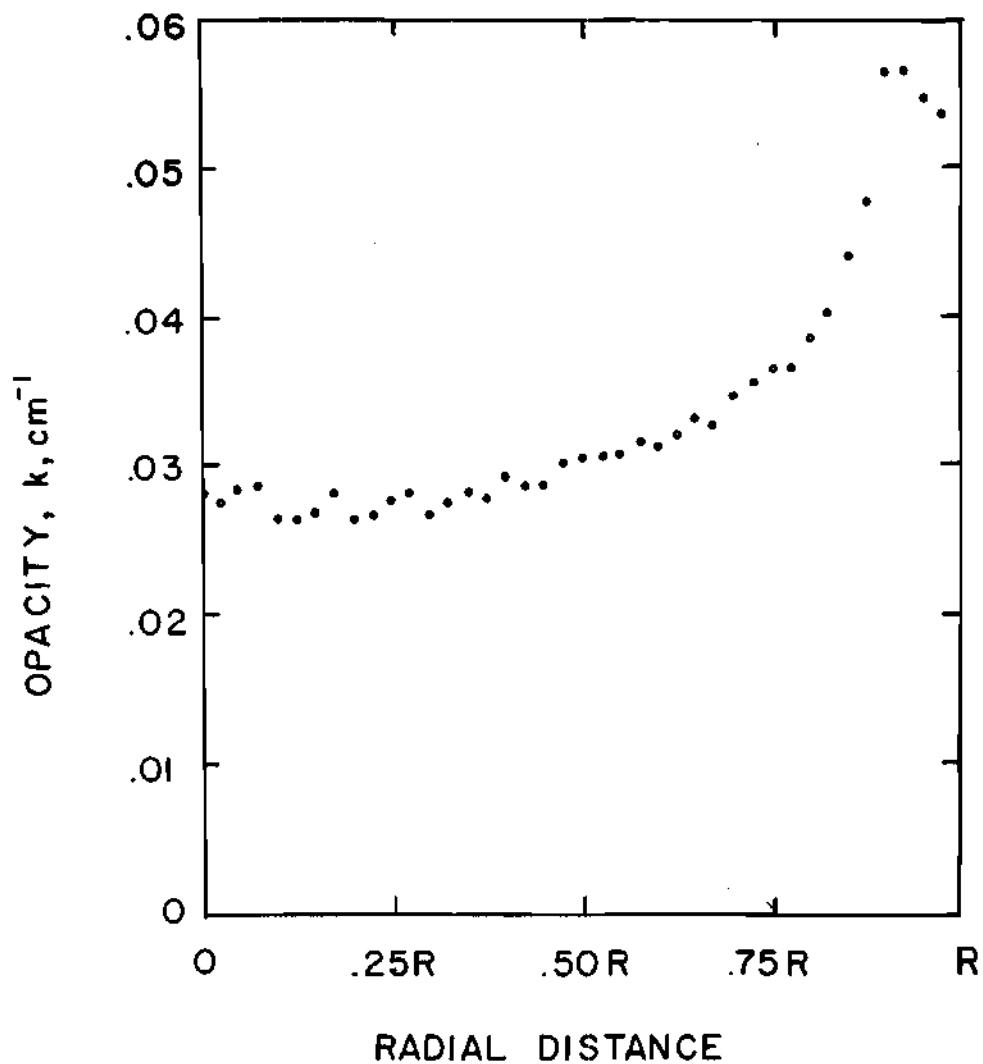


Figure 31. Opacity Profile of Tungsten-Hydrogen Plasma with Inlet
Aerosol Density of $41.5 \times 10^{-6} \text{ gm/cm}^3$

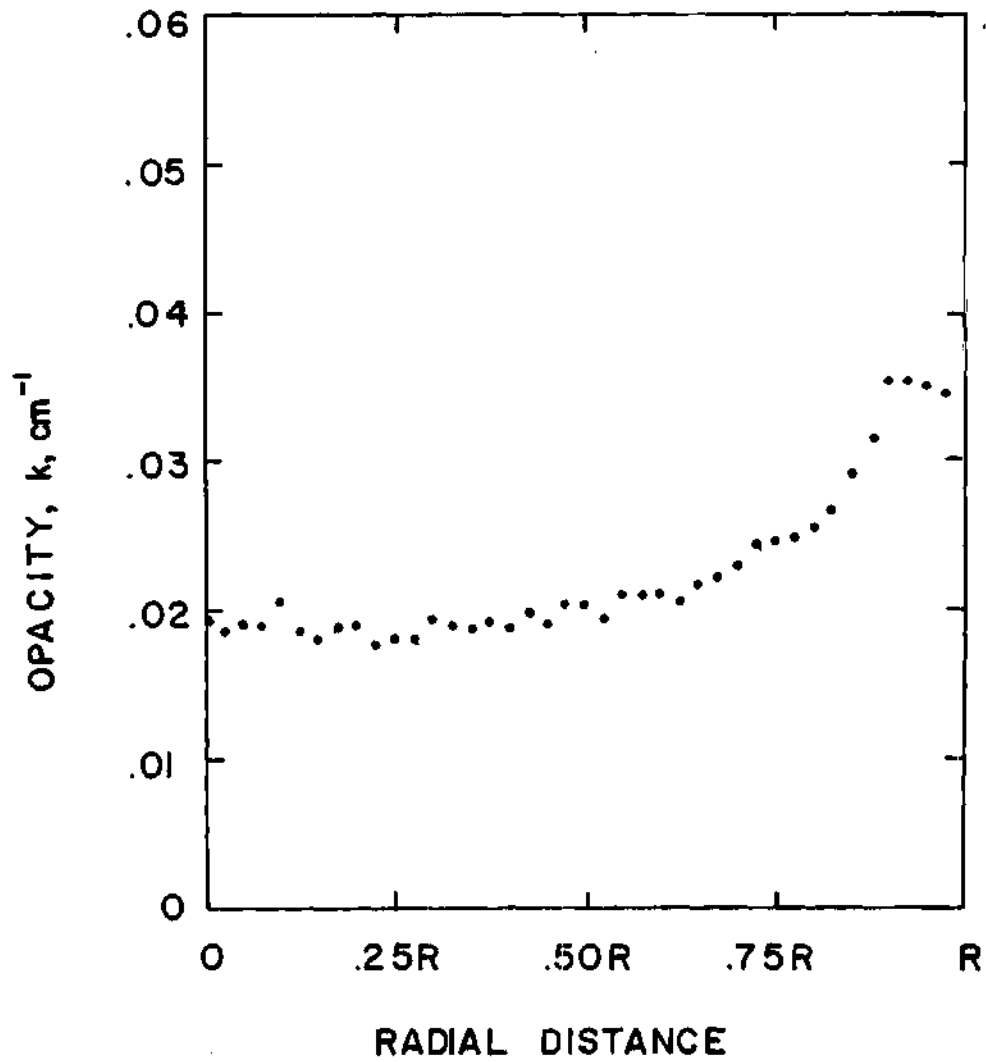


Figure 32. Opacity Profile of Tungsten-Hydrogen Plasma with Inlet Aerosol Density of $30.5 \times 10^{-6} \text{ gm/cm}^3$

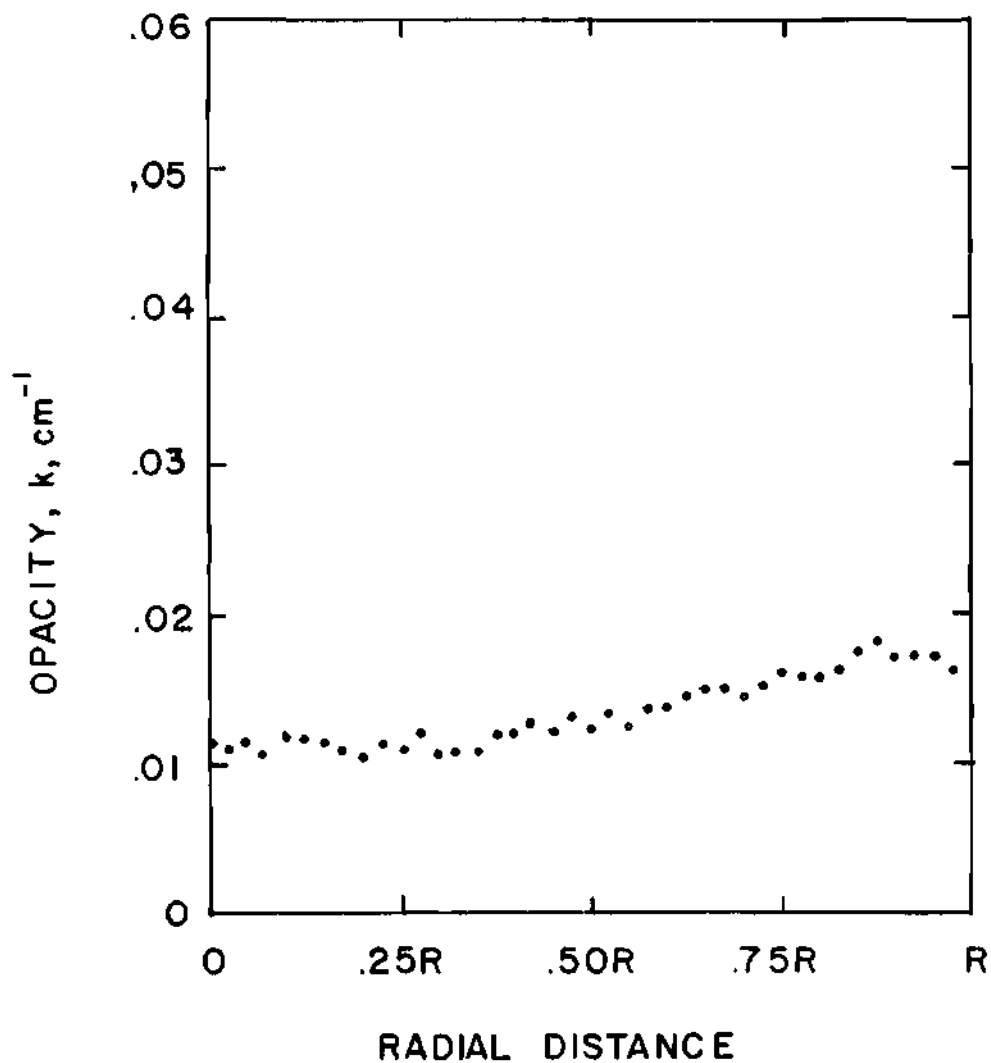


Figure 33. Opacity Profile of Tungsten-Hydrogen Plasma with Inlet Aerosol Density of $16.9 \times 10^{-6} \text{ gm/cm}^3$

Figure 31 is the measured opacity profile for a tungsten seeded hydrogen plasma with an inlet aerosol density of $41.5 \times 10^{-6} \text{ gm/cm}^3$. The maximum opacity value occurs near the wall of the plasma torch, well beyond the plasma region. Tungsten particles exist in this region, and the attenuation of the laser beam is due to the same mechanisms described by A. Shenoy and W. Partain.³³ During seeded hydrogen plasma operation the torch wall operates near the softening point of quartz, about 1950°K , and it is reasonable to assume that the hydrogen aerosol in this region is near the temperature of 2000°K . Assuming that the tungsten aerosol is distributed according to the hydrogen density, a seed density of $6.10 \times 10^{-6} \text{ gm/cm}^3$ exists in this region near the torch wall. The measured opacity of $.055 \text{ cm}^{-1}$ in this region corresponds to an extinction parameter of $.9 \times 10^4 \text{ gm/cm}^2$, which also compares favorably with the experimental data taken in this research and with data taken by A. Shenoy.³³ This tends to validate the assumptions made about the temperature profile and aerosol distribution in the region near the wall of the torch.

The opacity decreases from a value of $.055 \text{ cm}^{-1}$ at a radius of $.9 \text{ R}$ to a value of $.031 \text{ cm}^{-1}$ at a radius of $.55 \text{ R}$. The radius of $.55 \text{ R}$ corresponds roughly to the "edge" of the plasma. The "edge" of the plasma is taken to be the region where the plasma intensity is noticeably reduced from the intensity of the center region of the plasma. The opacity of the plasma region is fairly constant at a value of $.028 \text{ cm}^{-1}$. The flat opacity profile in the plasma region indicates that the temperature profile in this region is also fairly flat. Plasma diagnostic work done by United Aircraft with induction heated argon plasmas has shown that the

temperature profile of an induction plasma is relatively flat with about a five percent drop in temperature near the center.²³ Figures 31, 32, and 33 show a slight opacity increase near the center of the plasma, which according to theoretical work discussed in the Appendix, indicates a slight drop in the temperature of this region.

A heat balance on a tungsten seeded hydrogen plasma shows that the plasma equivalent black-body radiating temperature is 4100°K and that the actual plasma temperature is 8700°K . Once again assuming uniform distribution of tungsten in the plasma torch, a tungsten density of about $1.43 \times 10^{-6} \text{ gm/cm}^3$ existed in the plasma region of the torch during this data run. The experimental opacity of $.028 \text{ cm}^{-1}$ for this tungsten density compares to Krascella's theoretical value of $.005 \text{ cm}^{-1}$. It was not expected that the experimental and theoretical values would closely match, due to the fact that Krascella's theoretical research, as discussed in the Appendix, is only a semi-empirical model based upon several questionable assumptions.

Figures 32 and 33 show opacity data for seeded hydrogen plasmas with inlet aerosol densities of $30.5 \times 10^{-6} \text{ gm/cm}^3$ and $16.9 \times 10^{-6} \text{ gm/cm}^3$, respectively. Each opacity profile can be analyzed as done previously with similar results. The opacity profile of Figure 33 does not show as clearly the decrease in opacity in the plasma region. This is probably due to the errors discussed in Chapter VI, which are more prevalent with plasmas produced with low density aerosols.

It should be noted that, despite many attempts to measure pure hydrogen or argon opacity, no attenuation was ever noted in argon or

hydrogen plasmas which were not seeded with tungsten. Thus, all attenuation measured is due to the tungsten aerosol and vapor.

The equivalent black-body radiating temperature of the plasma was determined by performing a heat balance on the plasma generator. It was determined that approximately 70 kilowatts was effectively coupled to a plasma load with a surface area of about 6.9 sq in. The assumption is made here that all the energy coupled to the plasma is radiated. This is an assumption frequently made in studies of argon plasmas.^{22,23} Although hydrogen has a higher thermal conductivity, the seeded plasmas are much more opaque at lower temperatures, and this increased opacity therefore results in greater thermal radiation at lower operating temperatures. This is a radiant heat flux of 15.9 kW/in², or a black-body radiating temperature of 4100°K. Assuming an emissivity of .05, a value which corresponds to the measured opacity shown in Figure 31, a plasma temperature of 8700°K results.

CHAPTER VIII

CONCLUSIONS AND RECOMMENDATIONS

Conclusions

One atmosphere pressure hydrogen plasmas, seeded with metallic particles to simulate the working fluid of a gaseous core nuclear reactor, have been produced by a suitably designed radio frequency induction heating generator operated at four MHz. Approximately 110 kilowatts of input power to the plasma generator is required to sustain a seeded hydrogen plasma. The plasma must be initiated with a flow of pure argon at a reduced power level of about five kilowatts.

A two inch diameter, air cooled, plasma torch has been developed which has flat windows to allow for spectral observations of the plasma. The plasma torch has a relatively short life (60 to 180 seconds) during seeded hydrogen operation. The equivalent black body radiating temperature of a seeded hydrogen plasma produced in this torch is about 4000°K , which corresponds to an actual plasma temperature of about 8000°K .

The opacity of the plasma was measured by scanning the plasma with a helium-neon laser and recording the transmitted intensity as a function of axial distance from the center of the plasma. A modified Abel inversion technique transformed these data to radial dependent opacity data. Measurements on a tungsten aerosol with no plasma present yielded an extinction parameter of $1.27 \times 10^4 \text{ cm}^2/\text{gm}$, which showed the reliability of the opacity measurements and the accuracy of the Abel inversion technique.

The attenuation of one atmosphere pressure hydrogen and argon plasmas is negligible as far as this research is concerned. All attenuation is due to the tungsten aerosol and vapor.

Using a helium-neon laser the measured opacity of a tungsten seeded hydrogen plasma is $.028 \text{ cm}^{-1}$ for an inlet aerosol density of $41.5 \times 10^{-6} \text{ gm/cm}^3$. This corresponds to an extinction parameter of $(1.95 \pm .62) \times 10^4 \text{ cm}^2/\text{gm}$, which is typical of all opacity data taken during this research. The seed-hydrogen opacity window expected in the temperature range which extends from the vaporization point of tungsten (5000°K) to the point where hydrogen itself becomes opaque ($10,000^\circ \text{K}$) does not appear to be as transparent as had been expected. The heat transfer in the gaseous core nuclear reactor evidently will not suffer much due to the seed-hydrogen opacity window.

Recommendations

It is evident that the opacity of the tungsten vapor should be measured at several points within the wavelength spectrum of interest since Krascella's theoretical research (see the Appendix) predicts that the opacity is significantly wavelength dependent.

Plasma diagnostic measurements to confirm the assumptions made relating to aerosol density distribution and temperature profiles should be conducted. Additional seed materials, such as uranium, should be studied. Since there is no attenuation in pure argon or hydrogen plasma, and all the attenuation is due to the tungsten aerosol and vapor, the plasma diagnostic research could be conducted using argon as the carrier gas. Under these conditions the torch life would be extended to over

half an hour, and maintenance required by the plasma generator would be sharply reduced. If this is not done, a better plasma torch utilizing water cooling possibly could be designed.

APPENDIX

ABSORPTION OF RADIANT ENERGY IN HYDROGEN AND TUNGSTEN VAPOR

At low temperature, the hydrogen atoms are essentially all in the ground state, and radiant energy of 1216 Å wavelength or shorter is required to excite or ionize the atom. This means that hydrogen atoms in the ground state are incapable of absorbing radiant energy of wavelengths greater than 1216 Å. At higher temperatures, a significant number of hydrogen atoms are thermally excited to the first excited state ($n = 2$). Radiant energy of wavelengths as long as 6563 Å will cause ionization. At slightly higher temperatures, the third excited state becomes sufficiently populated to permit significant absorption of radiant energy of wavelengths as long as 18,760 Å.^{48,49}

N. L. Krascella computed the theoretical composition (partial pressures of H_2 , H , H^+ , H^- , e^- , and quantum states 1 through 5 of H) and total spectral absorption of hydrogen for pressures from 1 to 1000 atmospheres, and for temperatures from 1667°K to 111,111°K. These characteristics were computed for wave numbers from 1000 cm^{-1} to $400,000 \text{ cm}^{-1}$.⁷ R. W. Patch performed similar calculations and included the hydrogen triatomic molecular ion, H_3^+ , in his work.^{50,51}

Krascella determined composition of the hydrogen by a simultaneous solution of the following relations⁷:

Dalton's law of partial pressure--

$$P = P_{H_2} + P_{H_2^+} + P_H + P_{H^+} + P_{H^-} + P_{e^-} \quad (\text{A-1})$$

Electrical Neutrality--

$$P_{H_2^+} + P_{H^+} = P_{H^-} + P_{e^-} \quad (A-2)$$

Dissociation of Hydrogen--

$$K_p = P_{H_2} / (P_H)^2 \quad (A-3)$$

where K_p is the equilibrium constant.

Saha equations--

$$P_{H^+} \left(\frac{P_{e^-}}{P_H} \right) = \frac{AT^{5/2}}{Q_H} \exp \left(- \frac{hc I_H}{kT} \right) \quad (A-4)$$

$$P_{H_2^+} \left(\frac{P_{e^-}}{P_{H_2}} \right) = 2AT^{5/2} \exp \left(- \frac{hc I_{H_2}}{kT} \right) \quad (A-5)$$

$$\frac{P_H P_{e^-}}{P_{H^-}} = A Q_H T^{5/2} \exp \left(- \frac{hc I_{H^-}}{kT} \right) \quad (A-6)$$

where Q_H is the partition function of atomic hydrogen, I_H is the ionization potential of atomic hydrogen, I_{H_2} is the ionization potential of molecular hydrogen, I_{H^-} is the ionization potential of the negative hydrogen ion, and A is the Saha equation constant. The partial pressures of the excited states were found from

$$P_{H(n)} = \frac{P_H g_n}{Q_H} \exp \left(- \frac{hc \omega_n}{kT} \right) \quad (A-7)$$

where g_n is the statistical weights of the n^{th} quantum level, and ω_n is

the term value of the n^{th} quantum level. Figure 34 illustrates the composition of hydrogen as a function of temperature at one atmosphere pressure.

Krascella included the following processes in calculating the spectral absorption coefficient:

a) Photoionization, or bound-free, transition, where H can have different principal quantum numbers.



The Lyman, Balmer, Ritz-Paschen, Brackett, and Pfund continua are considered on the basis of Kramer's continuum approximation:

$$a_{H(n)}^{\text{bf}} = \sigma_{H(n)} \frac{N_0 P_{H(n)}}{RT} \quad (\text{A-9})$$

where $a_{H(n)}^{\text{bf}}$ is the bound-free absorption coefficient of the $H(n)^{\text{th}}$ species in cm^{-1} , N_0 is Avogadro's number, R is the gas constant, $82.06 \text{ cm}^3 \text{ atm} \cdot (\text{mol}, ^\circ\text{K})^{-1}$, $P_{H(n)}$ is the partial pressure of the $H(n)^{\text{th}}$ species in atmospheres, T is the absolute temperature, $^\circ\text{K}$, and $\sigma_{H(n)}^{\text{bf}}$ is the bound-free cross-section of the $H(n)^{\text{th}}$ species.

$$\sigma_{H(n)}^{\text{bf}} = \frac{16 e^2 R_y^2 G_n^{\text{bf}}}{3\sqrt{3} m_e c^2 n^5 \omega^3} \quad (\text{5-10})$$

where e is the electronic charge, 4.8×10^{-10} esu, R_y is the Rydberg, $1.09 \times 10^5 \text{ cm}^{-1}$, G_n^{bf} is the bound-free Gaunt factor, m_e is the electron mass, c is the velocity of light, and ω is the wave number, cm^{-1} .⁵⁰

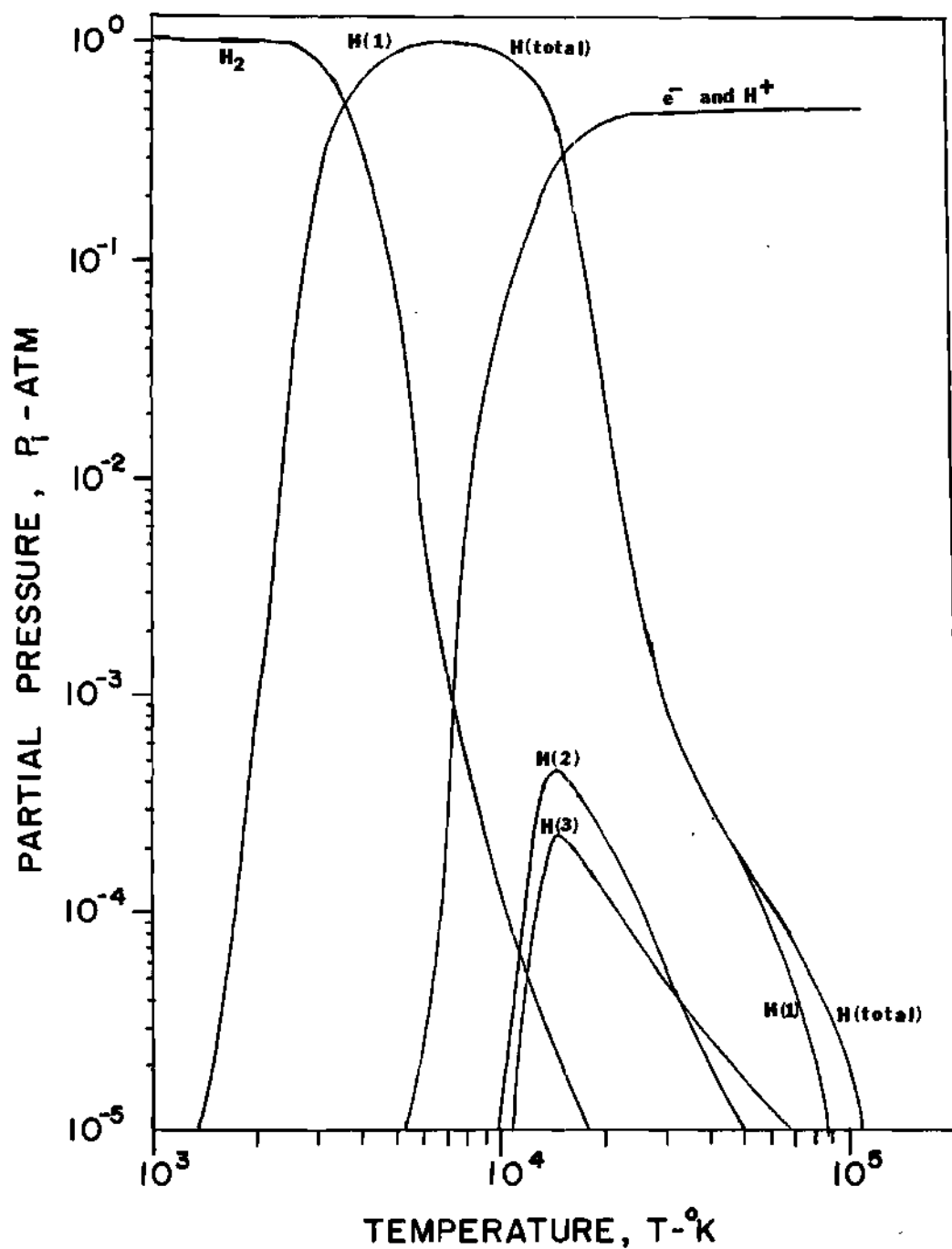
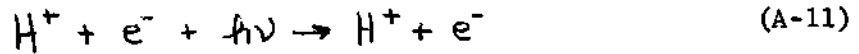


Figure 34. Composition of Hydrogen as a Function of Temperature at a Pressure of One Atmosphere (Reference 7)

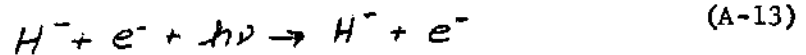
b) Positive hydrogen ion free-free transition, also known as inverse bremsstrahlung.



$$a_{H^+}^{ff} = \sigma_{H^+}^{ff} \frac{N_0 P_{H^+}}{RT} \quad (A-12)$$

where $a_{H^+}^{ff}$ is the free-free absorption coefficient of the H^+ species, and $\sigma_{H^+}^{ff}$ is the free-free cross-section of the H^+ species. Expressions for $\sigma_{H^+}^{ff}$ are given in References 7 and 52.

c) Negative hydrogen ion free-free transitions.



$$a_{H^-}^{ff} = \sigma_{H^-}^{ff} \frac{N_0 P_H P_{e^-}}{RT} \quad (A-14)$$

The free-free cross-section of the H^- ion species is given in References 7 and 53.

d) Negative hydrogen ion bound-free transition.



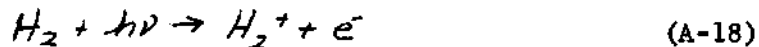
$$a_{H^-}^{bf} = \sigma_{H^-}^{bf} \frac{N_0 P_{H^-}}{RT} \quad (A-16)$$

The bound-free cross-section of the H^- species is tabulated in References 7 and 54.

e) Photodissociation and photoionization of the hydrogen molecule. These transitions were considered collectively because the sum of the two absorption coefficients is measured experimentally.



This is photodissociation where H_2 is assumed to be in the ground state, and H^* is in an electronically excited state.



This is photoionization. Both of these transitions are bound-free. The bound-free absorption coefficient for these transitions is given by

$$\alpha_{H_2}^{bf} = \sigma_{H_2}^{bf} \frac{N_0 P_{H_2}}{RT} \quad (\text{A-19})$$

where the bound-free cross-section of H_2 is listed in Reference 7.

f) The wings of the Lyman- α resonance line of atomic hydrogen.

$$\alpha_{H(1)}^{bb} = \sigma_{H(1)}^{bb} \frac{N_0 P_{H(1)}}{RT} \quad (\text{A-20})$$

where the bound-bound cross-section of $H(1)$ is given by

$$\sigma_{H(1)}^{bb} = \frac{e^2}{mc^2} f_{\alpha} \frac{\Gamma}{T} \left(\frac{\omega}{\omega_0} \right)^2 \left[\frac{1}{(\omega - \omega_0)^2 + \Gamma^2} + \frac{1}{(\omega + \omega_0)^2 + \Gamma^2} \right] \quad (\text{A-21})$$

where f_{α} is the Lyman- α line oscillator strength, ω_0 is the wave number

of the Lyman- α line, $8.22 \times 10^4 \text{ cm}^{-1}$, ω is the wave number, and Γ_T is the total line half width.

$$\Gamma_T = \Gamma_R + \Gamma_C \quad (\text{A-22})$$

where Γ_R is the resonance broadened line half width, and Γ_C is the collision broadened line half width.

Patch's work on hydrogen opacity differed from that of Kracella mainly on two points. Patch concluded that Krascella's expression for the absorption of the Lyman- α line was accurate only over a very small range of wave numbers about the line center. Patch neglected absorption of the far wings of the Lyman- α resonance line because of the lack of valid theory, believing that this procedure caused less error than including it incorrectly. Patch's work also included the hydrogen triatomic molecular ion H_3^+ in the composition. Patch found that including the H_3^+ significantly increased the number densities of e^- and H^- at high pressures. However, number densities of e^- and H^- were less dependent on the inclusion or neglect of H_3^+ at lower pressures.^{8,50} Krascella calculated the theoretical spectral opacity of 100 atmosphere hydrogen at $11,111^\circ \text{K}$ for 6667 \AA to be $.337 \text{ cm}^{-1}$, compared to $.272 \text{ cm}^{-1}$ calculated by Patch.

At temperatures above the boiling point of the seed material (approximately 5600°K for tungsten) evaporated seeds will absorb radiation at high wave numbers (short wavelengths) by bound-free transitions, and at low wave numbers (long wavelengths) by bound-bound transitions, which give rise to spectral lines. In some gases spectral "windows" between the widely spaced bound-bound transitions occur. Heavy atom gases usually have dense line structure over wide spectral regions, and although there

are small "windows" between each of these lines, the "windows" are essentially eliminated due to line broadening.⁵⁵ An exact analytical determination of the composition and opacity of heavy atom gases is not possible due to lack of information concerning ionization potentials, term values, and oscillator strengths, and to the extreme spectral complexity of the species involved. Estimates of the opacity of tungsten gas have been arrived at using a semi-empirical model. This work was done by N. L. Krascella at United Aircraft Corporation.

The principal assumptions in the analytical description of the atomic model are:

- 1) All energy levels are uniformly spaced and degenerate.
- 2) Energy level spacing is small relative to the ionization potential of the species.
- 3) All upward transitions are allowed, and all downward transitions are prohibited.
- 4) An oscillator strength sum rule is applicable.
- 5) A modified oscillator strength band-type distribution in the bound-bound region which is varied to match the calculated tungsten line spectrum to measured results is assumed.

The model tungsten atom consists of a number of equally spaced energy levels, ξ_i , for each ionization species, with the actual number of levels being a function of species ionization potential, I_i , and the mean level spacing, τ_i (Figure 35). Ionization potentials for the treated ionization species (neutral, and singly ionized) were taken to be 7.98 eV and 14.0 eV.⁵⁶ A mean level spacing of .4 eV was employed. This value was selected on the basis of an examination of known spectral data for

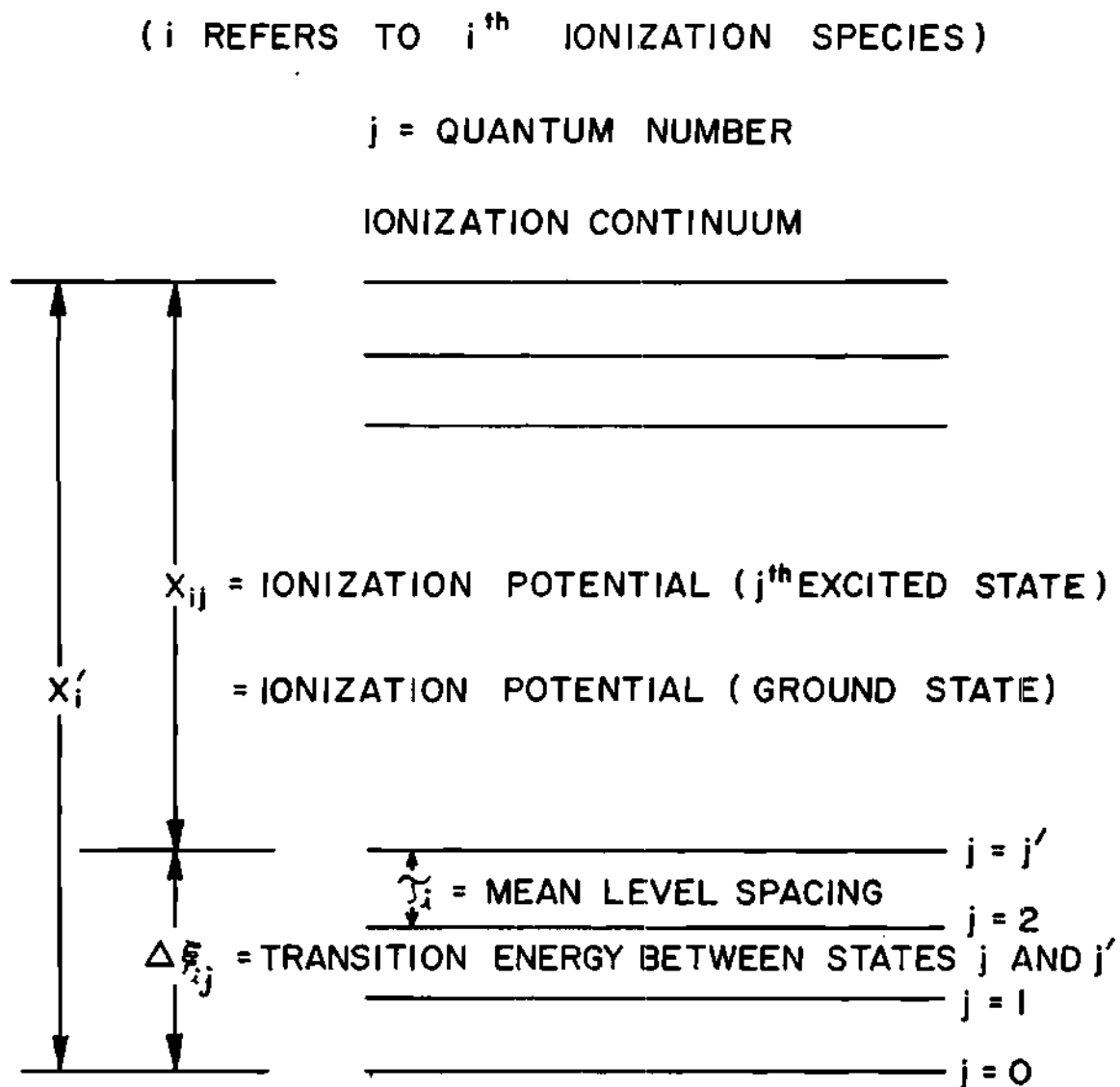


Figure 35. Energy Level Diagram of the Model Fuel Atom
(Reference 55)

heavy atom gases.^{29,57} Examination of Figure 35 shows the following relationships to hold:

Ionization potential from level j ,

$$X_j = I' - (j-1)\tau \quad (\text{A-23})$$

Energy of level j ,

$$E_j = (j-1)\tau \quad (\text{A-24})$$

Energy difference between levels of j and j' ,

$$\Delta E_{jj'} = (j' - j)\tau \quad (\text{A-25})$$

Wave number of spectral line,

$$\omega_{jj'} = \frac{\Delta E_{jj'} B_1}{hc} = \frac{(j' - j)\tau}{hc} B_1 \quad (\text{A-26})$$

where B_1 is a conversion factor, 1.602×10^{-12} erg-ev⁻¹. It should be noted that the subscript i refers to a species, while the j subscripts refer to atomic energy levels.

Some knowledge of the transition probabilities or oscillator strengths associated with the transitions under consideration is required in order to calculate the spectral opacity of a species. Relatively little is known of the oscillator strengths in heavy atom species. It was necessary to specify a procedure to describe the distribution of oscillator strength with photon energy. Krascella assumed a hydrogenic distribution of oscillator strength to apply in the bound-free spectral region

$\left(\frac{df^{bf}}{dE} \propto \frac{1}{E}\right)$. In the bound-bound region (below a photon energy corresponding to the ionization potential X_{ij}) an oscillator strength distribution

of the following form was assumed.

$$\left(\frac{df^{bb}}{dE}\right)_{ij} = b_i \left[\sum_j a_{ij} \sin^2 \left\{ m_i \pi \left(\frac{X_{ij} - E}{X_{ij}} \right) \right\} + d_i \right] \quad (\text{A-27})$$

where a_{ij} are arbitrary amplitudes, m_i the number of peaks, and d_i are constants of arbitrary magnitude. Figure 36 shows schematically the oscillator strength distribution. The quantities a_{ij} , m_i , and d_i of equation A-27 were adjusted until the major features of the experimental intensity data for neutral tungsten were reproduced. The normalization factor b_i in equation A-27 was adjusted to satisfy the sum rule, which states that the total oscillator strength is of the order of the number of valence electrons, V_N ,⁵⁹ such that,

$$\int_0^{X_{ij}} \left(\frac{df^{bb}}{dE}\right)_{ij} dE + \int_{X_{ij}}^{\infty} \left(\frac{df^{bf}}{dE}\right) dE = 2.0 \quad (\text{A-28})$$

Krascella arbitrarily fixed V_N at 2.0 to account for the possibility of more than one valence electron. The oscillator strength in the bound-free region is given by⁵⁷

$$\left(\frac{df^{bf}}{dE}\right)_{ij} = \frac{2A_1 X_{ij}^2}{E^3}, \quad E > X_{ij} \quad (\text{A-29})$$

where A_1 is a constant found by extrapolating equation A-29 to zero energy and applying the sum rule. The constant A_1 is found from

$$\int_0^{\infty} \left(\frac{df^{bf}}{dE}\right) dE = \int_0^{\infty} \frac{2A_1 X_{ij}^2}{E^3} dE = V_N = 2.0 \quad (\text{A-30})$$

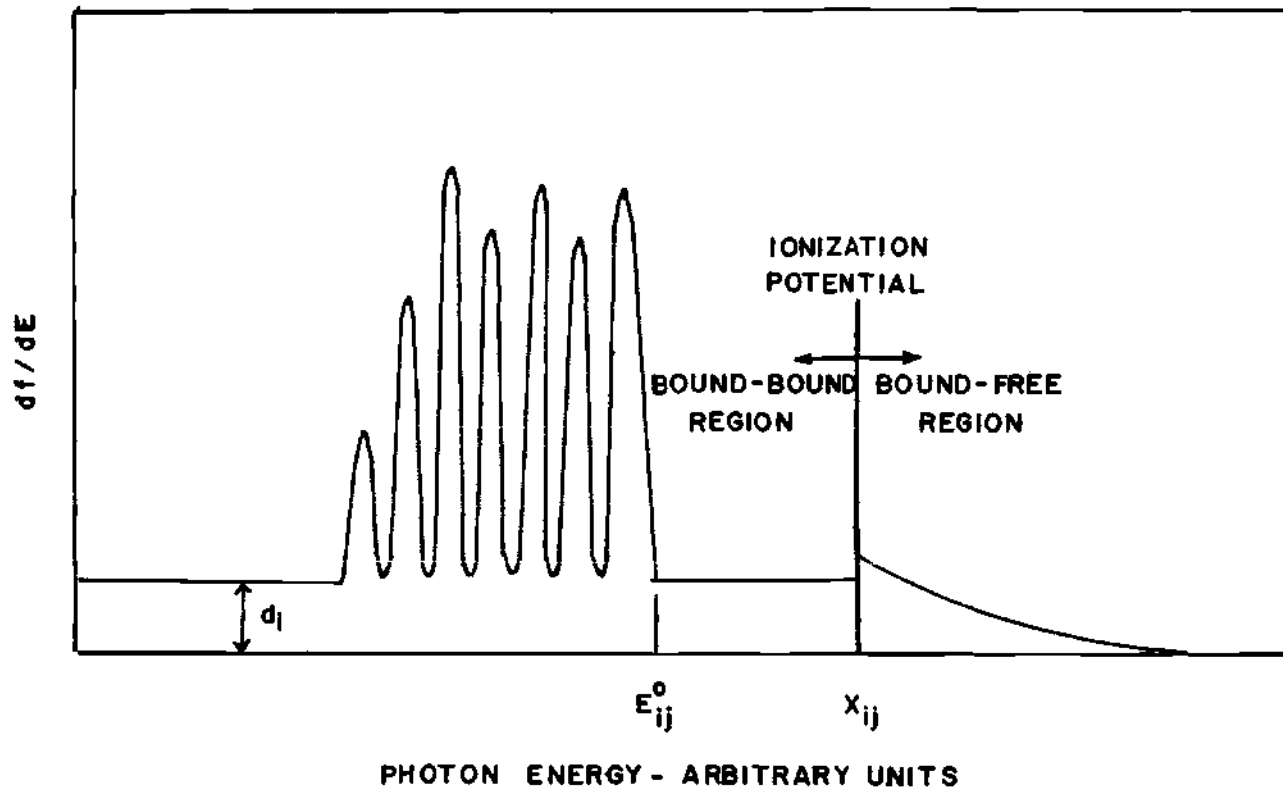


Figure 36. Assumed Oscillator Strength Distribution Used in the Heavy Atom Model as a Function of Photon Energy (Reference 55)

Once this constant, A_1 , is known, equation A-28, which also must satisfy the sum rule, is solved for the normalization factor, b_1 , of equation A-27 which defines the oscillator strength distribution in the bound-bound energy region (below X_{ij}).

Although the bound-free oscillator strength is given by the assumption of a hydrogenic distribution of oscillator strengths to be

$$f_j^{bf}(X_j \rightarrow E) = A_1 [1 - (X_j/E)^2], \quad E > X_j \quad (\text{A-31})$$

it remains for f_j^{bb} to be defined. It is evident from Figure 36 that,

$$f_j^{bb}(0 - E_{j'}) = \sum_{j=j'}^{j=j'} f_{jj'}^{bb} \equiv \int_{j'} f_{jj'}^{bb} dj' \quad (\text{A-32})$$

It has already been shown that

$$\xi_{j'} = (j-1)\tau, \quad \text{so} \quad \frac{d\xi_{j'}}{dj'} = \tau \quad (\text{A-33})$$

and from A-32

$$\frac{df_j^{bb}}{d\xi_{j'}} \frac{d\xi_{j'}}{dj'} = f_{jj'}^{bb} \quad (\text{A-34})$$

so,

$$f_{jj'}^{bb} = \tau \frac{df_j^{bb}}{d\xi_{j'}} = \tau \frac{df_j^{bb}}{dE} \quad (\text{A-35})$$

So $f_{jj'}^{bb}$ is found by multiplying the oscillator strength distribution by

the level spacing, τ .

The composition of the tungsten gas was determined by Krascella from the following four basic relations:

Dalton's Law of Partial Pressures:

$$P = P_{W^+} + P_{W^{++}} + P_{W^{0+}} + P_{e^-} \quad (\text{A-36})$$

Electrical Neutrality:

$$P_e = P_{W^+} + P_{W^{++}} \quad (\text{A-37})$$

Saha equations:

$$\frac{P_{W^0} P_{e^-}}{P_{W^+}} = A_2 T^{5/2} \left(\frac{Q_{W^0}}{Q_{W^+}} \right) \exp \left(- \frac{I_{W^0}}{kT} \right) \quad (\text{A-38})$$

$$\frac{P_{W^+} P_{e^-}}{P_{W^{++}}} = A_2 T^{5/2} \left(\frac{Q_{W^+}}{Q_{W^{++}}} \right) \exp \left(- \frac{I_{W^+}}{kT} \right) \quad (\text{A-39})$$

Where the partition function ratio Q_{W^0}/Q_{W^+} has been shown to be close to one,⁵⁶ and the partition function ratio $Q_{W^+}/Q_{W^{++}}$ has been assumed to be one^{29,53}. As previously mentioned, $I_{W^0} = 7.98$ eV and $I_{W^+} = 14.0$ eV. Number densities are given by

$$N_i = \frac{N_0}{RT} P_i \quad (\text{A-40})$$

where N_0 is Avogadro's number and R is the gas constant.

For strongly overlapping lines, the line contribution to opacity may be represented by²⁹

$$\alpha_i^{bb} \approx \frac{\pi e^2 h}{m c} \frac{1}{B_i} \left\langle N_{ij} f_{ij}^{bb} \right\rangle \rho_{i \Delta j} \quad (\text{A-41})$$

where an average value of the product in the brackets over the energy interval defined by Δ_j is indicated. $\rho_i \Delta_j$ is the line density in the same energy interval.

According to Boltzmann statistics

$$N_{ij} = \frac{N_i g_{ij} \exp(-\epsilon_{ij} B_i / kT)}{Q_i} \quad (\text{A-42})$$

Thus the desired average is

$$\langle N_{ij} f_{ij}^{bb} \rangle = \frac{1}{m_{\Delta j}} \left[\sum_j \frac{N_i g_{ij} \exp(-\epsilon_{ij} B_i / kT)}{Q_i} f_{ij}^{bb} \right] \quad (\text{A-43})$$

where $m_{\Delta j}$ is the number of degenerate lines in the given energy interval.

The line density is defined by

$$\rho_i \Delta_j = \frac{m_{\Delta j}}{\tau_i} \quad (\text{A-44})$$

Substituting A-42, A-43, A-44 into A-41 yields

$$Q_i^{bb} = \frac{\pi e^2 h N_i}{B_i m_e c \tau_i Q_i} \left[\sum_j g_{ij} \exp\left(-\frac{\epsilon_{ij} B_i}{kT}\right) f_{ij}^{bb} \right] \quad (\text{A-45})$$

Making the following substitutions

$$Q_i = \sum_j g_{ij} \exp(-\epsilon_{ij} B_i / kT) \quad (\text{A-46})$$

$$g_{ij} \equiv 1 \quad (\text{A-47})$$

yields,

$$\alpha_i^{bb} = \frac{\pi e^2 h N_i}{m_e c B_i \tau_i} \frac{\sum_{j=1}^{j=(I_i/\tau_i)-1} f_{ij}^{bb} \exp[-(j-1)\tau_i B_i/kT]}{\sum_{j=1}^{j=(I_i/\tau_i)-1} \exp[-(j-1)\tau_i B_i/kT]} \quad (\text{A-48})$$

where $\Delta_j = 1, 2, 3, \dots \left(\frac{I_i}{\tau_i} - 2 \right)$

The line contribution in the bound-bound region is fully defined upon inserting the expressions for oscillator strength from equation A-35.

Krascella utilized the bound-free cross-section, σ_i^{bf} , given by reference 52,

$$\sigma_i^{bf} = \frac{\pi e^2}{m_e c} \left| \frac{df_{ij}^{bf}}{d\nu} \right| = \frac{\pi e^2}{m_e c} \left| \frac{dF_{ij}^{bf}}{d\omega} \right| \quad (\text{A-49})$$

where it has been shown,

$$\frac{df_{ij}^{bf}}{dE} = \frac{2A_i X_{ij}^2}{E^2} = \frac{2A_i X_{ij}^2}{h^3 c^2 \omega^3} \quad (\text{A-50})$$

Thus,

$$\sigma_i^{bf} = \frac{2\pi e^2 A_i B_i^2}{m_e h^2 c^2} \frac{X_{ij}^2}{\omega^3}, \quad \omega \geq \frac{B_i X_{ij}}{hc} \quad (\text{A-51})$$

and the bound-free absorption coefficient, a_i^{bf} , is given by,

$$\alpha_i^{bf} = \sum_{j=1}^{j=(I_i/\tau_i)-1} \sigma_i^{bf} N_{ij} \quad (\text{A-52})$$

where σ_i^{bf} is given by A-51 and N_{ij} is given by A-42.

The total spectral absorption coefficient is ^{29,55}

$$a_{\omega} = \sum_i (a_{i,bb} + a_{i,bf}) \quad (\text{A-53})$$

Inclusion of stimulated emission yields^{29,58}

$$a_{\omega}^* = a_{\omega} \exp(-hc\omega/kT) \quad (\text{A-54})$$

Figure 37 illustrates the results of Krascella's work. The effect of wave number on the spectral absorption coefficient of tungsten gas is shown. Figure 38 shows the expected emission spectrum for the gas core reactor. These results of calculations of the bound-bound and bound-free spectral absorption coefficients of tungsten vapor must be considered rough calculations since the absorption coefficient may vary several orders of magnitude depending upon the selection of atomic model parameters and oscillator strength distributions.²⁹

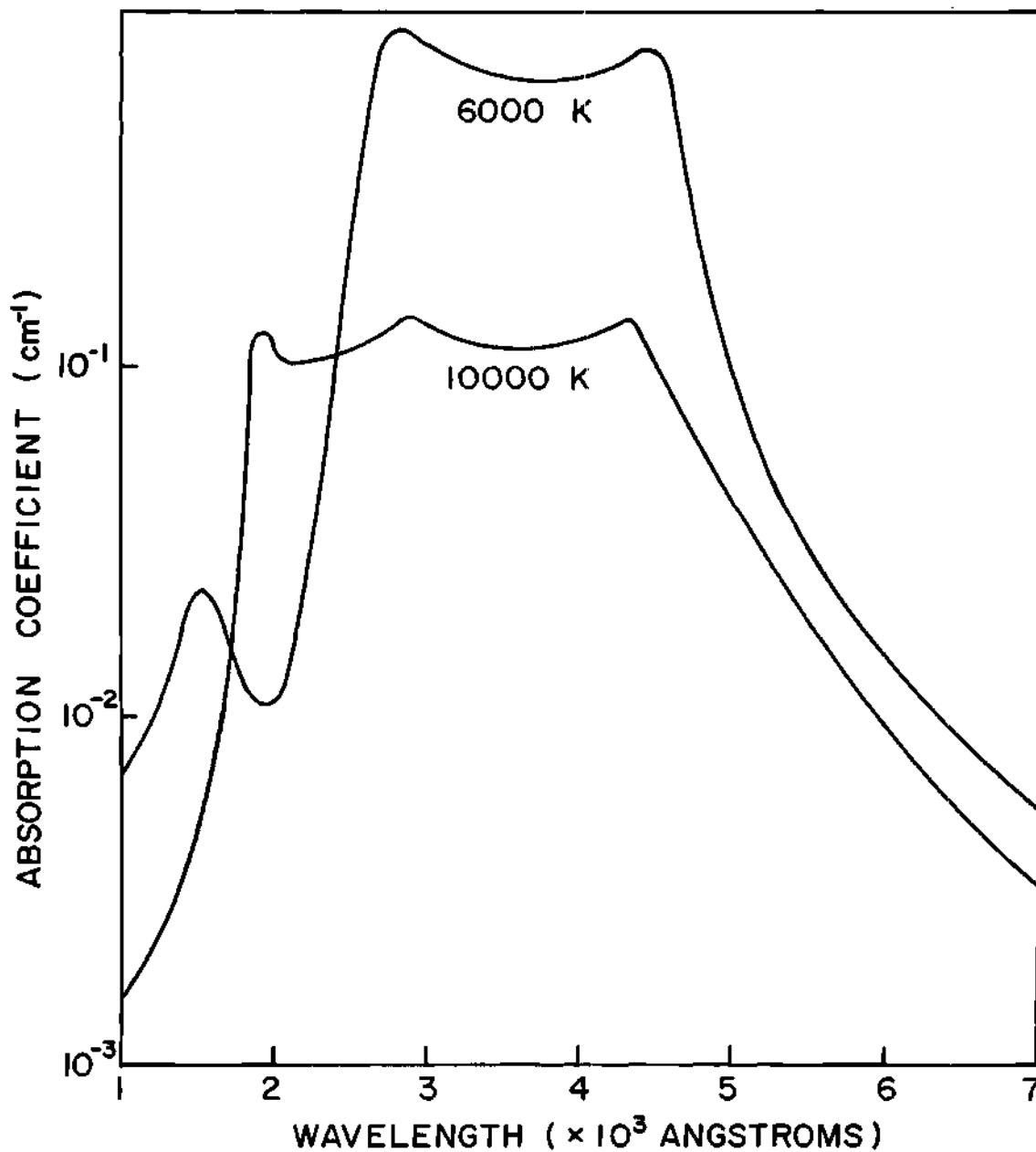


Figure 37. Spectral Absorption Coefficient of .01 Atmosphere Tungsten Vapor at 6000° K and 10000° K (Reference 56)

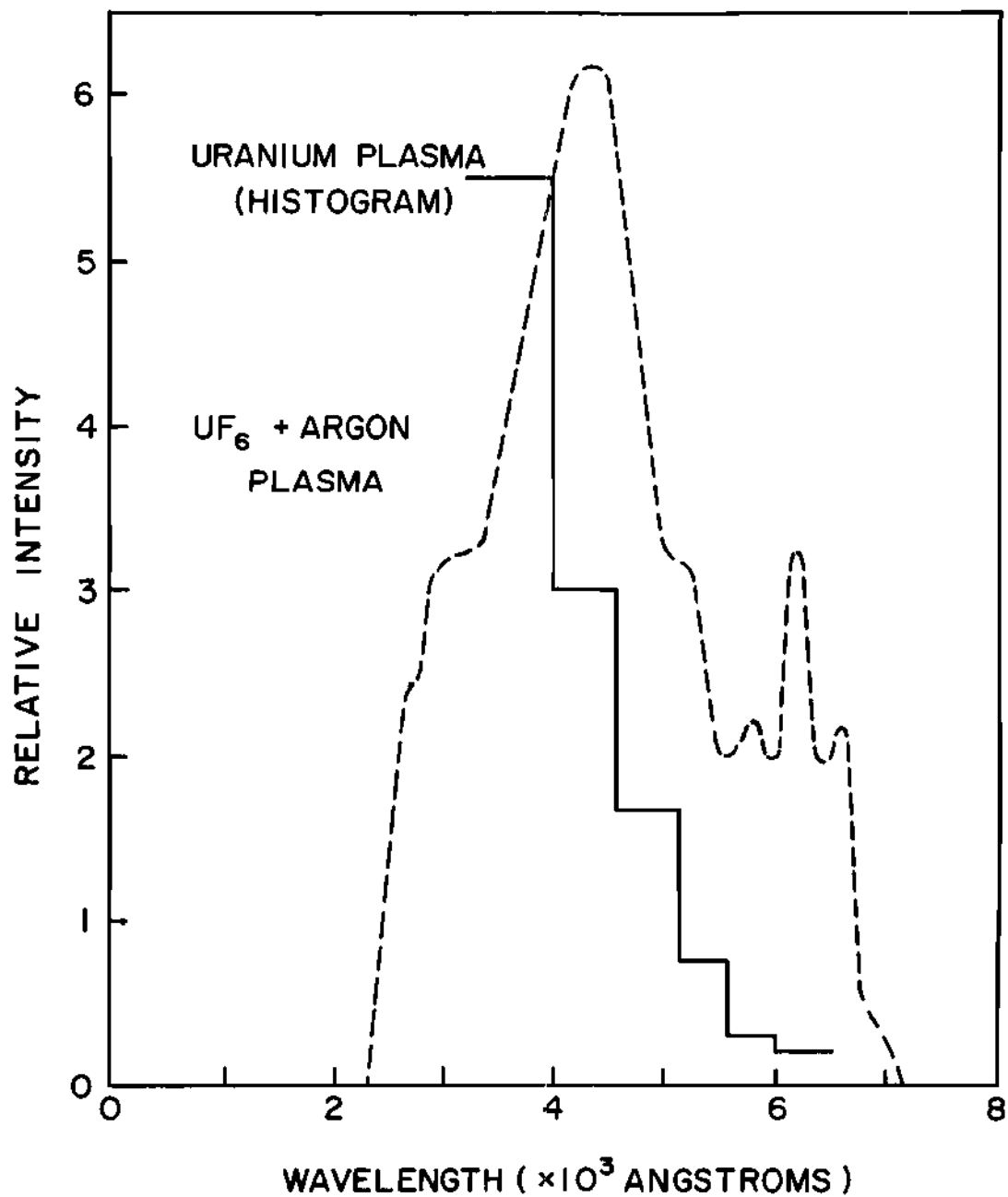


Figure 38. Experimental Emission Spectrum of Uranium Plasma at 8000°K (References 9 and 10)

BIBLIOGRAPHY

1. J. D. Clement and J. R. Williams, "Gas Core Reactor Technology," Reactor Technology, No. 3, 226-251, June, 1970.
2. F. E. Rom, "Coaxial Flow Gaseous Nuclear Reactor Concept," Proceedings of an Advanced Nuclear Propulsion Symposium, Los Alamos Scientific Laboratory Report LA-3229, 177-179, January, 1965.
3. G. H. McLafferty and J. W. Clark, "Summary of Research on the Nuclear Light Bulb Reactor," University of Florida Symposium on Uranium Plasmas and Their Technological Application, January, 1970.
4. F. C. Schwenk and C. E. Franklin, "Comparison of Closed and Open Cycle Systems," Proceedings of the Symposium on Research on Uranium Plasmas and Their Technological Applications, January, 1970.
5. D. E. Parks, G. Lane, J. C. Stewart, and S. Peyton, "Optical Constants of Uranium Plasma, Gulf General Atomic Report #8244, NASA-CR-62348, February, 1968.
6. R. G. Ragsdale, "Relationship Between Engine Parameters and the Fuel Mass Contained in an Open-Cycle Gas-Core Reactor," NASA TM X-52733, January, 1970.
7. N. L. Krascella, "Tables of the Composition, Opacity, and Thermodynamic Properties of Hydrogen at High Temperatures," NASA Sp-3005, 1963.
8. R. W. Patch, "Interim Absorption Coefficients and Opacities for Hydrogen Plasma at High Pressure," NASA TM X-1902, 1969.
9. P. J. Marteney, A. E. Mensing, and N. L. Krascella, "Experimental Investigation of the Spectral Emission Characteristics of Argon-Tungsten and Argon-Uranium Induction Heated Plasmas," United Aircraft Research Laboratories Report No. G-910092-11, 1968.
10. A. G. Randol, III, "Determination of High Pressure High Temperature Uranium Plasma Properties," Ph.D. Thesis, University of Florida, August, 1969.
11. A. S. Shenoy, "The Attenuation of Radiant Energy in Hot Seeded Hydrogen," Ph.D. Thesis, Georgia Institute of Technology, June, 1969.
12. J. W. Cable, Induction and Dielectric Heating, Reinhold Publishing Corp., New York, 1954.

13. T. B. Reed, "Induction Coupled Plasma Torch," Journal of Applied Physics, Volume 32, Number 5, May, 1961.
14. M. L. Thorpe and L. W. Scammon, "Induction Plasma Heating," NASA CR-1343, May, 1969.
15. J. A. Kendall and W. C. Roman, "Initial Radio-Frequency Gas Heating Experiments to Simulate the Thermal Environment in a Nuclear Light Bulb Reactor," UARL Report G-910091-17, September, 1968.
16. M. L. Thorpe, "Induction Plasma Heating: System Performance, Hydrogen Operation, and Gas-Core Reactor Simulator Development," NASA CR-1143, April, 1968.
17. P. H. Dundas, "Induction Plasma Heating: Measurement of Gas Concentrations, Temperature, and Stagnation Heads in a Binary Plasma System," NASA CR-1527, February, 1970.
18. C. E. Vogel, "Curved Permeable Wall Induction Torch Tests," NASA CR-1764, March, 1971.
19. C. E. Vogel et al., "Radiation Measurements and Low Frequency and High Pressure Investigation of Induction Heated Plasma," NASA Contract NA53-13227, August, 1970.
21. J. A. Kendall and W. C. Roman, "Initial Radio-Frequency Gas Heating Experiments to Simulate the Thermal Environment in a Nuclear Light Bulb Reactor," UARL Report G-910091-17, September, 1968.
22. W. C. Roman, J. F. Klein, and Paul G. Vogt, "Experimental Investigations to Simulate the Thermal Environment, Transparent Walls, and Propellant Heating in a Nuclear Light Bulb Engine," UARL Report H-910091019, September, 1969.
23. W. C. Roman, "Experimental Investigations of a High Intensity R-F Radiant Energy Source to Simulate the Thermal Environment in a Nuclear Light Bulb Engine," UARL Report J-9100900-4, September, 1970.
24. A. E. Mensing and J. F. Jaminet, "Experimental Investigations of Heavy Gas Containment in RF Heated and Unheated Two Component Vortexes," UARL Report H-910091-20, September, 1969.
25. A. E. Mensing and J. F. Jaminet, "Experiments of Simulated Fuel in Unheated and Heated Vortexes," Proceedings of the Symposium on Uranium Plasmas and Their Technological Applications, January, 1970.
26. H. D. Campbell, R. T. Schneider, C. D. Kylstra, and A. G. Randol, "Spectroscopic Study of a Uranium Arc Plasma," Proceedings of the Symposium on Uranium Plasmas and Their Technological Applications, January, 1970.

27. P. J. Marteney, A. E. Mensing, and N. L. Krascella, "Experimental Investigation of the Spectral Emission Characteristics of Argon-Tungsten and Argon-Uranium Induction Heated Plasmas," UARL Report G-910092-11, September, 1968.
28. A. E. Mensing and L. R. Boedeker, "Theoretical Investigations of RF Induction Heated Plasmas," UARL Report G-910091-18, September, 1968.
29. N. L. Krascella, "Theoretical Investigations of Spectral Opacities of Hydrogen and Nuclear Fuel," Air Force Systems Command Report RTD-TDR-63-1101, November, 1963.
30. M. H. Miller, T. D. Wilkerson, and D. W. Koopman, "Uranium Plasma Opacity Measurements," Proceedings of the Symposium on Research on Uranium Plasmas and Their Technological Applications, January, 1970.
31. C. D. Lanzo and R. G. Ragsdale, "Experimental Determination of Spectral and Total Transmissivities of Clouds of Small Particles," NASA-TN-D-1405, September, 1962.
32. E. Keng and C. Orr, "Investigations of Radiant Heat Transfer to Particle Seeded Gases for Application to Nuclear Rocket Engine Design," NASA-CR-953, November, 1967.
33. J. R. Williams, W. L. Partain, A. S. Shenoy, and J. D. Clement, "Thermal Radiation Absorption by Particle Seeded Gases," Journal of Spacecraft and Rockets, Vol. 8, No. 4, April, 1971.
34. W. R. Jacobs and J. R. Williams, "Measurement of Thermal Radiation Scattering Characteristics of Submicron Refractory Particles," Second Symposium on Uranium Plasmas: Research and Applications, November, 1971.
35. L. Hartshorn, Radio Frequency Heating, Reinhold Publishing Corporation, New York, 1949.
36. L. L. Langton, Radio Frequency Heating Equipment, John Wiley & Sons, Inc., London, 1949.
37. P. H. Dundas, "High Temperature Induction Furnaces," Research Applied in Industry, London, Vol. 14, July, 1961.
38. A. von Engle, Ionized Gases, Oxford University Press, 1965.
39. Radio Amateur's Handbook, American Radio Relay League, Inc., 1971.
40. R. I. Sutherland, Care and Feeding of Power Grid Tubes, Eimac Division of Varian, 1967.

41. W. H. McAulay, Eimac Division of Varian, Private Communication.
42. R. S. Glasgow, Principles of Radio Engineering, McGraw-Hill, New York, 1936.
43. G. C. Blascoe, Private Communication.
44. J. F. Poteet, Private Communication.
45. W. E. Benns, Private Communication.
46. B. Waldie and I. Fells, "An Experimental Study of Gas Borne Suspensions of Thermionic Emitters as MHD Working Fluids," Royal Society (London) Philosophical Transactions, Ser. A, 261, July, 1967, pp. 490-5.
47. J. S. Cory and A. Bennett, "Thermal Absorption in Seeded Gases," Douglas Report DAC-60779, February, 1969.
48. R. W. Patch, "Methods for Calculating Radiant Heat Transfer in High Temperature Hydrogen Gas," UARL Report M-1492-1, November, 1961.
49. J. R. Williams, A. S. Shenoy, and J. D. Clement, "Theoretical Calculations of Radiant Heat Transfer Properties of Particle-Seeded Gases," NASA CR-1505, February, 1970.
50. R. W. Patch, "I. Composition, Absorption Coefficients for Hydrogen," Journal of Quantitative Spectroscopy and Radiative Transfer, Vol. 9, 1969.
51. R. W. Patch, "Composition of a Hydrogen Plasma Including Minor Species," NASA TN D-4993, 1969.
52. D. H. Menzel and C. L. Felseris, "Absorption Coefficients and Hydrogen Line Intensities," Monthly Notices of the Royal Astronomical Society, Vol. 96, November, 1935.
53. T. Ohmura and H. Ohmura, "Continuous Absorption Due to Free-Free Transitions in Hydrogen," Physical Review, Vol. 121, No. 2, January, 1961.
54. S. Chandrasekhar, "On the Continuous Absorption of the Negative Hydrogen Ion," Astrophysical Journal, Vol. 104, 1946.
55. N. L. Krascella, "Theoretical Investigation of the Opacity of Heavy-Atom Gases," United Aircraft Research Laboratories Report D-910092-4, September, 1965.
56. N. L. Krascella, "Theoretical Investigation of the Composition and Line Emission Characteristics of Argon-Tungsten and Argon-Uranium Plasmas," UARL Report G-910092-10, September, 1966.

57. E. A. Sziklas, "Method for Estimating the Opacity of a Heavy Atom Gas," United Aircraft Research Laboratories Report M-1688-1, September, 1961.
58. N. L. Krascella, "Theoretical Investigation of the Absorptive Properties of Small Particles and Heavy-Atom Gases," NASA CR-693, January, 1967.
59. C. W. Allen, "Astrophysical Quantities," University of London, The Athlone Press, 1955.
60. P. J. Marteney, A. E. Mensing and N. L. Krascella, "Experimental Investigation of the Spectral Emission Characteristics of Argon-Tungsten and Argon-Uranium Induction Heated Plasma," United Aircraft Research Laboratories Report No. G-910092-11, 1968.

VITA

Robert Allan Bennis was born on October 20, 1946, in Columbia, South Carolina. He was raised in Washington, D.C., where he attended grammar school and one year of high school. In 1962 he moved to Chattanooga, Tennessee, where he graduated from Chattanooga High School in 1964.

Mr. Bennis attended the Georgia Institute of Technology and worked as a co-op student at Combustion Engineering in Chattanooga. He received his Bachelor of Science degree in Physics in 1968. Mr. Bennis entered graduate school in the Nuclear Engineering Department at the Georgia Institute of Technology in 1968, and received his Master of Science degree in 1970. While studying for his Master's degree Mr. Bennis became associated with a research grant investigating the radiant heat transfer in gaseous core nuclear reactor concepts by utilizing induction heated plasmas. He later began his Ph.D. work in this technical area.

Mr. Bennis is the principal author of "Measurements of Seeded Argon-Hydrogen Plasma Properties," which he presented at the Second Symposium on Uranium Plasmas in Atlanta, Georgia. He is also principal author of "RF Seeded Plasma Diagnostics" published in the Proceedings of the First Topical Conference on RF Plasma Heating.

Mr. Bennis is married to the former Christine Marshall of Tampa, Florida, and they have one child, David. He is a member of the ANS and Sigma Xi.